Mechanical Engineering.

Mechanical Engineering
Individual Investigative Project

Development of a novel gene screening platform for cells exposed to flow

Britta Moers

August 2017

Supervisors: Dr Cécile M. Perrault and Prof Paul Evans

Dissertation submitted to the University of Sheffield in partial fulfilment of the requirements for the degree of Master of Philosophy

Abstract

Flow is a key regulator of endothelial function and therefore cardiovascular disease development. Nonetheless, the application of flow to cultured cells is a non-trivial challenge. Results obtained from *in vitro* flow systems must be critically reviewed as several technical limitations exist within each system. Recent developments of molecular high throughput techniques are constantly changing the scientific demands of life science laboratories. In order to meet this demand, there should also be the possibility to increase the throughput for flow studies. However, at present there is no high throughput device commercially available to apply flow to cells *in vitro*. Therefore there is a strong need for a novel high throughput technology that can effectively monitor the impact of shear stress on cells.

Endothelial cells (EC) form the inner lining of the arterial wall, thus acting as a barrier between the vessel wall and flowing blood. EC are subjected to wall shear stress (WSS), a force created by the flowing blood. Although Atherosclerosis is associated with systematic risk factors like Diabetes or smoking, disease characteristic plaques occur predominantly near branches and bends, where EC are exposed to low or bidirectional WSS; thus illustrating the physiological importance of WSS.

This project aims to develop a high throughput *in vitro* system for functional screening of gene regulation in EC exposed to flow. The development of an *in vitro* device for application of flow to cells in 96 well plates will allow screening to identify genes involved in cellular responses to flow. It is envisaged that the system will be used in future studies to identify novel putative therapeutic targets for the prevention or treatment of atherosclerosis. Therefore, the proposed high throughput device is designed to be compatible with standard cell culture methods. Briefly, flow will be generated in a standard 96 well cell culture plate using 96 individual stirring cones mounted in a re-usable lid. Each cone will be rotated by a magnetic stirrer, placed underneath the 96 well plate. Due to the device's compatibility with plate readers it will be an ideal addition to existing flow studies to perform fluorescent *in situ* staining.

Table of Contents

Nomenclature

List of Greek letters and SI Units

Symbol	Description	SI-Unit
Δ	distance	[m]
γ_n	normal strain	[dimensionless]
γ_s	shear strain	[rad]
μ	effective viscosity	[Pa s]
ω	angular velocity	[s^{-1}]
π	constant- ratio circle circumference	[dimensionless]
ρ	density	[kg m^{-3}]
τ	shear stress	[Pa]
τ_w	wall shear stress	[Pa]
ν	kinematic viscosity	[m^2 s^{-1}]

List of Latin letters and SI Units

Symbol	Description	SI-Unit
c	substance concentration	[mol l^{-1}]
D	diffusion coefficient	[m^2s^{-1}]
f	frequency	[Hz]
J	diffusion flux	[mol $m^{-2}s^{-1}$]
m	mass flux	[kg $m^{-2}s^{-1}$]
Q	Volumetric flow rate	[ms^{-1}]
r	radius	[m]
T	Tesla	[kg s^{-2} A^{-1}]

List of figures

List of tables

List of abbreviation

3D printing	3 dimensional printing
AC	Analog current
cDNA	Copy DNA
CAD	Computer assisted design
CFD	Computational fluid dynamics
CT	Cycle threshold
CO_2	Carbon dioxide
DC	Digital current
ID	Inner diameter
DAPI	4',6-diamidino-2-phenylindole
DNA	Deoxyribonucleic acid
DNase	Deoxyribonuckease
DNMT	DNA methyltransferase
dNTP	Deoxyribonucleotide

ECGF	endothelial cell growth factor
E-SELECTIN	Endothelial selectin
EC	Endothelial cell
eNOS	Endothelial NOS
FCS	Fetal calf serum
FITC	Fluorescein isothiocyanate
GND	ground
H/D ratio	height to diameter ratio
HDL	High density lipoprotein
HPRT	Hypoxanthine-guanine phosphoribosyltranserase
HUVEC	Human umbilical vein endothelial cell
IgG	Immunoglobulin G
LDL	Low density lipoprotein
LRM	Large rotating magnet
M199	Media 199
MCP1	Monocyte chemoattractant protein 1
MF	Magnetic field
mRNA	Messenger RNA
NaOH	Sodium hydroxide
NF-κB	Nuclear factor kappa B
OD	Outer diameter
P53	Protein 58
PBS	Phosphate buffered saline
PCR	Polymerase chain reaction
PDMS	Polydimethylsiloxane

PFA	paraformaldehyde
PWM	Pulse width modulation
qPCR	Quantitative real-time PCR
RNA	Ribonucleic acid
RNAi	RNA interference
RNas	ribonuclease
RPM	Revolutions per minute
RT	Room temperature
VE-cadherin	Vascular endothelial cadherin
WSS	Wall shear stress

Acknowledgement

First and foremost I would like to thank Dr Cécile Perrault from the Department of Mechanical Engineering at the University of Sheffield for supervising this project. She introduced me to the world of mechanical engineering, gave continuous support and helpful mentorship. Moreover she taught me to trust and follow my own ideas, no matter how strange they were, she always appreciated and encouraged me to think outside the box and beyond.

I also would like to thank Prof Paul Evans from the department of Infection, Immunity & Cardiovascular Disease for giving me the opportunity and freedom of this part-time project whilst I worked as research technician in his group. A special thanks to the departmental technical team and all members of the Evans group, in particular to Dr Matthew Bryan who supervised this project on a day-to-day basis. Matt's passion for research and innovation constantly reminded me to see the bigger picture of this project which motivated me to keep going even in challenging times. I also would like to thank my tutor Dr Tim Chico for really helpful discussions and advice on fundamental questions.

Moreover I would like to thank Dr Candice Majewksi and Wendy Birtwistle for advice and help with the 3D print as well as Simon Rawson and John Wilson from the medical workshop at the Royal Hallamshire Hospital for implementing the practical built of the novel device.

Last but not least I thank my fabulous family and friends: Hiltrudis, Heribert, Christoph and Sandra Mörs; Aaron, Josefine amd Elisa Ganther; Philip Dennis, Liam Murphy, Stefanie Pletz, Martin Grey, Tanja Kalle, Martina Jahn, Ingo Fleschen, Hayley Duckles, Neil Bowden, Ismael Gauci, Rosemary Kim, Sarah Tull, Marc Beurskens and Roshana Thambyrajah.

Thank you - Dankeschön - Dank je wel - Merci beaucoup - Bohoma istouti - Gomawo

1 Introduction

Atherosclerosis is a lipid-driven inflammatory disease of arteries that is characterised by the accumulation of cells, lipids and extracellular matrix in the artery wall. This process of plaque formation can result in narrowing of the vessel lumen and, in some cases, to complete occlusion leading to heart attack or stroke, dependent upon the vessel type occluded. Atherosclerosis is initiated by pro-inflammatory activation of EC which promotes the recruitment of inflammatory cells from the circulation to the artery wall via the leukocyte adhesion cascade and by EC apoptosis (Libby 2012; Tricot *et al*. 2000). Although atherosclerosis is associated with systemic risk factors such as age, high cholesterol and obesity, plaque formation occurs predominantly at branches and bends that are exposed to disturbed patterns of blood flow (Ku 1985; Warboys *et al*. 2011).

The focal nature of EC injury and activation is related to WSS, a force exerted on EC by flowing blood (Davies 2007; Caro 2009a). Regions of arteries exposed to low, oscillatory WSS are susceptible to injury, inflammation and lesion formation. Recent experimental procedures are focusing on microarray studies coupled to bioinformatics to correlate WSS with the endothelial transcriptome in porcine arteries (Passerini *et al*. 2004; Chaudhury *et al*. 2010; Serbanovic-Canic *et al*. 2016). Those studies should be elaborated by using human derived EC *in vitro*. Therefore there is a strong need for an *in vitro* high throughput device for distinct mechanical conditions. Consequently, the device proposed in this dissertation will help to reduce the duration of identification of novel putative therapeutic targets for the prevention or treatment of atherosclerosis.

2 Background and literature review

2.1 Atherosclerosis

Atherosclerosis is a cardiovascular disease that underlies coronary heart disease and stroke. It accounts for 46% of all deaths in Europe; equivalent to 4.1 million deaths per year (Nichols *et al*. 2013).

Atherosclerosis is a, chronic inflammatory disease of the macrovasculature, characterised by the formation of lesions in the arterial wall. This plaque development is associated with an abnormal endothelial function. Risk factors promoting this arterial disease exert homeostatic inbalance on arterial function, e.g. hyperlipidaemia, smoking, hypertension, age, sex and diabetes (Libby 2012).

Atherosclerotic plaques are initiated by inflamed early lesions, called fatty streaks. During disease progression, lipids, cells and extracellular matrix accumulate in early atherosclerotic lesions. This leads to larger and even more inflamed plaques which narrows the vessel lumen to complete occlusion. Thereby, atherosclerotic plaque development is a cause of endothelial cell (EC) dysfunction. A damaged endothelial layer is associated with the loss of the barrier function, and consequently, circulating monocytes can enter the vessel wall (Figure 2-1). These monocytes then differentiate to lipoprotein ingesting macrophages causing production of foam cell which are important in plaque development (Libby, 2002; Sumpio *et al*., 2002).

However, Libby 2002 and Glagov *et al.* 1987 have shown that an initial sign of atherosclerosis is an artery enlargement, where normal vessel lumen and blood flow is retained. Nonetheless, with disease, and therefore with plaque progression, normal lumen size cannot be maintained since plaque progression can lead to inward remodelling of arteries which consequently reduces lumen area and reduces blood flow (Glagov 1994).

Atherosclerotic plaques can be stable or unstable, see Figure 2-2. Stable plaques are characterised by an intact and thick fibrous cap. This stabilising fibrous cap is rich in smooth muscle cells, which have migrated from the medial layer, and accumulated collagen (Finn *et al*. 2010). Unstable plaques are characterised by a thin fibrous cap, rich in inflammatory cells and macrophages (Boyle 2005).

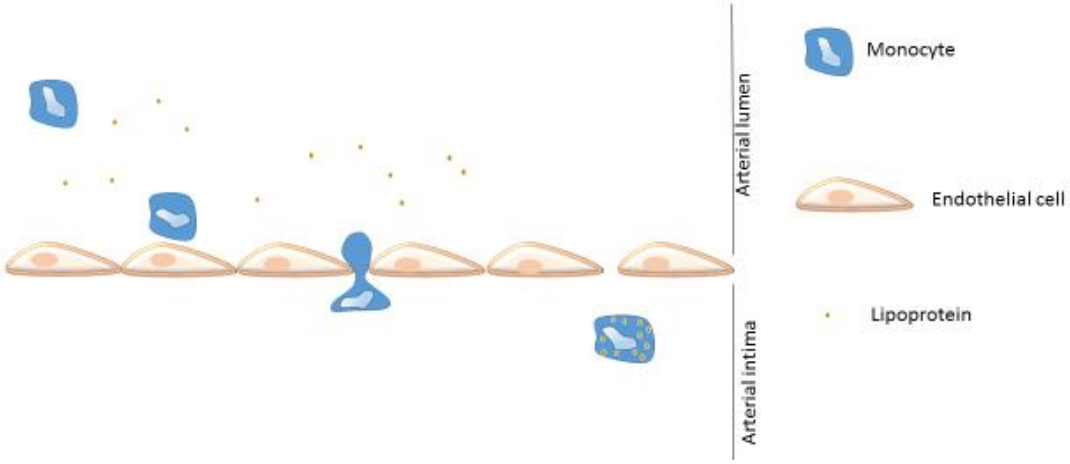

Figure 2-1 **Atherosclerosis plaque development**.

From left to right: Circulating monocytes and lipoprotein in the arterial lumen cannot enter the healthy endothelial layer. Healthy and functional endothelial (shown in brown) creates a barrier between vessel and circulating blood. A damaged endothelial layer loses this barrier function. As a consequence circulating monocytes (shown in blue) can enter the vessel wall. Once the monocytes entered the arterial intima they are subjected to differentiation. Differentiated monocytes have the capability to ingesting lipoproteins, resulting in the accumulation of lipids in the monocytes cytoplasma.

Endothelial cells

A key regulator for the development of atherosclerosis is the endothelium. The endothelium is the inner layer of the arterial wall that acts as a barrier between the flowing blood and the underlying vascular bed and is composed of endothelial cells (EC) Rather than simply channelling blood flow, the endothelium is able to respond to its surrounding environment. Thus, the endothelium may be considered as a dynamic "organ", regulating immune and inflammatory responses, haemostasis and vascular tone (Sumpio *et al*. 2002).

2.2 Endothelial dysfunction and Atherosclerosis are focal

Considering atherosclerosis' risk factors, like hypertension or hyperlipidaemia, are uniformly distributed in the vasculature, this could lead to the prediction that atherosclerotic plaques would develop uniformly or randomly in the vasculature. However, atherosclerotic lesions occur preferentially in specific regions, e.g. arterial branches or bends, and are therefore focal in nature. Hence an additional factor for lesion formation must be considered (Caro *et al*. 1969; Ku 1985).

Atheroprone sites, like arterial branches and bends, are more likely to be subjected to low and disturbed flow, in contrast to high and unidirectional flow in straight vessels at atheroprotected sites. This division implies that endothelial cells are responsive to mechanical as well as chemical stimuli, see Figure 2-3 (Dai *et al.* 2004). There are currently two hypotheses for endothelial dysfunction and plaque development at atheroprone sites (Tarbell *et al*. 2014):

1. Mass transport: prolonged duration of pro-atherosclerotic factors, in particular lipoproteins (e.g.LDL), may promote their influx into the arterial wall and subsequent plaque formation (Schwenke & Carew 1989);

2. Wall shear stress (WSS): blood flow generates diverse frictional forces to the vessel wall, which may trigger varied biomechanical responses at atheroprone and atheroprotected sites (Caro & Nerem 1973).

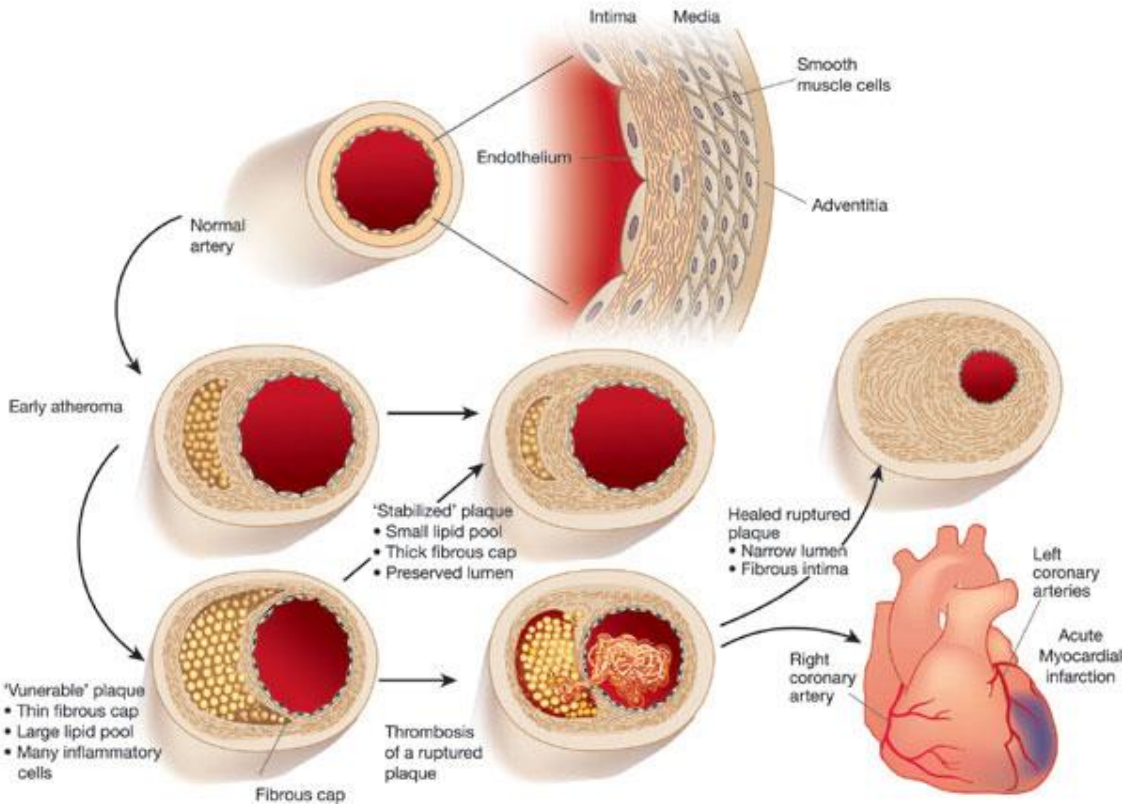

Figure 2-2 Atherosclerosis plaque progression

(Libby 2002, with permission of Nature publishing group)

The endothelium forms the inner lining of the arterial wall; thus acting as a barrier between the flowing blood and the underlying vascular bed. Atherosclerotic plaques find develop as inflamed early lesions. The early atheroma is characterised by accumulation of inflammatory cells as well as lipids which leads to larger and even more inflamed plaques. Those plaques can be either stable or unstable. Stable plaques are characterised by a thick intact fibrous cap, a small lipid pool and a preserved lumen. In contrast to unstable plaques, which are characterised by a thin fibrous cap, a large lipid pool and many inflammatory cells. On the one hand, unstable plaques can lead to inward remodelling of the arteries, which reduces the lumen area and consequently reduces blood flow. On the other hand unstable plaques can lead to thrombosis and consequently to myocardial infarction.

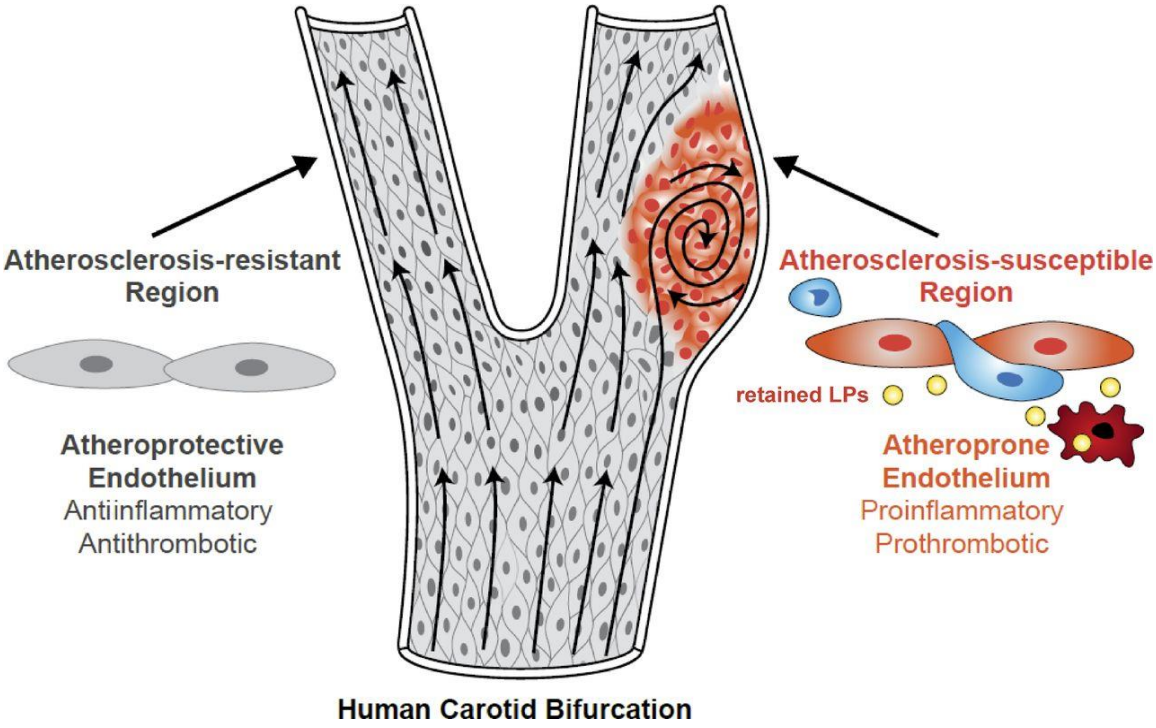

Figure 2-3 The focal nature of atherosclerosis

(from(Tabas et al. 2015, *with permission of Rockefeller University Press*))

In this figure velocity vectors (arrows) are used to illustrate the magnitude (arrow lenghts) and direction (arrow shape) of a fluid velocity field in a human carotid bifurcation. Arterial branches are subjected to low and disturbed flow at bifurcations (shown as eclipsed and bended arrows), and high and unidirectional flow in straight vessels (straight green arrows). Low and disturbed flow regions resulting in atherosclerosis-susceptible sites which can be found predominantly at bifurcations. Atherosclerosis-resistant sites are subjected to high and unidirectional flow.

2.3 The link between Rheology and Atherosclerosis

Atherosclerotic plaques occur at branches and bends, where the endothelium is exposed to low or bidirectional wall shear stress (Dai *et al*. 2004). Research to further investigate atherosclerosis is thus a multidisciplinary approach, combining biology and the study of the deformation and flow of fluids or solids (Caro 2009), a field called rheology (Bingham 1846).

Blood flow in the human body is driven by the cardiac cycle originating from the pumping heart and is therefore unsteady by increasing and decreasing blood velocities dependent on the state of cardiac cycle (Davies et al. 2013). In addition, the human vasculature is a complex structure and in combination with unsteady velocities shear stress effects on the vasculature are divers (Davies 1995). In order to distinguish between different flow magnitudes and flow directions in the vasculature please see the following definitions (Davies 1995):

Laminar Flow: The motion of a fluid in a unidirectional streamline with definite layers and paths which usually occurs at low velocities. Laminar flow is described with Poiseuille's law. This law describes the pressure drop of an incompressible Newtonian fluid through a long pipe. Low shear stress typically occurs in regions of laminar flow

Disturbed flow: Streamline and paths are irregular regarding the fluids magnitude and directions. Disturbed flow is a result of breaking down regular laminar flow, usually through high velocities and geometrical irregularities. A specific type of disturbed flow is oscillatory flow which occurs in areas of the curvature in the vicinity of those branch points.

High shear stress (HSS): Flow typically occurring in large arteries in the ranging from 20-40 dyn/cm^2. HSS usually occurs in the uniform vasculature away from branches and bends.

Experiments conducted by Cheng *et al*. (2006) provide a direct link between atherosclerosis and blood flow. The authors showed that plaques are directly inducible by altering blood flow *in vivo*. Thereby low shear stress induces unstable plaques and oscillatory shear stress induces stable plaques (Figure 2-2).

Vasculature structure and blood flow (haemodynamics) exhibit a dynamic bidirectional relationship. The development of blood vessels and the initiation and progression of atherosclerosis are on the one hand flow-dependent processes (Geudens & Gerhardt 2011). On the other hand, the build-up of plaques can modify the geometrical structure of the vasculature which in turn alters blood flow (Saxer *et al*. 2013).

"Everything flows" (Heraclitus), and therefore even Ohm's Law is applicable to blood flow which originally describes the flow of electricity (Ohm 1891; Bingham 1846). Equation 2-1 shows that current flow is the ratio of potential difference and resistance. Therefore, changing the potential difference or the resistance has an impact on the total amount of current flow in the closed system.

Equation 2-1 $$Current\ flow = \frac{Potential\ Difference}{Resistance}$$

Bingham (1846) adapted Equation 2-1 by applying it to circulating blood in the human body. This simplified concept states that blood velocity is the ratio of pulsatile pressure difference created by the heart and resistance, see Equation 2-2.

Equation 2-2 $$Velocity = \frac{pulsatile\ Pressure\ Difference}{Resistance}$$

2.4 WSS calculation - laminar flow conditions

Stress is the force per unit area and shear is described as the movement of parallel adjacent layers. The degree of rheological deformation caused by stress is called: strain (y). A shear strain (y) therefore describes the rheological deformation of parallel layers on the same plane. The rate of shear strain change with time is called shear rate ($\dot{y}$). Thereby shear rate can be defined as the time dependent rheological displacement of parallel layers on the same plane. Shear rate is expressed in reciprocal seconds [sec^{-1}]. Fluid shear stress (τ) is the force per unit area acting parallel to the surface causing the movement of adjacent fluid layers, expressed in [Pa]. Consequently, WSS (τ_w) is the

specific shear stress force acting on the inner vessel wall, which is the location of the endothelium (Jacobs 2013).

Laminar flow is the smooth movement of parallel layers and is thereby characterised by the change of magnitude only, contrary to turbulent flow. Calculations for WSS under laminar flow through a straight vessel are derived from Poiseuille's law. This law describes the pressure drop of an incompressible Newtonian fluid through a long pipe. Further adjustments to address viscosity were made from Navier (Sutera & Skalak 1993). Equation 2-3 and Figure 2-4 illustrating WSS calculation; where Q is the volumetric flow rate [L $h^{-}1$], πr^3 [m^3] the vessel size and μ the viscosity [Pa s]. The impact of viscosity on the fluids motion is described in more detail in the following section.

Equation 2-3 $$\tau_W = \frac{4\,\mu\,Q}{\pi\,r^3}$$

Equation 2-3 illustrates that WSS is dependent on viscosity, flow rate, and vessel size. In addition it shows that viscosity and velocity are directly proportional. If one of them increases, that in turn increases the WSS, given a constant vessel size. The equation also shows that a smaller vessel diameter increases the WSS and a larger vessel diameter decreases WSS, given constant viscosity and velocity. This might be one explanation why atherosclerosis is a disease of the macrovasculature (Fung 1996).

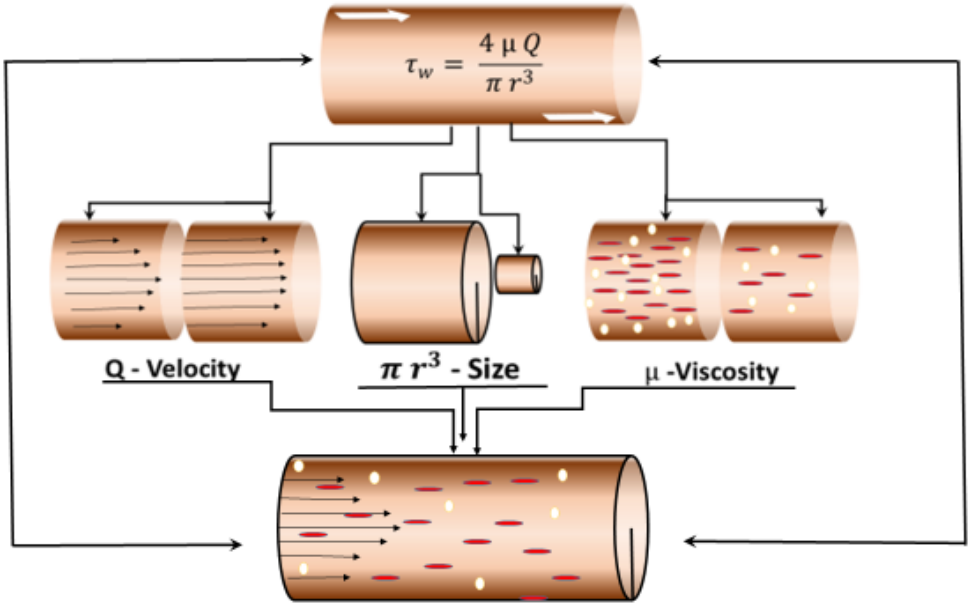

Figure 2-4 Wall shear stress calculation.

The figure illustrates wall shear stress equation factors for calculations of laminar flow in a straight vessel. Wall shear stress is dependent on viscosity (μ), volumetric flow rate (Q), and vessel size (πr^3).

This equation shows, that wall shear stress is strongly reliant on the vessel size. Thereby a smaller vessel diameter increases WSS whereas a larger vessel diameter decreases WSS, given a constant viscosity and velocity. However, viscosity and velocity are inverse proportional, an increase would consequently result in an increase of the shear stress magnitude.

2.4.1 Influence of viscosity on WSS

Viscosity is the resistance to flow, mathematically expressed as internal pressure per second [Pa s], the ratio of shear stress (τ) to shear rate ($\dot{\gamma}$), Equation 2-4 (Thurston 1972). Therefore WSS equation can be extended with this equation, forming Equation 2-5.

Equation 2-4 $$\mu = \frac{\tau}{\dot{\gamma}}$$

Equation 2-5 $$\tau_w = \frac{4\,\mu\,Q}{\pi\,r^3} = \frac{4(\frac{\tau}{\dot{\gamma}})\,Q}{\pi\,r^3}$$

Empirical viscosity measurements can be performed with a cone-and-plate rheometer. Thereby it must be noted that viscosity is strongly temperature dependent. Measurements at standard room temperature (25°C) are not reliable for *in vitro* applications at 37°C (Barnes *et al*. 1989).

Interestingly, it has been shown that atherosclerosis risk factors such as diabetes, LDL and smoking are accompanied with increased blood viscosity (Leonhardt *et al*. 1977; Sloop & Mercante 1998; Ernst *et al*. 1986). However, this seems to be controversial considering that an increased viscosity increases the WSS in a straight vessel with laminar flow (see Equation 2-5) and that high WSS has atheroprotective characteristics. Therefore it would be interesting to further investigate into this specific theoretical considerations.

Newtonian vs Non-Newtonian fluids

Dependent on the rheological behaviour between viscosity and shear rate, fluids are categorised into Newtonian or Non-Newtonian.
Isaak Newton was the first who derived the relationship of shear stress and shear rate in fluids. If the relationship between shear stress and shear rate is linear, fluids are called Newtonian fluids. Thereby shear stress is the force per unit area acting parallel to the surface and shear rate is the velocity gradient (see figure 2.4).

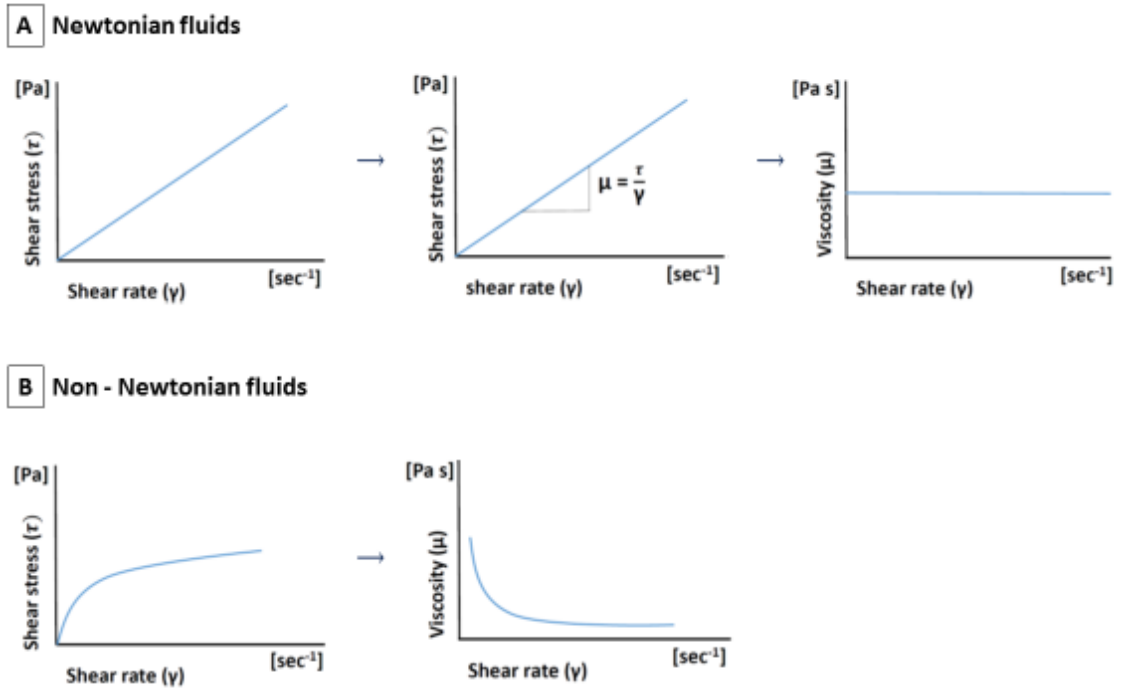

Figure 2-5 Flow- and viscosity plot of Newtonian- and Non-Newtonian fluids

(A) left plot: shear stress (τ) as a function of shear rate (γ); middle plot: the ratio of shear stress to shear rate provides information about the liquids' viscosity; right plot: viscosity as a function of shear rate.
Newtonian fluids show a linear correlation of shear stress and shear rate. Thereby showing a proportional behaviour of viscosity to shear rate.

(B) left plot: shear stress (τ) as a function of shear rate (γ); right plot: viscosity as a function of shear rate.
Non-Newtonian fluids show a non-linear function of shear stress to shear rate. The curve form shows a smaller increase of shear stress to shear rate, compared to Newtonian fluids. Thus, an increased viscosity results in decreased shear rate. Therefore Non-Newtonian fluids are viscoelastic and dependent on viscosity and shear rate.

Viscosity is the resistance to flow and can be determined through the slope of shear stress and shear rate. In order to determine the relation between viscosity and shear rate, they can be plotted against each other; this graph shows that shear rate is independent of viscosity. This means that with all possible shear rate points the viscosity remains the same. Blood plasma is a Newtonian fluid and can be described on the basis of the Navier-Stokes equation.
However, whole blood is a complex fluid and does not follow Newton's law. Those fluids are called Non-Newtonian fluids. Non-Newtonian fluids show a non-linear relationship between shear stress and shear rate.

Whole blood may be described from a biologist's point of view as tissue, as it contains several types of cells, and proteins; those are surrounded by plasma which may be considered as the intercellular liquid component. A fluids mechanical engineer may describes whole blood as a two-phase liquid or as a solid-liquid suspension (Baskurt *et al*. 2003). Erythrocytes may be accountable for the rheological changes of whole blood most of all. With a haematocrit of approximately 40%, erythrocytes occupy the largest amount of solid components in the blood. However, red blood cells (RBC) may be considered as liquid caused by their viscoelastic nature. This means that at high shear rates erythrocytes are being deformed and oriented to the flow streamlines, which decreases the viscosity. The viscoelastic nature of erythrocytes is particularly striking in small capillaries, which is described by the Fahraeus-Lindqvist effect. The Fahraeus-Lindqvist effect shows that with decreasing microvessel diameter (5 – 7 µm) the viscosity decreases. However, if the capillary is smaller than the RBC itself, then the RBC is still able to move through the capillary due to its viscoelastic nature. High shear rates the RBC to deform and therefore adapt to the capillary size. In contrast, low shear rates cause lead to RBC aggregation, or rouleaux formation and is therefore accompanied with an increased viscosity.

Although whole blood is a Non-Newtonian fluid, it shows the characteristics of a Newtonian fluid in a large straight vessel under laminar flow and high shear conditions (Dutta & Tarbell 1996). Therefore a non-Newtonian fluid can have Newtonian fluid characteristics but not *vice versa* (Barnes *et al*. 1989). Thus blood can be assumed to be Newtonian for most fluid dynamics calculations (Sochi 2013).

2.5 Turbulent flow - Reynolds number

Turbulent flow is characterised by the change of magnitude and direction. Therefore blood flow may be turbulent in some circumstances and can be expressed with the dimensionless Reynolds number. The Reynolds number (Re) is the ratio of the inertial force and the viscous force, where the inertial force is the result of volumetric flow rate (Q) multiplied with the vessel size. The viscous force is described as kinematic viscosity (υ), expressed as [$m^2\ s^{-1}$], and is the ratio of viscosity and fluid density (ρ), expressed as [$kg\ (m^3)^{-1}$], Equation 2-6.

Equation 2-6

$$Re = \frac{inertial\ force}{viscous\ force} = \frac{Q\ x\ \pi r^3}{\upsilon} = \frac{Q\ x\ \pi r^3}{(\frac{\mu}{\rho})}$$

Equation 2-6 illustrates that the Reynolds number depends on flow rate, viscosity and vessel diameter. The inertial force determinants, velocity and vessel diameter, are directly proportional; thus an increase of the inertial force results in an increased Reynolds number, given a constant viscous force. This means that an increased flow rate and/or larger vessels are more prone to higher Reynold numbers. When the Reynolds number exceeds a critical value of 2300, flow is considered to be turbulent (Fung 1996).

2.6 Techniques to predict and model fluid dynamics

In order to further investigate the interplay between fluid dynamics and atherosclerosis lesion formation *in silico* and *in vitro* techniques have been developed. Those techniques allow the creation of shear stress maps to predict fluid dynamics. Conventional simulating methods are computational fluid dynamics (CFD) and particle imaging velocimetry (PIV) which will be reviewed here in more detail.

2.6.1 Computational fluid dynamics

The increasing potential of computer data processing possibilities in the last decades allow researchers to predict larger and more complex rheological principals in biological systems *in silico* (Henninger *et al*. 2010). CFD software, e.g. FLUENT, became

commercially available in the 1980s and during the last decade publications of CFD studies have increased nearly exponentially (Xiang *et al*. 2014).

A CFD simulation resolves rheological principals numerically by solving a mathematical equation. This equation describes a problem, the specific physical properties of the fluid; e.g. the Navier-Stoke-equation can be used for computational prediction of Newtonian fluids, see section 2.4.1 (Pekkan *et al*. 2005).

However, flow characteristics are strongly dependent on the geometrical vessel structure, see 2.4. Therefore the geometrical structure needs to be modelled, e.g. a vessel. This geometrical structure is then used to create a mesh. The mesh, also called a grid, divides the model into small segments. These smaller segments are called cells; in this way CFD is capable to solve complex structures.

For finite element CFD simulation, the mathematical equation is then applied to each cell of the mesh, where each cell has input and output locations. The mathematical calculation for one cell starts with the pre-processing at the input, is then processed to solve the problem and finishes at the output with the post-processing. Neighbouring cells then use the post-processed data as their input signal. This procedure is continued until all cells of the mesh are processed (Versteg & Malalasekera 2007). Figure 2-6 briefly sketches this CFD principle.

The major limitation of CFD is currently the computer power. The computer power needed to solve a CFD model is dependent on the fineness of the created mesh and the numerical input of the solver.

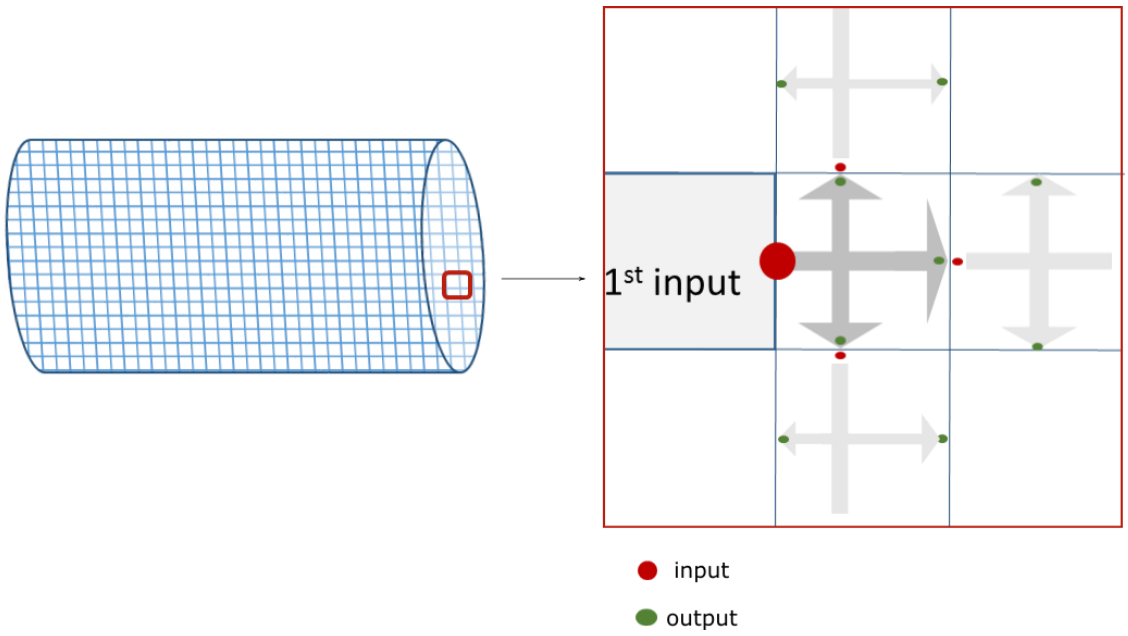

Figure 2-6 Simplified principle of computational fluid dynamic

CFD is used to predict fluidic behaviour and is therefore an essential tool for studies of vascular response to flow.

Left hand side: In order to simulate the flow behaviour the geometrical structure of the area of interest is modelled. For further processes a grid is applied to this model to divide into smaller cells.

The right hand side shows a cluster of 9 cells; red circle illustrating the input- and the green circle the output signal. The mathematical equation is applied to the input signal and processed to the output signal. Neighbouring cells then using this output signal as their input signal.

2.6.2 Particle imaging velocimetry

PIV is a direct measurement of fluidic dynamics and mostly used in order to validate and complement CFD predictions, mostly *in vitro*. Adrion (2005) defines PIV as "the accurate, quantitative measurement of fluid velocity vectors at a very large number of points simultaneously". Tracer particles are added to the flow and their movement is recorded. Flow direction and velocity is then determined by following the particle displacement between the recorded frames (Buchhave 1992). Since the time delay between frames is known, the displacement of a particle between frames allows to track the distance of the particle per frame and therefore time.
The particle itself should be as small as possible to avoid flow disruption. However, larger particles improve light scattering and thereby allow accurate analysis of the flow dynamic (Melling 1997).

Micro-PIV experiments in liquid flows can also be performed with fluorescent labelled particles and usually a microscope with a camera is used to track the particle displacement (Raffel *et al*. 2007). Thereby the field of view is rather planar, and the tracking analysis does not provide information on the third dimension.

2.7 Mechanotransduction

In order to respond to stimuli and adapt to their environment multicellular organisms have developed mechanoresponsive mechanisms e.g. the sense of touch, hearing or balance (Lumpkin *et al*. 2010). In the vasculature EC are exposed to WSS, a mechanical force created by the flowing blood. EC are able to respond to their local mechanical environment including WSS. Consequently, EC are considered to be mechanoresponsive, but the mechanism of shear stress sensing by EC and the mechanotransducers involved are poorly understood. However, various studies were able to identify surface receptors and cytoskeleton components, which are able to transduce the shear stress signal to a biochemical response (Davies 2009), Figure 2-7.

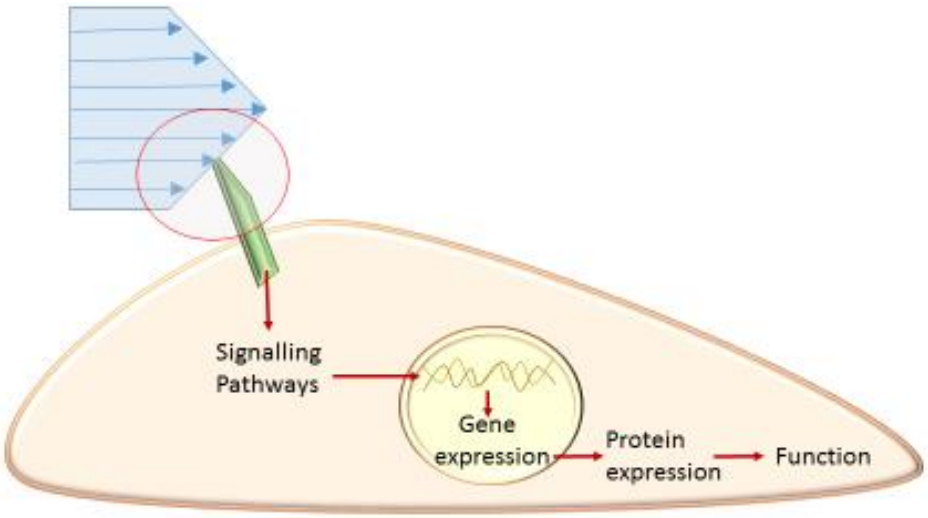

Figure 2-7 Schematic endothelial mechanotransduction.

Mechanical cell sensors on the cell surface, shown in green, sense extracellular mechanical signals. Those signals are created amongst others by blood flow, shown in blue. The mechanical signal is translated into a biochemical signal, activating certain signalling pathways and subsequently altered gene expression. Thereby triggering gene expression and finally resulting in adapted functionality transmitted by proteins.

Research of Tzima *et al*. (2005) shows a mechanosensory complex to transduce mechanical forces in endothelial cells. This complex compromises of: platelet endothelial cell adhesion molecule-1 (PECAM-1); vascular endothelial cell cadherin (VE-cadherin); and VEGFR2, where PECAM-1 transmits the mechanical force, VE-cadherin functions as adaptor molecule and VEGR2 activates specific kinase activity. In 2008, Goel *et al*. and Harry *et al*. were able to show that PECAM-1 has different functions on specific sites implying PECAM-1's flow dependency.

Furthermore, the surface, glycocalyx, cytoskeleton, integrins, plasma membrane, actin filaments, ion channels and cilia have been proven to be flow responsive (Huebsch *et al*. 2010; Matthews *et al*. 2010; Batra *et al*. 2012; Bellin *et al*. 2009; Barbee *et al*. 1994; Weinbaum *et al*. 2011; Weinbaum *et al*. 2003; Zhou *et al*. 2014; Tarbell & Pahakis 2006; Hierck *et al*. 2008; Van der Heiden *et al*. 2011).

The effects of mechanical forces on downstream signalling events in EC has been studied intensely in the last decade. Several transcriptome studies, coupled to CFD have analysed the relationship between shear stress and endothelial gene expression (Passerini *et al*. 2004; Civelek *et al*. 2009; Serbanovic-Canic *et al*. 2016).

On the one side, these transcriptome studies reveal that low shear increases the gene expression of pro-inflammatory and pro-apoptotic signalling pathways, which are known to support endothelial dysfunction and consequent atherosclerotic plaque formation. Important flow responsive pro-inflammatory genes include NF-κB and p38/JNK MAPK whereas important flow responsive pro-apoptotic genes are: XBP-1, JNK, p53, Caspase-3 (see
Figure 2-7).

On the other side, those studies also show that high shear rates decrease gene expression of inflammatory and apoptotic pathways and increases expression of anti-inflammatory and anti-apoptotic pathways. Anti-inflammatory, and therefore atheroprotective, upregulated genes including MKP-1, Nrf2, and Cezanne. Differently expressed anti-apoptotic genes include c-Jun, VEGF, eNOS and IAP (Amini *et al*. 2014; Hajra 2000; Cuhlmann *et al*. 2011; Hayden & Ghosh 2004; Van der Heiden *et al*. 2010; Zakkar *et al*. 2011; Zeng *et al*. 2009; Heo *et al*. 2011; Garin *et al*. 2007; Enesa *et al*. 2008; dela Paz *et al*. 2012; Jin *et al*. 2002; Taba *et al*. 2003).

Furthermore it has been shown that flow has an impact on cell alignment. Davies (2005), describes the EC alignment in the direction of flow as a ‘healthy phenotype’ whereas lack of cell-alignment under bidirectional flow was associated with EC dysfunction. Further research showed that the no-alignment phenotype occurs at atheroprone-regions, with increasing apoptosis and the inflammatory genotype (Davies 2008; Tzima *et al*. 2005; Barbee *et al*. 1994). It will be important in future to investigate, if cell alignment in the direction of flow influences the mechanotransmitting surface properties of EC, or whether inflammation and apoptosis are independent of alignment.

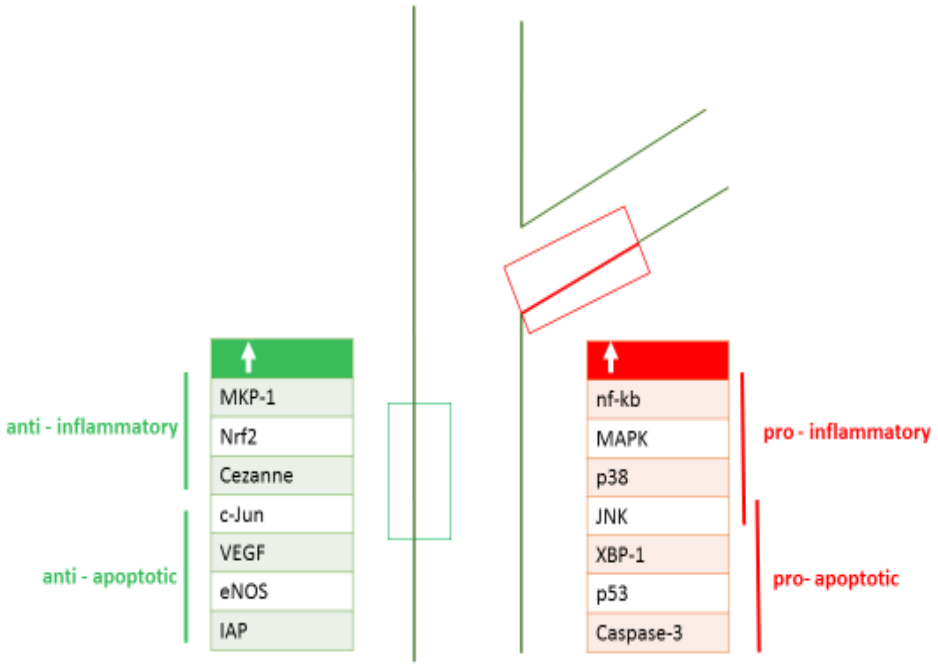

Figure 2-8 Differentially expressed genes of high and low shear regions

High shear regions (green) express increased anti-inflammatory and anti-apoptotic genes, shown in green table. Anti-inflammatory genes include MKP-1, Nrf2, Cezanne; Anti-apoptotic genes include c-Jun, VEGF, eNOS, IAP.

Whereas low shear regions (red) express increased pro-inflammatory and pro-apoptotic genes, shown in red table. Pro-inflammatory genes include nf-κb, MAPK, p38, JNK; Pro-Apoptotic genes include JNK, XBP-1, p53, Caspase-3.

2.8 Review on existing flow devices and high throughput compatibility

The endothelium is subjected to WSS, a frictional force created by the flowing blood, which triggers biomechanical responses resulting in atheroprone and atheroprotected sites in the vasculature. In order to investigate the cellular response to shear stress *in vitro* devices for flow application have been developed. A common feature of all devices is the principal to move the cell culture media and thereby create shearing force on the cells.

2.8.1 Orbital shaker

The orbital shear stress model was described by Dardik *et al*. (2005) and Salek *et al*. (2011). It is a medium throughput system, exposing cells to flow using commercially available 6-well tissue culture plates placed on an orbital shaker in a cell culture incubator. Several plates can be positioned on the shaker platform and in addition they can be stacked on top of one other (Warboys *et al.* 2010a).

Equation 2-7 describes the estimation of the applied shearing force in mechanical shakers, where: "a" is the orbital radius of the shakers rotation [m]; "μ" is the viscosity [Pa s]; "ρ" is the density [kg (m3)-1]; and "f" is the frequency of rotation [rotations sec^{-1}] (Hubbe 1981; Alan Dardik *et al*. 2005).

Equation 2-7

$$\tau_{max} = a\sqrt{\mu\, p\, (2\pi f)^3}$$

In order to quantify fluid dynamics in the single 6-well exposed to the orbiting force, CFD analysis and PIV have been performed (Dardik *et al*. 2005; Kostenko *et al*. 2010; Salek *et al*. 2011).

Given an orbital shaker radius of 10 cm; the viscosity and density of the cell culture medium at 37°C, a rotational speed of 210 rpm, the fluid velocity and therefore the shear stress is found to be different in the 6-well plate. A high shear region is found in the periphery of the well whereas the centre of the well is exposed to low shear and greater flow disturbances. Consequently, cells in the periphery align with flow direction in contrast to cells in the centre (Dardik *et al*., 2005).

On the one hand the ability to generate different shear stress regions are beneficial for studying EC response to physiological flow; high shear regions merge with low shear and bidirectional flow regions. Under physiological conditions biochemical factors are

carried and shared amongst different shear stress regions by the blood, which is partly mimicked by the orbital shaker system *in vitro*.

On the other hand, flow studies that test only specific magnitudes are not feasible with the orbital shaker system, since it is not possible to impose a single specific flow pattern on cells.

Orbital shaker as high througput system?

The orbital shaker is a very user friendly system to apply flow to cells. Currently the orbital shaker is used with 6-well plates and the orbital shaker itself is placed in the incubator. However, the system has been validated for 6 well plates filled with 3 ml media only. It certainly would be a reasonable idea to do further validations for different media volumes and different tissue culture plates, e.g. a 12 well plate.

Salek *et al.* (2012) suggest that two variables alter the flow motion: firstly, the media volume and secondly, the shaker speed. Therefore one possibility to increase the sample throughput would be the numerical scale down of the 6 well plate system to e.g. a 96 well plate with a constant shaker speed. In biotechnological processes a scale down is calculated via the height to diameter ratio (H/D ratio). The 6-well plate wells are filled with 3 ml media and are orbited at a speed of 210 rpm. 3 ml media in a 6 well thereby equals a volume height of 7 mm in the 6 well. The 6 well diameter is 35.43 mm. The H/D ratio of the 6-well filled with 3 ml media is therefore: 0.2. The diameter of a 96 well is: 0.96 mm. In order to achieve an H/D ratio of 0.2 the media height in the 96 well has to be 1.4 mm. A medium height of 1.4 mm equals approximately 50 µl of cell culture medium. This volume may be not enough to culture cells for an averaged timed experiment. Another possibility would be to increase the orbital shakers speed in order to be able to increase the cell culture volume and therefore the created shearing force. However, it is questionable if the non-uniform flow motion, which is created by the orbital movement of the shaker, is desirable itself.

2.8.2 Microfluidic chambers

Microfluidics chambers find their application as miniaturised platforms for a wide range of applications in the modern laboratory; for example, shear stress, stretch or intracellular architecture research (Kurth *et al*. 2012). These chambers are using the principal of "Lab-on a chip" by scaling down *in vitro* assays to a minimum size. Improved soft lithography

technology immensely simplified fabrication and customisation of microfluidic chambers for customised production (El-Ali *et al*. 2006).

Microfluidic chambers are widely used for mechanobiology studies and therefore also for shear stress applications. The cell culture medium flows through the chamber by pumping and thereby creating the shear stress on the adherent cells. The chamber itself can contain single-, multi- or y-shaped channels to address different applications and questions. However, since chambers can be easily prepared with polydimethylsiloxane (PDMS), there are infinite possibilities to create chambers for each application.

Commercially available microfluidic flow systems are available from cytodyne, which are based on parallel plate system, and ibidi. The ibidi system, reviewed here, consists of an air pressure pump connected to a fluidic unit. Both parts work together to create flow. Cells are seeded on a microfluidic slide which is connected to the fluidic unit to create unidirectional, oscillating or pulsating flow of the cell culture medium. This flow creates the shear stress which is applied to the cells on the slide. With help of a perfusion system, which is mounted on the fluidic unit, media is pumped back into the reservoirs followed by re-flowing it through the slide. Using the PumpControl Software it is possible to control all pump parameters (Kroutvar & Guttenberg 2013).The ibidi system is a low throughput system which is highly accurate and flow is distributed uniformly over the slide. The total cell number is limited due to the microfluidic chamber size and the cell culture medium is limited because of the reservoir volume. Although the pump is maintenance free, the costs for the slides are relatively high.

Microfluids as high throughput system?

Microfluidics chambers offer the possibility to work within microscales and therefore apparently provide the possibility to apply flow to cells on a larger scale as a high throughput system. However, one problem arises when considering microfluidics as a high throughput system: every chamber would need its own pumping system. Assumed that several microfluidics will be served by one pump, all chambers will be provided with the same cell culture media. During flow application, cells secrete signalling substances in the cell culture media, which will consequently be received by all chambers. Therefore, this set-up would not be a truly a high throughput system since the media may be considered as an internal contamination source. Consequently, it would be questionable if a single chamber in this set-up could be considered as individual sample number. The other scenario would be to set-up each microfluidic chamber with its own

pump. However, this may not be suitable as a high throughput setup either. This may involve long time periods for the manual set-up and may cause logistical space issues due to the number of pumps, cables and individual medium reservoirs. Overall the idea of constructing microfluidics to a high throughput system seems to be a user–unfriendly approach.

2.8.3 Cone-and-plate

The cone-and-plate device was originally invented as a rheometer, intended for viscosity measurement. It works with a stationary plate in combination with a rotating cone shaped insert above the stationary plate. The cone shaped insert achieves a constant shear rate on the cells grown on the stationary plate by linearising the angular velocity, see Figure 2-9 (Buschmann *et al*. 2005; Spruell & Baker 2013). Fluid dynamics can be calculated with the dimensionless Reynolds number. Thereby the radius (r) expressed in [m], the angle (α) and the angular velocity (ω) expressed in [rad·s^{-1}] are directly proportional as the ratio to viscosity (υ), expressed in [m^2 s^{-1}], Equation 2-8.

Equation 2-8

$$Re = \frac{r^2\,\alpha^2\,\omega}{12\,v}$$

The shear rate (D) can be determined as the ratio of the linear velocity to the gap considering the height (h), see Equation 2-9. The linear velocity is the proportional result of angular velocity (ω) and the radius (r)(McKennell 1954).

Equation 2-9

$$D = \frac{\omega\,r}{h}$$

Cone-and-plate as high throughput system?

The cone-and-plate device allows uniform and constant flow patterns and is therefore particularly suitable for the application of defined shear stress to endothelial cells (Nagel *et al*. 1994). In addition the system allows the application of specific atheroprotective and atheroprone wave forms for physiological flow applications (O'Keeffe et al. 2009a).

However, most cone-and-plate devices are made for large-scale viscosity measurements and therefore are not customisable. In addition the shear rate is highly dependent on the correct positioning of the cone insert, thus the usage of this device requires a certain degree of technical skills (Buschmann *et al*. 2005). This makes the cone-and-plate device a user-unfriendly and low throughput system.

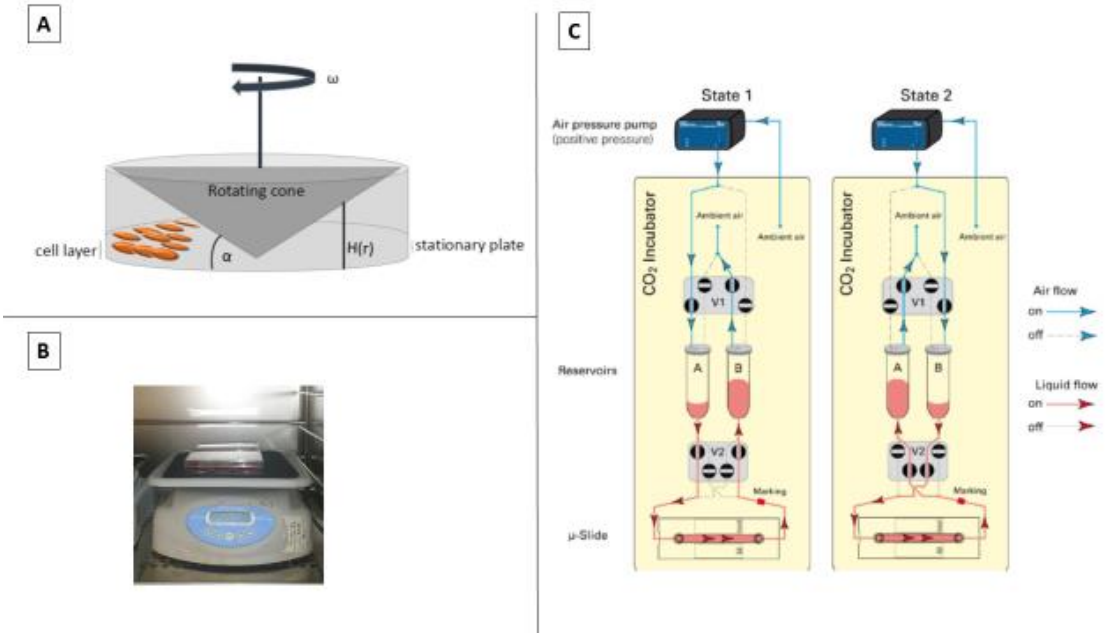

Figure 2-9 Existing in vitro systems for cellular flow exposure

To investigate the cell response to shear stress, in vitro systems have been developed. The most established systems are shown in this figure.

(A) Cone-and-plate device: Cells are seeded on the stationary plate and the shear is created by the rotating cone. For mathematical determination of shear rate and Reynolds number the angel (α), angular velocity (ω), height (H) and radius (r), play an important role.

(B) The Orbital shaker is placed in an incubator, providing optimal cell culture conditions, whilst applying orbiting movement and therefore creating the shearing force in a tissue culture 6-well-plate.

(C) Microfluidics (Kroutvar and Guttenberg, 2013; with permission from ibidi GmbH) The ibidi system consists of three elements, pump, fluidic unit and pump control. Flow is created with an air pressure pump, which is fully controllable with the pump control software. With help of two medium containing reservoirs, flow is created moving the medium in the reservoirs through air flow. Reservoirs and slide are connected with a perfusion set. The fluidic unit, holding reservoirs, perfusion set and slide, is placed inside of the incubator.

2.9 Principal idea of this project's novel device

Flow can be generated through pumping or shaking however, another possibility to create flow is via stirring. Each well could function as a medium reservoir itself by placing an individual stirrer in each well. Consequently, cells in each well are exposed to its own cell culture media only and therefore each well can be considered as individual sample number.

The cell culture media movement will generate the shearing force to the cells and the media movement can be achieved by rotating the stirrer. The possibility of moving the stirrers with one big motor controlling all 96 stirrers with help of a gearing system to equip 96 mini motors with stirrers on the motor's shaft was considered. However, those set-ups might be too complicated and may also result in a very user-/biologist-unfriendly device.

The project's device will use magnetic forces to move the stirrers. Thereby a magnetic field is created from moving magnets placed underneath the stirrers. In order to make the stirrers receptive to this magnetic field the magnetic stirrer itself will also be equipped with a magnet. Subsequently, the stirrers in the well plate shall move and follow the magnetic field transmitted from the moving magnets. This way the moving energy will be transmitted to the stirrers via a wireless magnetic field which will create a user-friendly approach.

However, cells cultured on the bottom of the well need to be protected from the moving stirrer itself, otherwise cells would simply be sheared off by the stirrer. Therefore, the stirrers will be mounted in a reusable lid which will allow a gap between the bottom of the well and the stirrer. In order to reduce friction and guarantee a smooth stirrer motion, the stirrer's are joined in a ball bearing which itself is mounted in the lid.

Sample number and throughput

Standard tissue culture well plates are available as 6, 12, 24, 96 and 396-well plate formats. Since a higher throughput system is aimed to be achieved 6, 12 and 24-well plates have not been further considered for this project; although the principal idea of the proposed device shall be applicable for other well formats. However, with the principal idea of creating flow in a single well via stirring a certain sized stirrer needs to be built. Therefore, 396-well plates have been excluded from further considerations, since it

would be very challenging task to build and design a stirrer to fit such small wells. For this project it was decided to work with a 96-well plate system. With 96 wells a much higher throughput will be achieved than is currently possible with any other flow devices at present. The surface of the wells is smaller than of most of currently used plates or wells; thus the 96-well format will be much more cost efficient since less reagents are needed for cell manipulations, e.g. siRNA or antibodies. Furthermore, the 96-well format is compatible with plate readers, which can be found in every life science laboratory. Due to the device's compatibility with plate readers it will be ideal to use for fluorescent *in situ* staining.

Nomenclature of the novel device

Whilst working on this project individual parts of the novel device have been named and established in the laboratory jargon, with collaborators from the University of Sheffield as well as those new nomenclatures have been used in presentations and abstracts. Therefore specific nomenclature relating to the device described in this dissertation are going to be explained in this section.

The device consists of three parts: Lid, stirrer's in the wells and a moving magnet. However, when communicating about the device, distinguishing between magnets of the stirrer's and the moving magnet has been an issue. In particular during the early stage of prototyping a magnetic stirrer was used for the moving magnet part whilst also prototyping the stirrers placed in the wells which are equipped with a magnet. Thus, whilst prototyping two separate parts it was suboptimal to refer to one part as stirrer magnet or magnetic stirrer. Therefore it has happened that the stirrer's placed in the wells were named Mörs stirrers. Mörs is the author's and inventors surname, whereby the original umlaut ö is replaced with oe by convention. Nonetheless, the ö's (œ) phonetic is identical to the "i" of stirrer and therefore the combination "Mörs stirrers" creates a harmonic tone colour.

Therefore, Mörs stirrers refer to stirrers equipped with magnets which are placed in the well plate, whereas laboratory magnetic stirrer refers to the moving magnet. However, an optimised prototype for this part of the device was renamed in large rotating magnet (LRM).

The jargon has further developed and the term Mörs stirrers is now used when referring to the overall system.

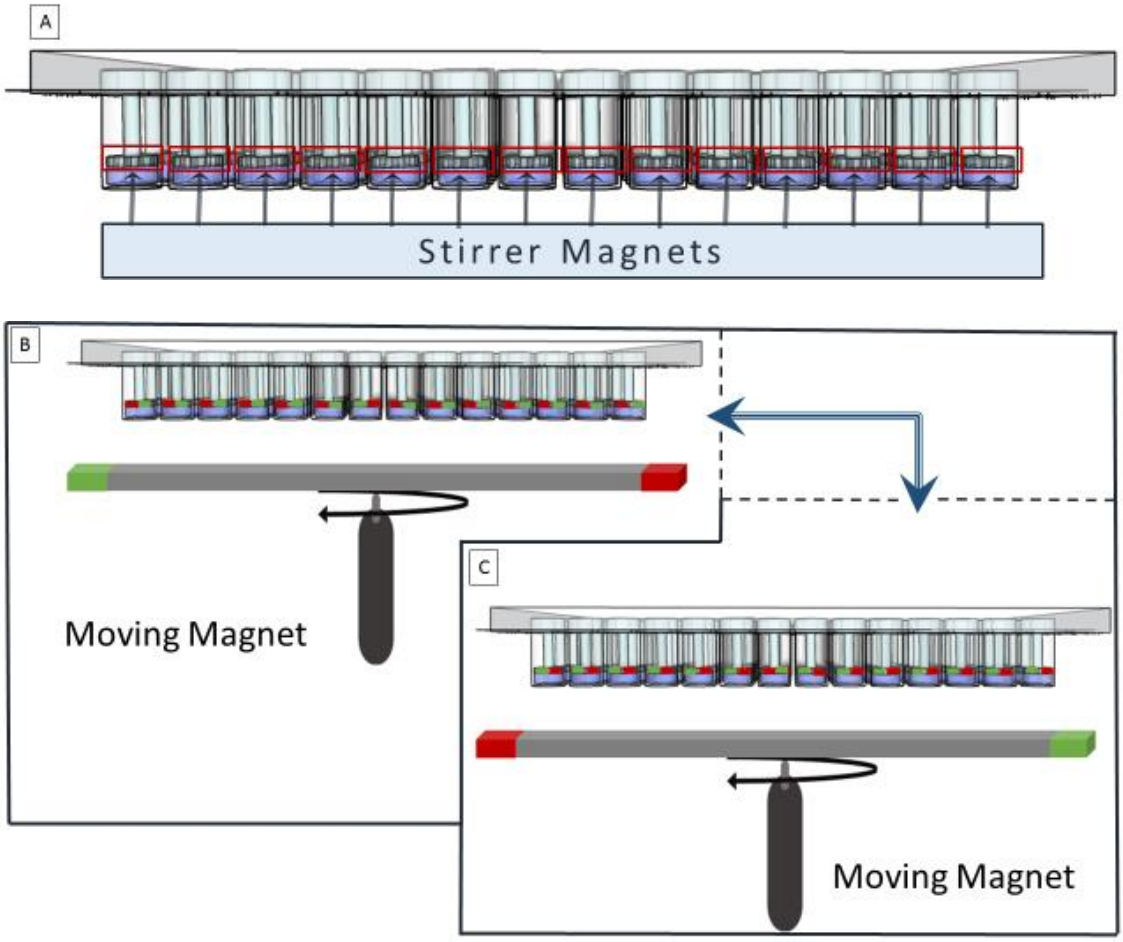

Figure 2-10 Mörs stirrers Working principal

(A) Mörs stirrers are individually equipped with a magnet and placed in a cell culture well plate. (B and C) The magnetic field of the moving magnet is achieved by opposing polarities of a magnet (shown in red and green). In order to achieve a moving magnetic field, the magnet requires an attachment to an axially moving element. Consequently, the magnetic field is transmitted to the magnets of the Mörs stirrers which shall adapt to the magnetic field. However, when the magnet moves, the transmitted magnetic field is constantly changing. This shall result in the continuous adaptation of the magnetic configuration of the Mörs stirrers. This adaption shall result in the horizontal stirring motion of the Mörs stirrer movement which is enabled through the attachment to the ball bearing mobile ring.

3 Material and Methods

Due to the interdisciplinary nature of this project, the material and methods chapter is split in in Engineering and Biological based content.

3.1 Engineering

3.1.1 Electronics

Electronics is the science of controlling electronic circuits and was used in this project to control certain parts of the novel device. The utilised electronic elements for this project are electronic circuits, microcontroller, programming and PWM and which are going to be explained in more detail in this section.

If not stated otherwise, all electronic components used in this project were purchased from the Arduino starter kit (SmartProjects, Italy).

Controller board

In order to control electronic components and circuits the Arduino Uno was used. This single board micro controller is an open source hard- and software project, designed to provide inexpensive and easy usage.

This single board micro controller runs with the Arduino firmware, communicating with a computer via USB. The most suitable application is to control connected components and sensors by assembling electronic circuits using a bread board, circuit components and software programming.

Electronic Circuits

Electricity is generated through electrons and can be either static or current. Static electricity is generated when electric charge is built up without electron movement. When electrons in this confirmation are re-arranged, a discharge of electrical energy may occur; for example, thunderstorm lightning. Contrarily, most human made electrical devices, e.g. mobile phones or drilling machines are based on current electricity which is based on moving or flowing electrons. Thereby, in an electric circuit, electricity flows from the higher potential energy to the lowest potential energy. The higher potential energy is referred as “+”, and the lowest potential energy as “–” or ground (GND). The ground is defined as zero potential, and therefore 0 volts. Within the circuit any voltages will be measured referring to the ground.

The strengths of current electricity and therefore its electron flow can be determined by Ohms law. Ohms law states that current flow is directly proportional to the input voltage and the amount of resistance within the circuit. In order to determine the current flow within an electronic circuit a voltmeter was used (Voltcraft VC135).

Bread board

A device for assembling electric circuits has been invented by Cruz Ruben in 1964. The so called bread board is a construction base to build circuits via conductive metal strips. The bus strips are vertically aligned and provide power to the electronic components. Besides the power supply strip there is one strip to ground the circuit. The terminal strips hold the electronic components. The circuit is built with jumper wires, connecting the electric components and the bus- and terminal strips.

Circuit components

A power supply is needed to provide the bread board with power; this can be either a battery or a direct supply via the wall socket. A jumper cable usually connects the bus- with the terminal strips on the bread board. Thereby a jumper cable is usually made of metal and therefore allows electrons to flow from one electronic component to another one. A jumper wire can therefore be described as an electron bridge between different components. Depending on the thickness of the jumper wire more or less electrons can travel through it. A thicker jumper wire consists of more metal wires compared to thin jumper wires. Therefore thin jumper wires have less capacity to transport electrons, whereas thick jumper cables have more capacity.

Capacitor and Resistor

Capacitors and resistors work in the opposite way and can be used to control an electronic circuit. A resistor converts electrical energy into heat and therefore resists electrical energy. The application of resistors is to reduce the current input for a downstream circuit element. The desired amount of resistance is chosen depending on the electrical component within the circuit. A potentiometer works as a variable resistor whereas a capacitor stores electrical energy from the circuit's power supply. The stored energy can be released back into the circuit if needed. Therefore a capacitor is used when the 5 V power from the microcontroller board is insufficient for an electrical component in the circuit.

H-Bridge (L293D) bidirectional drive

H-bridges are integrated circuits (IC) and able to control the motor's direction. To change the motor's direction a switch is needed. The L293D, used in this project, is made out of 16 pins. The respective number of the pins can be identified by the U-shape on top of the H-Bridge. The H-Bridge resembles a letter H, with four switches on the vertical line and the motor on the horizontal line. In case of: S1 and S4 are closed and S3 and S2 are open the motor's motion will be clockwise, whereas when S1 and S4 are open and S3 andS2 are closed the motor's motion will be counter clockwise. Opening another switch will stop the current flow, resulting in a motor stop.

Open S1 and S2 and closed S3 and S4 should be avoided. This results in a very high current, and leads to overheating. The same occurs if S3 and S4 are open and S1 and S2 are closed.

Table 3-1 H-bridge switch configuration

Function	**S1**	**S2**	**S3**	**S4**
Stop Motor	1	0	0	0
Stop Motor	0	1	0	0
Stop Motor	0	0	1	0
Stop Motor	0	0	0	1
High current	1	1	0	0
Stop Motor	1	0	1	0
Clockwise	1	0	0	1
Counter clockwise	0	1	1	0
Stop Motor	0	1	0	1
High Current	0	0	1	1

Alternating Current (AC) and Digital Current (DC)

Alternating current changes the electricity direction, therefore the output is sinusoidal, e.g. from a wall socket. Contrarily to digital current, which is constant unidirectional, e.g. from a battery.

Pulse Width Modulation (PWM)

Pulse Width Modulation is a technique to change the constant unidirectional electricity direction from a DC source to an analog-like behaviour. PWM provides full voltage power for a specific time. 100% PWM means full voltage power over time. 50% PWM only provides a train of full voltage pulses for half of the time. The voltage pulses (τ_0) which are repeated over time (τ_c) are called duty cycle. The regulated effective output voltage (V_{eff}) is a result of the input voltage and the duty cycle.

The PWM signal itself is usually received, converted and amplified by a transistor. However, in principal it is also possible to control the constant voltage with a resistor, or if a variable voltage is needed, with a potentiometer. However the optional range is limited for this application. Furthermore, resistors convert electrical energy into heat, which might result in overheating the system. With the affordable PWM it is much more practical to control the power output and was therefore used in this project.

Arduino motor shield

The Arduino motor shield is an extension module, consisting of the same pin configuration as the Arduino and can therefore be mounted on top of the Arduino. This controller board allows the control of direction and speed of two DC motors in parallel.

Programming

The Arduino is controllable with its own programming firmware and supports Java, C and C++ programming languages. The Arduino programming language can be divided into three main parts: structure, values and functions. The basic programming language consists of a “setup” and “loop”. In the “Setup” the language is prepared and the “loop” is the execution. The “setup” is used to name the used Pins and configure them as “input” or “output” pinMode. “input” are constantly switched on and in a high impedance state, whereas “output” are switched on, on demand. Therefore “output” pinMode are in a low impedance state.

3.1.2 Magnets and magnetic strengths measurement

A magnet is an object that transmits an external magnetic field around it. This field attracts certain materials, predominantly iron, steel, nickel and cobalt. It can be distinguished between three types of magnets: permanent-, temporary- and electromagnets. Permanent magnets produce their own magnetic field, caused by the magnetised material whereas temporary magnets are magnetised by an external magnetic field. Therefore, temporary magnets are going to lose their magnetism in the absence of an external magnetic field. The magnetic field produced by an electromagnet finds it origin in the flow of an electric current. Typically, an electric current runs through a coil of copper wire, which creates the magnetic field. However, when the electric current flow is stopped the coils become nonmagnetic immediately. A list of the magnets used for this project can be found in Table 3-2.

Magnetic strengths were determined with help of a gaussmeter. The gaussmeter functions on the basis of the Hall effect and contains a thin film of Hall probe, which is then placed in the magnetic field. The SI unit of magnetic field strength is Tesla.

Table 3-2 Magnet's used for this project

Magnet	**Supplier**	**Product Code**
2mm dia x 2mm thick N42 Neodymium Magnet	MAGNET Expert Ltd	F412-25
2mm dia x 1mm thick	MAGNET Expert Ltd	F321SC-50
1mm dia x 1mm thick N42 Neodymium Magnet	MAGNET Expert Ltd	F305-100
6mm O.D x 3mm I.D x 1mm thick Diametrically Magnetised N42 Neodymium Magnet	MAGNET Expert Ltd	SP631DM-10
130mm x 8 x 5mm thick N42 Neodymium Magnet	MAGNET Expert Ltd	F13085

3.1.3 Motor and Motor control

A motor is a device which converts electrical energy into mechanical energy. Consequently, we can control the mechanical energy output directly by controlling the input electrical energy. The motor used in this project was purchased from Polulo, product code: 1103.

H-bridges are equipped with current sensors and are able to change the direction of motor movement (clockwise or anti-clockwise) by switching to the opposite voltage. With help of pulse width modulation (PWM), which is built in the Arduino microcontroller, it is possible to control the motor speed. In the completed circuit PWM is also used to control the H-bridge.

3.1.4 Bearing

Bearings are machine elements that allow parts to move in connection with each other. In order to reduce frictional power loss bearings are widely used to precise mechanical movements. Different types of bearing designs have their own application and limitations

Contact bearings, used in this project, have mechanical contact between the parts, which limits the life span. The mechanical contact can be conducted via sliding or rolling. Rolling element bearings are built of two rings, rollers and a cage. The rolling friction of these bearings is much lesser than the sliding friction, due to the reduced contact area. Axial force is applied parallel to the shaft whereas the radial force is applied upright to the shaft. The bearing used is dependent on the applied load. Ball bearings and other rolling elements support both radial and axial load. Deep groove ball- and needle bearings are commonly used to support radial load.

The ball bearings used in this project were closed modelcraft miniature ball bearings 7 mm OD, 2 mm bore and 3 mm width (Rapid electronics, England) and metal shielded stainless flanged deep bearing 7 mm OD, 2 mm bore and 4 mm width (simply bearings, England).

3.1.5 Manufacturing

3D print

In this work the Object Eden260V 3D printer was used, along the resins Fullcore 840 VeroBlue, Fullcore 870 VeroBlack and Fullcure 705 Universal Support as supportive resin. The Objet Eden 260V was chosen since it prints 0.016mm thick layers, and is therefore suitable for small and precise printings.

3D printing is an additive manufacturing method to make a solid three dimensional object from a digital origin file. A 3D print works by adding successive layers of material on top of each other until the entire object is manufactured. Thereby every layer can be described as an individual horizontal cross section of the 3D printed object.

The gross supporting material was removed by hand and then further removed by incubating in 10% NaOH (Sigma) for 12 hours. Subsequently the stirrers were thoroughly wiped off, washed with water and dried at RT.

Lithography

Polydimethylsiloxane (PDMS; Sylgard 184, Dow Corning Corp) was used for moulding purposes. PDMS is supplied with two components, the polymer mixture and the crosslinking agent, which were mixed in a ratio of 8:1. Both materials were manually mixed and fully degassed in a vacuum before moulding. After moulding the PDMS mould was dried at 100˚C for one hour and the mould was removed from its container. Alternatively, the mould was hardened at RT for several days when heat sensitive materials were involved.

3.1.6 Computer programs

CAD

The open-source software "SketchUp" was used to create the computer assisted design (CAD) drawings for the 3D print. In order to export CAD drawings in a 3D printer compatible format, a plug in was installed to export the file as ".stl"; abbreviation for STereoLithography. The stl format reduces the CAD file to the necessary features for the 3D print by describing only the geometrical surface properties of the object.

imageJ

imageJ was used to track movements. Therefore videos were recorded and then imported as greyscale into imageJ. The video is shown as stack and the frames are individually displayed after one other. The camera used (Canon, Power Shot A650) recorded 30 frames in one second.

3.2 Biological

3.2.1 Cell culture

Primary human umbilical vein endothelial cells (HUVECs) were used for this study. HUVEC isolation and culture are described in the following sections.

All cell culture work was performed in a laminar flow cabinet (Heraeus LaminAir, HBB1228) to guarantee aseptic working conditions. The laminar flow cabinet and all subsequently added objects were cleaned with 70% ethanol prior to each cell culture work. All reagents were stored in the fridge and warmed up prior to use. Cell culture plastics were coated with 1% gelatine (Sigma) to improve the cell attachment surface. Furthermore the cell morphology was examined using a light microscope (Zeiss) every day.

HUVEC cell culture

HUVECs were cultured in complete growth media (see Table 3-3) and were incubated at 37 °C and 5% CO_2 (Incubator: Leec, Touch 190 S). The media contains a colour coded pH indicator (phenol red); a yellow medium colour indicates an acidic pH whereas a pink medium colour indicates an alkaline environment. Fungal or bacterial infection as well as a de-regulated CO_2 transfer would lead to a pH change. Once HUVECs were confluent the cells were washed with PBS and then lifted off the flask using 1 ml trypsin

(Life Technologies). Trypsin was incubated for approximately 2-3 min in the incubator until detachment and were neutralised with 10 ml of growth media. Subsequently, cells were transferred in a 15 ml Falcon tube and centrifuged for 5 min at 1000 rpm. The supernatant was discarded and the cell pellet was re-suspended in growth media and seeded in desired cell culture plastic. For HUVEC amplification, 1x T75 flask was usually split in a 1:3 ratio and cells were used for experiments up to passage 4.

Table 3-3 cell culture media

Incomplete growth media	**Complete growth media**
500 ml M199 (Sigma) + 50 μM L-Glutamine (Gibco) + 2 U/mL Penicillin-Streptomycin (Gibco) + and 50 ng/mL Amphotericin B (PAA)	160 ml Incomplete media + 20 ml FCS (Life technologies) + 20 ml FBS (Life technologies) + 5 ng/mL endothelial cell growth factor (ECGF, Sigma-Aldrich) + 90 ng/mL Heparin (Sigma-Aldrich)

HUVEC isolation

HUVECs were isolated from fresh umbilical cords obtained from the maternity department at the Jessops Hospital, Sheffield. The umbilical cords were stored in Eagle's Minimal Essential Media (Sigma) at 4 °C until isolation procedure. The cord was cleaned with Azowipes (Cavenmount) to remove blood remains on the outside and at the same time cords were gently massaged to liberate blood remaining's in the vein. The vein then was cannulated with a 14G intravenous cannula (SML Sentra Medical Ltd) and washed through with incomplete media until the media was free of any visible blood contamination. After the blood remains were cleaned, the cord was secured with a clamp on both end. The vein was then infused with collagenase (Roche, 0.5 mg/ml) in M199 and incubated for 15 mins at RT. To optimise the EC yield the cord was gently massaged for a few minutes whilst collagenase incubation. After incubation the collagenase-cell mixture was collected. The cord then was flushed through with incomplete media to further optimise the EC yield. HUVECs were then centrifuged for 5 min, 1000 rpm at RT. The supernatant was discarded and the cell pellet was re-suspended in 10 ml complete growth media and plated on a gelatinised T75 cell culture flask. 24 hours later

the media was changed to remove red blood cells and cell debris. HUVECs were then kept in the cell culture incubator until reaching confluence.

3.2.2 EC *in vitro* flow experiments

Orbital shaker

For flow studies HUVECs were cultured as confluent monolayers in a tissue culture 6 well plate. The cells were washed with PBS (Sigma) and precisely 3 ml of complete growth media were added to each well. The 6 well tissue culture plate was then put on the orbital shaker (Grant-Bio PSU-10i) in the cell culture incubator. Cells were then orbited at 210 rpm for 72 h. After 72 h the cell morphology was examined under the light microscope. Subsequently the cells were washed twice with ice-cold PBS (Sigma). The 6 well plate was then placed onto a shear stress map, which specifies flow regions created by the orbital shaker. Cells were harvested by scraping the desired flow regions using the rubber end of a 1ml syringe piston (BD). Cells were then transferred in a 15 ml Falcon tube and centrifuged for 5 min at 1500 rpm.

Mörs stirrers

The application of flow to cultures of HUVECs using the Mörs stirrers is described in the respective sections of this report, since cell culture conditions, materials and application times were changed during the prototyping process.

Biocompatibility tests

Biocompatibility tests were run with cultured HUVECs for 6h in the cell culture incubator. The tested materials were added to the cell culture medium and after 6 h or 24 h the cell morphology was examined. For further transcriptional analysis the cell culture media was removed and the cells were washed with ice cold PBS. Subsequently, the PBS was removed and the tissue culture plate was flash frozen on dry ice. The plates were then stored in a -80˚C freezer until RNA isolation.

RNA isolation from cultured HUVEC

For RNA isolation of cell pellets from 6 well plates, the cell pellets were suspended in 300 µl RLT buffer (Qiagen) supplemented with β-mercaptoethanol (10 µl/ml). Given the small surface area of a 96 well plate 50 µl RLT buffer (Qiagen), was added to 1x 96 well directly. Cells were lysed off the bottom of the well by pipetting the lysis buffer with

much power directly on the cells. In order to increase the RNA yield, cells harvested from 10x 96 wells were pooled.

This lysate was then homogenised by passing 10x through a 21 G needle and syringe (BD). Afterwards an equal volume of ethanol (70% (v/v), Sigma) was added and mixed though by gentle pipetting. The Qiagen RNaesy MiniKit was then used for total RNA isolation following the manufacturer's instructions. In the final step, the RNA was eluted using 30µl RNase –free water (Qiagen). The RNA concentration was measured with a NanoDrop-1000 using 1.5 µl of the isolated RNA. The absorbance at wavelengths 260 nm in relation to the absorbance at 280nm indicates the RNA purity. Only 260/280 ratios of 1.8 – 2.0 were used for further experiments.

The isolated RNA samples were stored for short term purposes at -20˚C and for long term storage in the -80˚C freezer.

cDNA synthesis

Following RNA isolation a cDNA synthesis Kit (BioRad) was used to convert RNA into cDNA. The cDNA synthesis kit was used following the manufacturer's instructions.

5 µl of 5x iScript Reaction Mix and 1 µl of iScript Reverse Transcriptase were added to a 200 µl plastic tube. The RNA template was normalised to the same appropriate quantity among all samples and was added to the tube. Nuclease free water was used to equalise the volumes of all sampled to 25 µl. The samples were incubated at 25°C for 5 minutes, followed by an incubation at 42°C for 30 minutes and then at 85°C for 5 minutes (Applied Biosystems, Verity, 96 well Thermal Cycler); cDNA samples were stored in the refrigerator until further use.

Quantitative real-time Polymerase Chain Reaction (qPCR)

qPCR is a technique that is able to simultaneously amplify and detect the cDNA template. For this purpose the highly sensitive dye SYBR Green is used which binds to double stranded DNA only. Therefore newly synthesised DNA strands are bound by SYBR green, which results in an increase of fluorescent intensity that is consequently proportional to the PCR quantity. Hence, with help of qPCR we are able to compare mRNA transcripts with each other.

SsoAdvanced SYBR Green Supermix (BioRad) was used following manufacturer's instructions. The qPCR reactions were run in 384 well plate using a reaction volume of 10 µl. Forward and reverse primers were used at a final concentration of 4 µM. Each sample was replicated in triplicate. The reaction was initiated for 3 min at 95°C, followed

by up to 60 amplification cycles of 5 seconds at 95°C and 30 sec and 60°C. Following the qPCR run, primer dissociation curves were plotted, in order to produce a melt curve for each primer pair. Melt curves were then examined if primer dimers or non-specific specific amplification were present which would appear as a secondary peak of the melt curve. Furthermore, Primer efficiency was tested by analysing amplification plots to make sure that the amount PCR product doubled with each amplification cycle. Therefore different primer concentrations per primer pair were tested.

Hypoxanthineguanine phosphoribosyltransferase (HPRT) expression was used as housekeeping gene, since HPRT's gene expression is not changed due to shear stress application. Relative gene expression was then calculated by relating the amount of cycles which were necessary to produce a threshold amount of product. The CT of HPRT was then subtracted of the each individual samples CT, this value is called ΔCT. This calculation also normalises the initial RNA quantity. The relative expressions of genes of interest from different samples were then compared using the 2- ΔΔCT method.

Primer design

Primers were designed to contain a minimum of 60% Guanine and Cytosine and the template lengths was chosen to be between 18-21 base pairs (Table 3-4).

Table 3-4 Primer targeting human genes

hMKP1 F	5' - CAGCTGCTGCAGTTTGAGTC
hMKP1 R	5' - AGGTAGCTCAGCGCACTGTT
hNrf2 F	5' - TACTCCCAGGTTGCCCACA
hNRF2 R	5' - CATCTACAAACGGGAATGTCT
hJNK1 F	5' - GAAGCTCCACCACCAAAGAT
hJNK1 R	5'- GGTTCTCTCCTCCAAGTCCA
hp53 F	5' - GCCCCCAGGAGCACTA
hp53 R	5' - GGGAGAGGAGCTGGTGTTG
hnf-kb F	5' -TCAAGATCTGCCGAGTGAAC

hnf-kb R	5'- TGTCCTCTTTCTGCAACCTTG
hKlf2 F	5' -GCACGCACACAGGYGAGAAG
hKlf2 R	5'- ACCAGTCACAGTTTGGGAGGG
hMCP1 F	5'-GCAGAAGTGGGTTCAGGATT
hMCP1 R	5'- TGGGTTGTGGAGTGAGTGTT
h e-selectin F	5'- GCTCTGCAGCTCGGACAT
h e-selectin R	5' - GAAAGTCCAGCTACCAAGGA
h eNOS F	5'- TGAAGCACCTGGAGAATGAG
h eNOS R	5'- TTGACCATCTCCTGATGGAA
h c-Jun F	5'-CAGCCCACTGAGAAGTCAAA
h c-Jun R	5'- CACCAATTCCTGCTTTGAGA

Immunofluorescence staining

HUVECs were cultures onto gelatine coated 96 well plates and were fixed after flow application using 50 µl of 4% PFA (VWR). Subsequently cells were permeabilised for 15 min using 70 µl of 0.1% TritonX (Sigma) at RT. Afterwards non-specific antibody binding was blocked using 50 µl of 20% (v/v) goat serum (Sigma) incubating at RT for 30 min. VE- Cadherin primary antibody (BD Biosciences 555661) was diluted in 5% (v/v) goat serum (Sigma) to a final working dilution of 5 µg/ml. 50 µl per well was used for an o.n. incubation at 4°C. The primary antibody was then aspirated and the cells were washed with PBS (Sigma). The cells were then incubated with the secondary antibody for 1h at RT in the dark whilst shaking. Subsequently the cells were washed three times in five-minute intervals with PBS at room temperature. DAPI was used for counterstaining at a concentration of 4 µg/ml, incubated for 15 min at RT. Afterwards the cells were washed three times in five-minute intervals with DNase free water (Sigma) at RT. The cell culture plates were stored light protected at 4°C until microscopy was carried out.

Microscopy

Phase contrast microscopy to examine the cell morphology was carried out using Nikon eclipse Ti. Fluorescence microscopy of immunofluorescent stained cells were performed using Leica AF600LX inverted microscope.

4 Mörs stirrer

4.1 Introduction

The Mörs stirrers will create the media movement which will consequently create the shearing force on the cells cultured on the bottom of the plate. Therefore the Mörs stirrers will be designed to fit in one single well of a 96 well plate. In order to hold the stirrer above the bottom of the well the stirrer needs to be mounted on top of the plate. However, due to the circular movement of the stirring motion the moving part of the stirrer will create friction on the static mounting part. Friction would reduce a smooth and uniform movement of the stirrer. Furthermore, it would cause material wear. To overcome frictional forces a ball bearing was used to attach the moving stirrer with the static lid and thereby generate a smooth movement of the stirrer.

The Mörs stirrer therefore consists of basically three elements: a magnet, the stirrer skeleton and a ball bearing. First stirrer prototypes were made of an acrylic rod and a bar- or disc magnet, using a hotplate to melt the acrylic material and glue it on the bar magnet. In another attempt a pencil sharpener was used to fit the acrylic rod in the magnetic disc and ball bearing.

Mörs stirrer – magnet

The magnet for the Mörs stirrer chosen to fit the stirrer's tip had with an O.D. of 6 mm and an I.D. of 3 mm. The stirrer's shaft diameter was designed accordingly. The chosen magnet is a Neodymium magnet which is diametrically magnetised allowing the magnet to move within in a vertical direction within the magnetic field.

Mörs stirrer – shape and design

The stirrers shape and design had to meet certain requirements. Firstly, the stirrer was designed to fit a single well of a 96 well plate. Secondly, the stirrer should have attachment sites for the magnet and the ball bearing. Thirdly, the stirrer shape should create a uniform fluid motion.

The diameter of a 96 well is 6.96 mm therefore, the stirrer tip was designed with a 6 mm diameter, in order to use most of the bottoms surface for cell culture. With a stirrer tip diameter of 6 mm, 86% of the 96 well's the surface is going to be covered. However, it would not be possible to use 100% of the surface and design the stirrers tip diameter to be 6.96 mm, since the stirrer would then collide against the well wall. Furthermore the region below the stirrer's mid-point is considered as a no flow region. This would cause an interruption of the stirrer's movement and would result in a non-uniform fluids motion. Therefore the stirrer's tip was designed with a tolerance of 0.49 mm to the outer well wall.

In order to generate reliable and reproducible data, the fluids motion during the measuring period should be as uniform as possible. Previous research of rheometer has indicated that various factors have a positive effect on the fluids motion. Rheometers are based on the cone and plate principal (see section 2.8.3). However, the principal of the cone and plate will be used for the design of the stirrers. In this analogy the stationary plate could be equated with the bottom of the well plate, and the rotating cone could be equated with the stirrer in the well.

Spruell and Baker (2013) investigated the fluid motion in a 96 well plate using a rotating cone. In detail this research shows that two factors greatly have an impact on the fluid motion; firstly, the shape of the cone, in particular the angle and secondly, the gap height between stationary plate and rotating cone. Both factors will be discussed in more detail in the following sections.

Cone angle

A number of studies have reported that a low angle cone creates a more uniform fluid motion (Voyvodic *et al.* 2012). Whilst the rotating cone moves axial centrifugation forces are developing, which causes a non-linear fluid movement across the surface. The low angle canonical formed tip linearises those centrifugation forces, and thereby creates uniform fluids motion, therefore the stirrers were designed with a 2˚ degree cone. The middle point of the stirrer will be the lowest point, and the 2˚ angle arises towards the stirrer's edge. Therefore, the stirrer's edge will be 0.105 mm higher than the mid-point of the stirrer.

Gap height

The gap height greatly influences the fluid motion which is already implicated in the equation for shear rate. The shear rate is a result of the angular velocity multiplied by the

fluid viscosity divided by the height. Consequently, the shear rate will be higher with a smaller height given a constant angular velocity. And *vice versa*, the greater the height the lower the shear rate. Several studies have estimated the optimal gap height of the cone and plate device, and came to the conclusion that a uniform flow motion is achieved with a zero gap (Bataineh 2014; Spruell & Baker 2013). This means that the rotating cone sits on the stationary plate. However, a zero gap would not be possible, since adherent cells will be grown on the bottom of the well. Therefore a gap height of 100 µm was chosen, which will allow the media to flow beneath and create the fluids motion across the cells.

With a well height of 10.9 mm the stirrer tip length was designed to be 2 mm long. The addition of the conical tip adds another 0.105 mm at the stirrers tip mid-point. Therefore, the stirrer's shaft lengths was chosen to be 8.794 mm long; taken together the stirrer tip (including cone) and the stirrer's shaft is 10.8 mm long. In theory this should create the 100 µm gap between stirrer and bottom of the well.

4.2 Results

4.2.1 Prototype 1 – Acrylic Rod

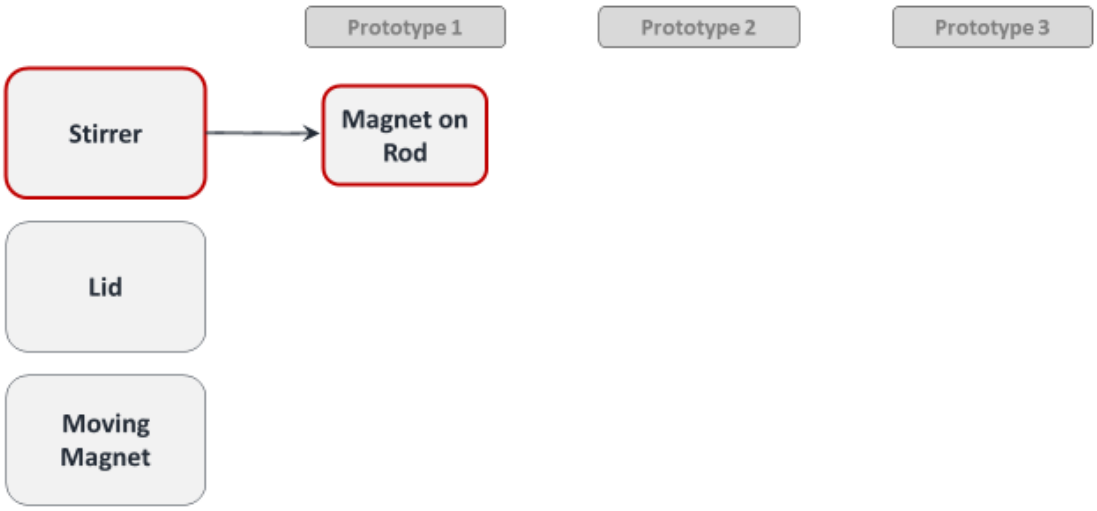

The first stirrer's prototyped had an acrylic rod on which the magnet and the ball bearing was attached. This was achieved by manually cutting the acrylic rod with a scalpel or a pencil sharpener or by melting the acrylic material in the magnet and ball bearing, see Figure 4-1.

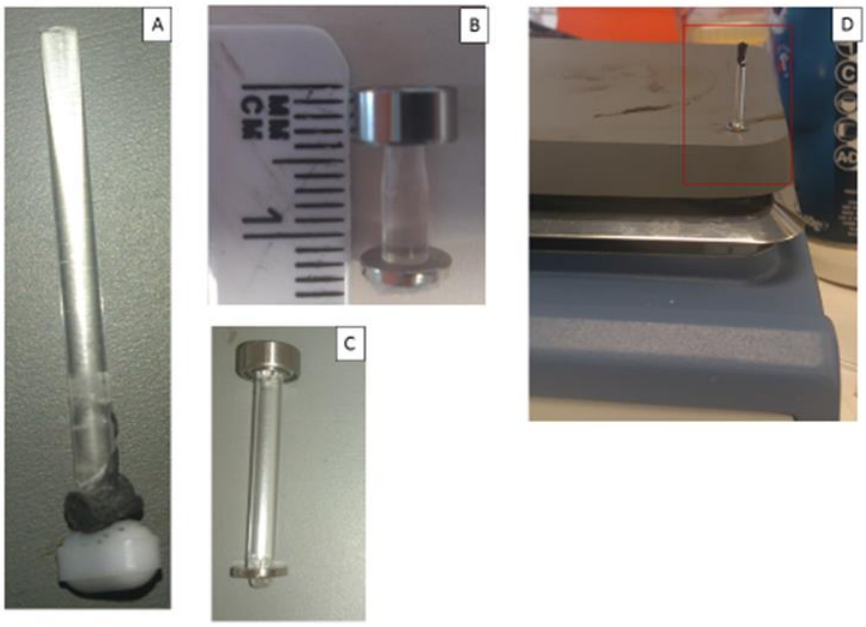

Figure 4-1 Mörs *stirrer Prototype 1 – Magnet attached to acrylic rod*

This figure illustrates different attempts of building prototype 1 Mörs stirrers. Panel A shows the very first attempt to melt an acrylic rod to a 6 mm long bar magnet. Further building attempts followed by using a pencil sharpener in order to fit the acrylic rod on a magnetic disc as well as in the ball bearing, as shown in panels B and C. In addition it was attempted to melt the acrylic stick in the magnet and the ball bearing, see panel D. Acrylic has a melting point of 160˚C therefore a laboratory hotplate was used to reach this melting point. Ideally, the acrylic material would melt and whilst hardening attach the magnetic disc on it.

Overall, the stirrers showed functionality in regard to rotational movement when exposed to an external magnetic field. However, the prototype 1 Mörs stirrer lacked an accurate build as well as reproducibility.

4.2.1.1 Result and Troubleshoot

The main limitation of the Mörs stirrers of prototype 1 is the poor reproducibility. Firstly, the acrylic material is a very strong and hard material and it is therefore a non-trivial challenge to cut or sharpen the attachment sides in a uniform way (Kishi et al. 2017). Secondly, the melting attempt was difficult to perform, since the acryl started to melt but does not change into the liquid phase at 160°C (Zhanhai et al. 2002). Both attempts were on the one hand difficult to manufacture and on the other hand did not meet the precise demands of the required stirrers.

4.2.2 Prototype 2 – 3D print

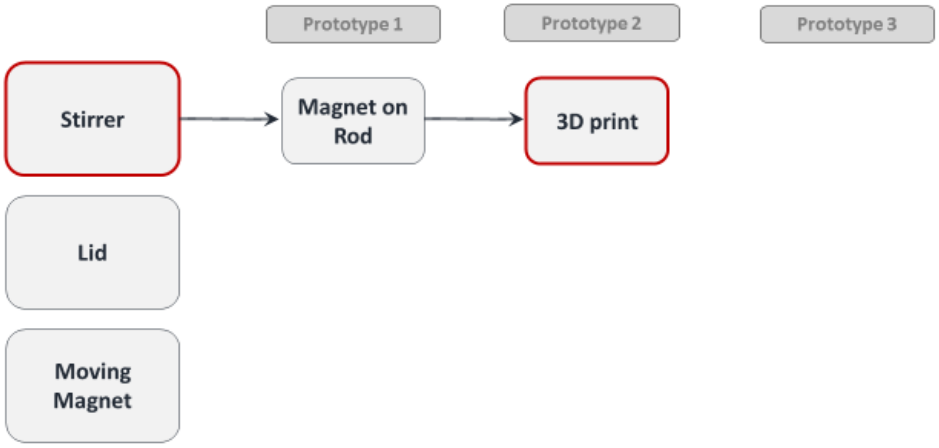

In order to address the reproducibility issues of the first stirrer prototype, it was decided to use 3D printing to manufacture the stirrers for the prototype. This way it was possible to produce identical stirrers which are designed to hold a 6 mm diametrically charged magnetic disc and to fit exactly in the bore of the ball bearing. With help of a CAD the stirrers were designed and subsequently printed. The supporting material was removed and the printing material tested for biocompatibility features. Furthermore, to remove excess material sodium hydroxide (NaOH) treatment was tested to see if a more refined structure could be produced and thereby enhance the biocompatibility of the supporting printing material. This method was suggested by Rua *et al*. 2015, investigating in the usage of 3D printed Microfluidics. Therefore the gross material of the 3D printed stirrers was removed and subsequently treated in a 10% (w/v) NaOH solution for 24 h at RT. HUVECs were cultured in 96 well plates until adherent, treated and untreated stirrers were mounted on a lid and placed in the cell culture media, without touching the bottom of the well. Cellular responses were investigated by qPCR testing inflammatory and apoptotic responsive genes, which itself were identified using results obtained from the orbital shaker system.

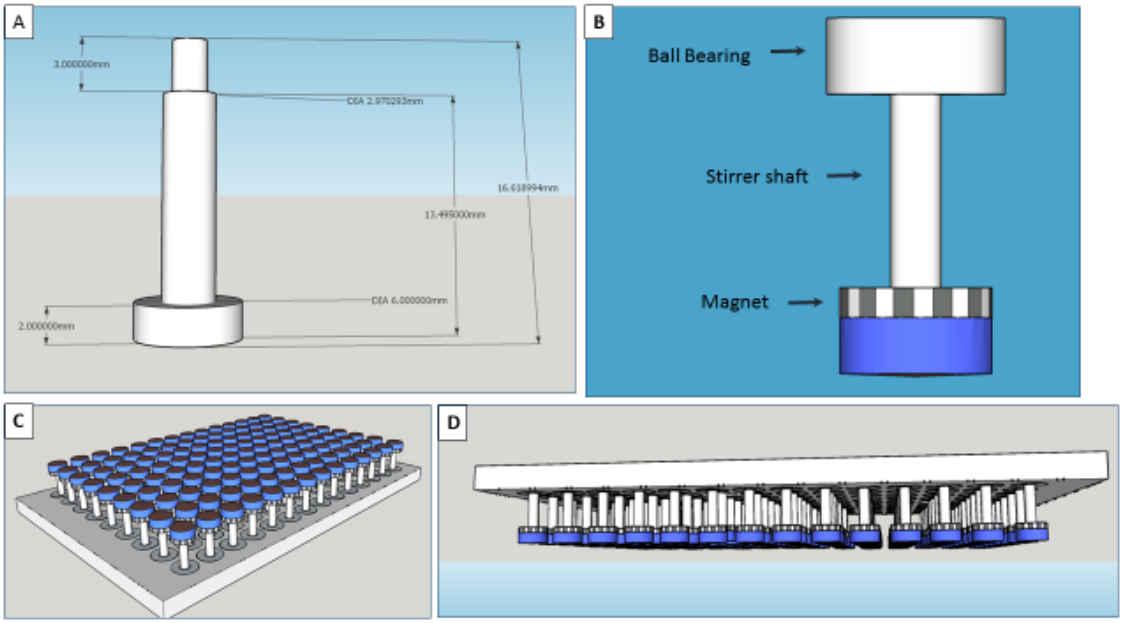

Figure 4-2 Mörs stirrers 2nd Prototype CAD drawing

The stirrer was designed using the CAD drawing program sketchup. This figure illustrates the design of a single stirrer (Panel A and Panel B) and the arrangement of 96 stirrers fitting a 96 well plate (Panel C and Panel D). A illustrates the digital origin for the 3D print including essential dimensions. The top of the stirrer is designed to fit a ball bearing whereas above the conical tip's top platform is designed to hold the magnet (Panel B). Overall the stirrer length and width is intended to fit in a standard 96 well plate. Therefore the aim is to fit 96 individual stirrers in a 96 well plate (Panel C and Panel D).

4.2.2.1 Result and troubleshoot

Gene selection for biocompatibility and flow experiments

In order to identify flow responsive genes for further experiments of this project, a qPCR analysis was performed using the well-established orbital shaker system. A set of possible genes was tested in order to select a set of four maximum responsive genes. Genes selected for further experiments are MCP1, e-selectin, eNOS and cJun (Chien 2003; Cicha *et al.* 2008). Genes selected will be used to test biocompatibility as well as flow application experiments performed in this project (see Figure 4-3).

Biocompatibility test of 3D printed stirrers

Figure 4-2 shows the CAD and the 3D printed stirrers with/without supporting material as well as an attached magnetic disc and ball bearing. The 3D printed stirrers were printed using two different resins. Firstly, the stirrer material resin itself, and secondly a supporting material resin. The supporting resin is needed for the 3D printing procedure in order to support the geometry of the stirrer in the printing process. A biocompatibility test was performed to test whether the 3D printed stirrers trigger a cellular response. Results obtained show that in particular the relative mRNA level of e-selectin and MCP1 are drastically increased, indicating an inflammatory response through the 3D printing material (Figure 4-4). In contrast the NaOH treated stirrer showed a reduced cellular response compared to untreated stirrer. However, comparing the NaOH treated and the control group, the stirrers still influence the cellular response.

The 3D printed stirrers were printed using two different resins. Firstly, the stirrer material resin itself, and secondly a supporting material resin. The supporting resin is needed for the 3D printing procedure in order to support the geometry of the stirrer in the printing process (Verhaar *et al.* 2015). However, it has been found that either one or both of those materials induce an inflammatory response in cultured HUVECs. In particular the mRNA level of e-selectin was greatly increased, indicating an inflammatory response through the 3D printing material (Pasceri *et al*. 2000). Furthermore, it was noted that the stirrers are very delicate and easily deformable after being in the incubator and the cell culture medium. This observation implies the material is suboptimal since this may change the

stirrers' dimensions and geometrical construction, and therefore a unique shear stress application in the 96 wells is not assured.

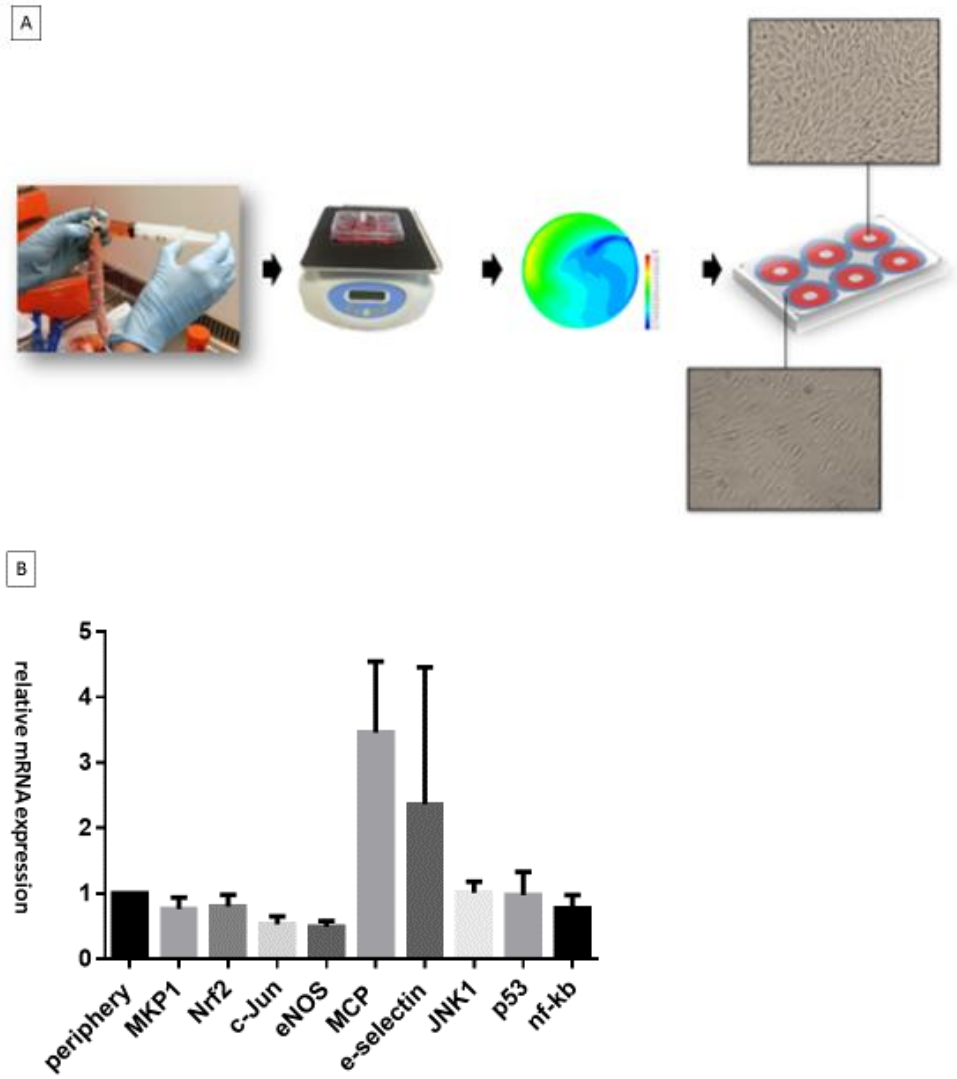

Figure 4-3 Flow application using the orbital shaker system

The figure shows the undertaken steps in order to identify the translational response of endothelial cells to flow. Panel A illustrates HUVECs isolation and afterwards being cultured in 6-well plates. Subsequently, the 6 well plate was placed on an orbital shaking plate and cells were exposed to orbital shaking at 210 rpm for 72 hours at 37 °C in a cell culture incubator. Cells were isolated from the centre of the well, which were exposed to disturbed flow patterns of low shear stress, and the periphery of the well, which were exposed to high shear stress.

Total RNA was isolated and the relative mRNA expression for a selection of genes was investigated by qPCR (Panel B). The experiment was performed using three different

donors, and cells exposed to low shear stress were normalised to cell from the high shear stress region.

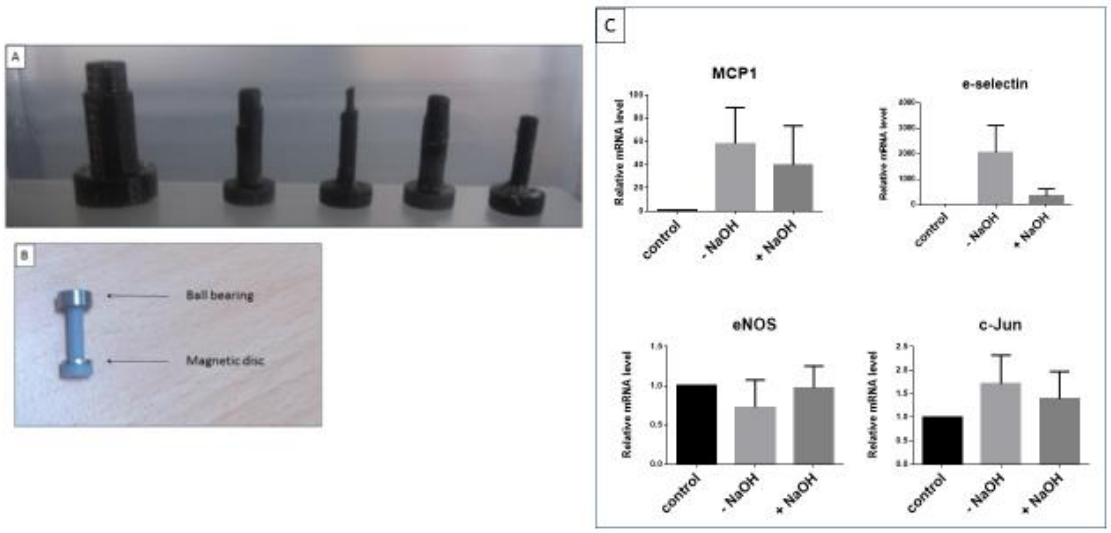

Figure 4-4 3D printed Mörs stirrers Biocompatibility

The figure shows 3D printed stirrers as well as biocompatibility features of selected genes.

Panel A: In order to meet the best tolerances to attach the ball bearing and the magnetic disc, several prints of optimisation have been performed. The ball bearing and the magnetic disc should have a tight grip on the printed stirrer.

Panel B shows the finished 3D printed stirrer with attached ball bearing and magnetic disc.

Shown in panel C is the biocompatibility result obtained from a qPCR screening for the genes MCP1, e-selectin, c-Jun and eNOS, normalised to cells cultured under static conditions. Supporting material of the 3D printed stirrers was removed manually or via the addition of NaOH solution for 24 h. HUVECs were cultured in 96 wells and stirrers were placed in the cell culture media for 6 h, followed by RNA isolation, cDNA synthesis and qPCR. qPCR results were analysed using ΔΔCT analysis and three different samples were run. The results shows that NaOH treatment reduces the cellular response of the selected genes.

4.2.3 Prototype 3 – manufactured stirrers

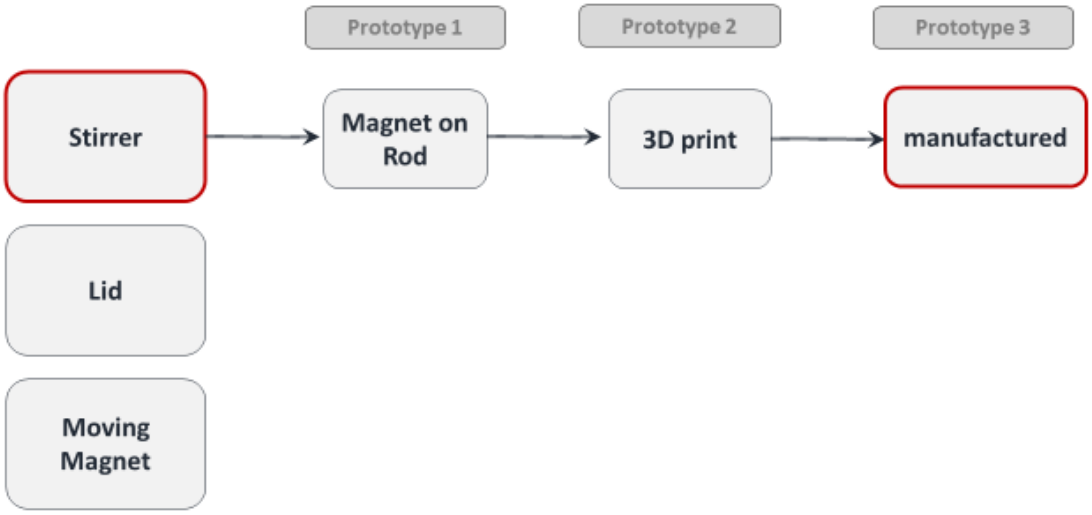

In order to address deformability and biocompatibility issues of the 2nd stirrer prototype, the material for the 3rd stirrer prototype was changed. However, a 3D printer which can produce the necessary precision and with a biocompatible material was not accessible. Therefore the final stirrer prototype was manufactured using delrin as stirrer material. The design for the 3rd prototype has extended the diameter of the cone tip by 0.49 mm. It was then aimed to place the magnet within the cone tip. The final step involved placing a surface on top of the cone/magnet in order to cover the magnet. After manufacturing the 3rd prototype the biocompatibility test was repeated as well as a test for biocompatible features of the stirrer magnet. Therefore only the magnet was placed in cell culture wells; by using magnetic forces, the magnets were placed next to each other in the cell culture media above the cells. This way it was possible to place the magnet in the cell culture media, without directly touching the cells (see Figure 4-5 C).

The delrin stirrer's were manufactured by the medical workshop in the Royal Hallamshire Hospital Sheffield.

4.2.3.1 Result and troubleshoot

Due to technical difficulties it was not possible to manufacture stirrers holding the magnet within the material. Thus, it was only possible to place an additional material on top on the magnets. However, part of the magnets are still exposed to the cell culture media.

Furthermore the biocompatibility tests showed that the delrin material did not start to deform (Sengupta *et al.* 2007). It was observed that the stirrer had the same stiffness than without incubation in cell culture conditions. The result stirrer biocompatibility result shows that the delrin stirrer do not significantly change the cellular response of selected genes in HUVECS (see Figure 4-5).

Moreover, the 2nd biocompatibility test of the magnet showed, that HUVECs died after being exposed to the magnet whereas the control wells still showed a healthy phenotype. In a second experiment the cells were observed after 16 h incubation, and the cells showed an apoptotic phenotype. However, after 6 h incubation a healthy phenotype was observed and the biocompatibility result shows that there is no significant change to the cellular response caused by the magnet. Nonetheless, it needs to be noted that the stirrer's magnet is not biocompatible for long term application on HUVECs.

The 3rd stirrer prototype was manufactured with the material delrin. The results of the biocompatibility test shows that delrin does not significantly affect the mRNA expression of eNOS, e-selectin, MCP1 and c-jun (see Figure 4-5). Furthermore, delrin exhibited better material stability in the cell culture environment since no material deformation was observed after incubation in the incubator for 6 hours (Zhanhai *et al.* 2002).

Unfortunately, it was technically impossible to enclose the magnet in the stirrers cone tip, this would have been ideal to cover the magnet. The results obtained from a set of biocompatibility tests with the magnet alone in the cell culture shows that the magnet itself has toxic effect on cell. Cell toxic effects may originate from the magnet's Nickel coating (Abudayyak *et al.* 2017). Thus, this prototype needs to be further improved since parts of the magnet are still freely exposed to the cell culture media. However, it has been shown that after 6 hours incubation the cells do not show a significant change of mRNA expression of selected genes. For experiments greater than 6 hours, the prototype should be further improved, for example with a coating.

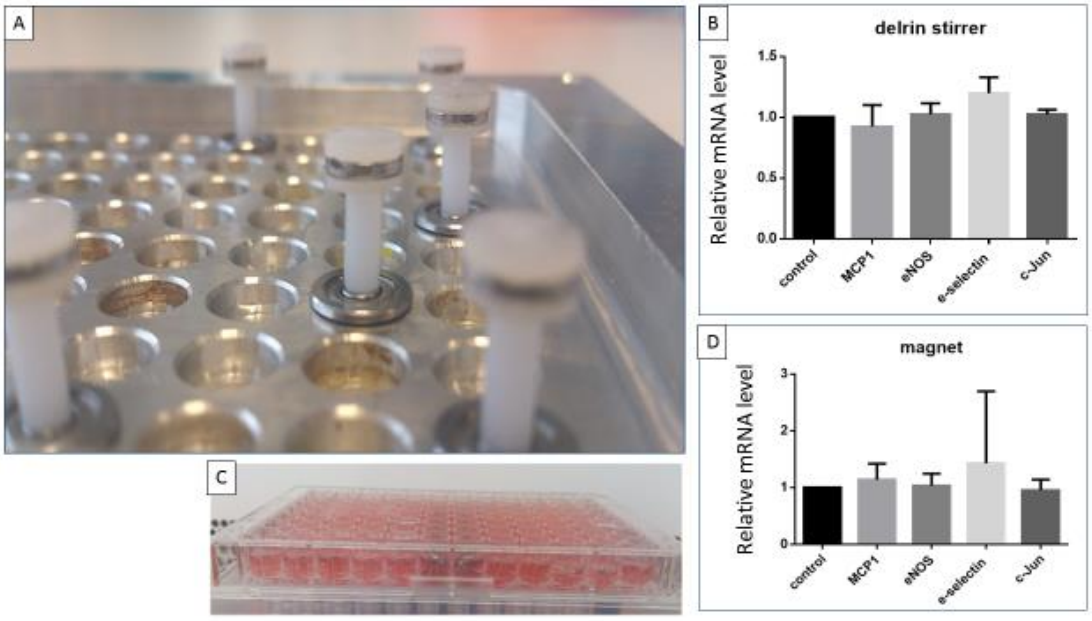

Figure 4-5 Prototype 3 Mörs stirrer – Manufactured

The figure shows the 3rd stirrer prototype which was manufactured using delrin.
Panel A shows the delrin stirrer's attached to a ball bearing held in the lid. The delrin covers the top surface of the magnet in order to limit the interaction of the magnet surface with the cell culture media.

Panel B and D showing the biocompatibility result obtained from a qPCR screening for the genes MCP1, e-selectin, c-Jun and eNOS. HUVECs were cultured in 96 wells and stirrers (Panel B) or magnets (Panel D) were placed in the cell culture media for 6 h, followed by RNA isolation, cDNA synthesis and qPCR. qPCR results were analysed using ΔΔCT analysis. This was performed with three different independent patient samples. Differences between mRNA levels of control vs stirrer or control and magnet were calculated by an un-paired, two-tailed t-test. The result showed that delrin stirrers or magnets do not significantly change the cellular response of selected genes in HUVECS after 6 h, n=3.

Panel C shows the arrangement of magnets on the cell culture wells without stirrers. Subsequent biocompatibility results were obtained as explained in the text.

4.2.4 Determining gap distance

In order to attempt to measure the distance from the cone tip to the bottom of the 96 well plate a PDMS mould was performed. PDMS was poured in a 96 well and the stirrers were placed in the well. Subsequently, the PDMS was allowed to solidify for at least three days at room temperature. The stirrers and PDMS were removed from the well and the PDMS mould was cut in cross sections to measure the gap distance using a light microscope.
In principal this method should solve issues arising from determining the gap distance. Unfortunately this method was not very precise and technically challenging. It was problematic removing the stirrers from the hardened PDMS, and the measured distance varied depending on the vertical angle of the cross-section. And finally, under the microscope, the cross section did not show a sharp border, and therefore an accurate measurement was very challenging.

Figure 4-6 shows a cross section of the obtained PDMS mould. The measurement shows that the gap distance is above 400 µm and therefore exceeds 100 µm. Furthermore the PDMS mould indicates that the stirrer's tip is conical shaped, since the distance in the middle is smaller compared to the outer side measurement.
Although the result must be reviewed critically, it indicates that the gap distance is much bigger than expected. Therefore this aspect of the Mörs stirrer is not optimal solved and requires improvement. Furthermore another method needs to be found to measure effectively the gap distance, or the current method, using a PDMS mould, needs to be improved.

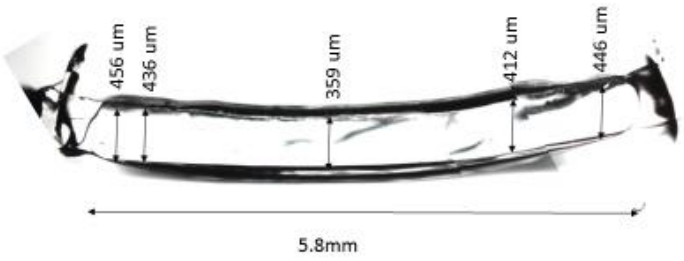

Figure 4-6 PDMS mould of gap distance

The figure shows a cross section of a PDMS mould between stirrer and well. PDMS was poured in a 96 well and the stirrer placed in the well. Subsequently, the PDMS solidified and a cross section was cut from the mould. The cross section was then measured using a light microscope. The picture shows that the distance between stirrer tip and bottom of the well is ~440 µm long. This result is suboptimal, since a gap distance of 100 µm was desirable for the current system configuration. However, this result must be very critically reviewed due to technical limitations as described in the text.

4.3 Discussion

The function of the Mörs stirrer is the movement of the cell culture media, which will subsequently create the shearing force on the adherent cultured cells in a well of a 96 well plate.

The main challenge of building the Mörs stirrers was the functional combination of the stirrers' elements consisting of the magnet, stirrer skeleton and the ball bearing in order to prototype a working element for the system. The magnet and ball bearing were purchased commercially and therefore had limited availability regarding sizes and materials. In particular the magnetic disc used to build the Mörs stirrers, was the only magnet which fit in the 96 well and the stirrer skeleton. However, this magnet occupies the ideal function, by being diametrically magnetised (Jang *et al*. 2012). The stirrer's skeleton was designed in order to fit the magnet and the ball bearing. Nonetheless, when one of those parts needs to be changed the stirrer skeleton will need to be adapted as well.

The Mörs stirrer therefore consists of basically three elements: a magnet, the stirrer skeleton and a ball bearing. First stirrer prototypes were done using an acrylic rod and a bar- or disc magnet, using a hotplate to melt the acrylic material and glue it on the bar magnet. In another attempt a pencil sharpener was used to fit the acrylic rod in the magnetic disc and ball bearing. A stirring motion was achieved with this prototype when the stirrer was exposed to an external magnetic field. However, the first prototype was not reproducible and it was technically impossible to build the cone angle as well as the exact stirrers lengths. Therefore 3D printing technology was used to address those limitations. The 3D printed stirrers were more accurate as well as more reproducible. Nonetheless, the 2nd prototype was found not to be biocompatible, as pro-apoptotic and pro-inflammatory genes were found to be up-regulated when testing selected flow induced genetic makers (Bryan et al. 2014). Thereby the supporting printing material seems to have cell toxic effects. In order to address this issue the chemical treatment was used to further remove supporting material (Rua *et al.* 2015). The repeated biocompatibility test shows that cell toxic effects were greatly reduced. However, respective genes were still upregulated compared to cells not exposed to the stirrers. Consequently it can be concluded that the printing material shows cell toxic effects itself. Unfortunately it was not possible to find a different 3D printer using a different 3D printing cartridge in order to optimise these results.

Therefore the 3rd prototype was manufactured professionally. This way it was possible to choose a biocompatible stirrer material and to keep a high precision regarding the stirrer's dimensions and shape. Delrin was chosen for the stirrer's skeleton since it has been shown to be biocompatible (Sucosky *et al.* 2008; Urban 1985). Furthermore this material is easy to handle and therefore simplified the manufacturing process *(*Rusina *et al.* 2007). Since it has been shown that the magnet confers cell toxic effects, it was aimed to enclose the magnet completely within the stirrer. However, this was not possible due to technical limitations. Nonetheless, it was shown that the magnets do not trigger a cell toxic response up to six hours. However, in due course this issue needs to be addressed in order to run long term experiments. One possibility would be to coat the stirrers with parylene or alternatively change the type of magnet (Chang *et al.* 2007). Another possibility may be to change the machinery, in order to enclose the magnet within the stirrer, which would be a good solution. Nonetheless, the final stirrer prototype works well in the overall system.

General optimisations are advisable when the system will be used in a professional manner. One possibility may be to attach the ball bearings on a vertically movable platform. This way the gap distance could be changed depended on the experiment. In order to quantify the existing gap distance a light barrier could be built in the system. Thereby a beam of light would be placed in the known distance of the bottom of the 96 well plate. When the stirrers are closer to bottom of the well the beam of light will be refracted from the stirrers. Therefore, the accurate distance can be determined by the distance when the light beam just about passes through to the opposite side of the 96 well plate.

5 Lid

5.1 Introduction

The lid occupies two functions. Firstly, the lid holds the ball bearing and secondly the lid assigns the position of the stirrer in the well. As already discussed, there is a minimal tolerance of 0.49 µm from stirrer tip to the edge of the well, therefore the lid must be designed to ensure the stirrer's mid-point is placed on the same axis as the well's mid-point, and the minimal gap distance between stirrer tip and 96 well bottom must be ensured. Furthermore, the ball bearing should be placed in the lid at 100 % vertical alignment. This also allows the stirrer to be vertically aligned in the well. Figure 5-1 Figure 5-2illustrates the importance of the lid for correct positions of the ball bearing and subsequently the positioning of the stirrer in the well.

Ball bearing

In order to reduce friction, which will be caused by the rotating movement of the stirrer, a ball bearing was used to connect the stirrer with the lid (Chen & Chen 2005). Therefore the ball bearing has three functions in this system: Firstly, the ball bearing connects the moving part with the static part. Secondly, the ball bearing regulates the height of the stirrer in the well. Thirdly, the ball positions the stirrer in the middle of the 96 well. Figure 5-2 demonstrates the ball bearings function as connector of lid and stirrer.

In order to meet those requirements, the ball bearing was chosen to have a smaller bore than the stirrer's shaft, ensuring that the ball bearing is situated on the ball bearing attachment site only, and consequently does not overlap the stirrer's shaft. This way it is possible to control the stirrer's vertical lengths as well as the horizontal positioning of the ball bearing in the well. If the ball bearing were to overlap the stirrer's shaft below the ball bearing attachment site, this would reduce the stirrer's shaft length and would result in an increased gap between stirrers tip and the bottom of the well (Figure 5-1, panel 4). Furthermore, the ball bearing attachment site guarantees that the stirrer will align in a 100% vertical position within the well. Thus, this will prevent an angled stirrer tip and unwanted fluid flow (**Error! Reference source not found.**, panel 2 and 3). Moreover, the ball bearing attachment to the lid will make sure that the stirrer is exactly placed in the middle of the well (Figure 5-1, panel 1).

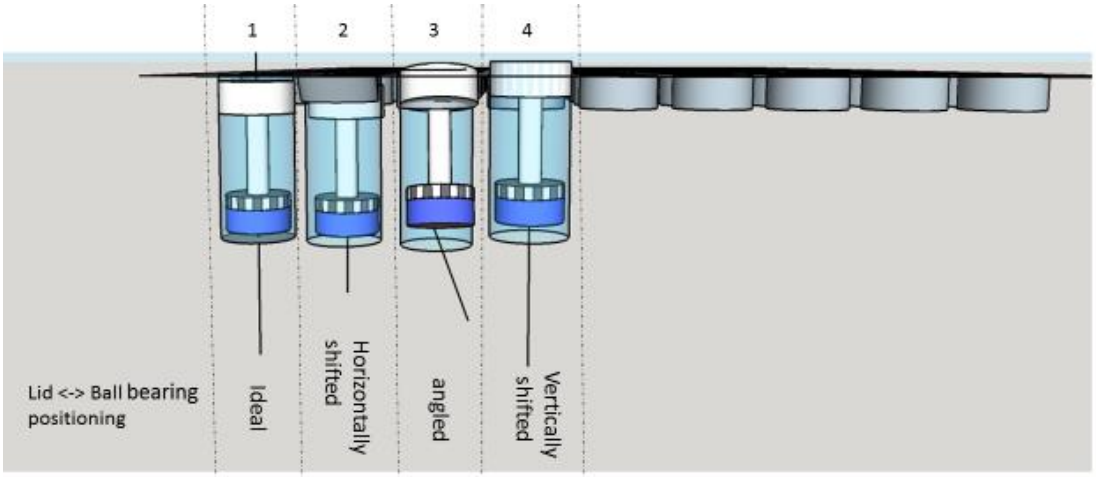

Figure 5-1 Ball bearing positioning in lid

This figure illustrates the importance of the lid for the correct positioning of the ball bearing in the well by demonstrating four different scenarios.

Panel 1 shows the ideal positioning; the ball bearing is positioned in the lid 100% horizontally, thereby the lid positions the ball bearing exactly over the well, resulting in a continuous line of the axis from the well mid-point, over the stirrers tip mid-point to the ball bearing mid-point of its moving element.
Panel 2 illustrates a horizontal shift of the ball, which results in the dispositioning of the stirrer. Although the stirrer is vertically aligned to the well, the well mid-point is not in line with the mid-point of the stirrer tip. This configuration is suboptimal, since the motion of the moving stirrer may be interrupted by contacting the wall.
Panel 3 displays a scenario where the lid dysfunctions by positioning the ball bearing in an angled position. This results in an angled position of the stirrer in the well and subsequently results in non-uniform fluid motion.
Panel 4 shows an altered vertical alignment of the stirrer by adjusting the ball bearing position distance, increasing the distance between the stirrer tip and the bottom of the well.

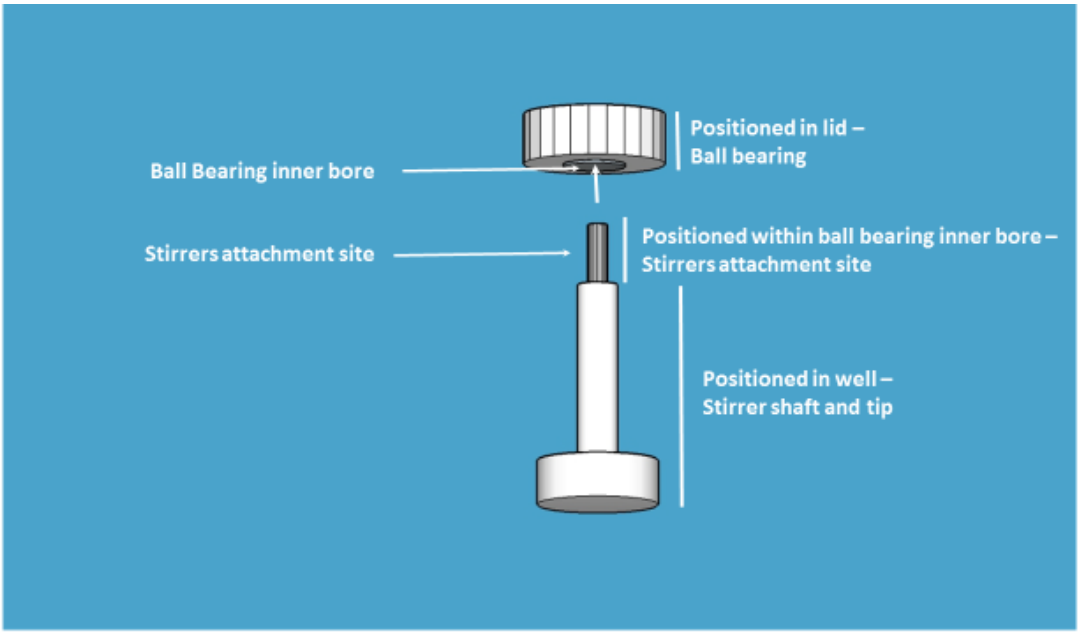

Figure 5-2 Attachment of stirrer to ball bearing

This figure illustrates the principal build-up of stirrer and its connection to the ball bearing. Thereby the ball bearing reduces friction in the system and moreover it functions as connector between lid and stirrer. This figure illustrates the specific connection between stirrer and ball bearing. Thereby the stirrer was designed to fit the inner bore of the ball bearing, whereas the stirrer's shaft is designed with an extended circumferential surface. This way the ball bearing normalises the stirrer's lengths in the well. In turn the ball bearings static part is positioned in the lid. Consequently, the lid plays an important role in positioning for the stirrer in the well.

5.2 Result

5.2.1 Prototype 1 – Pipette tip box holder

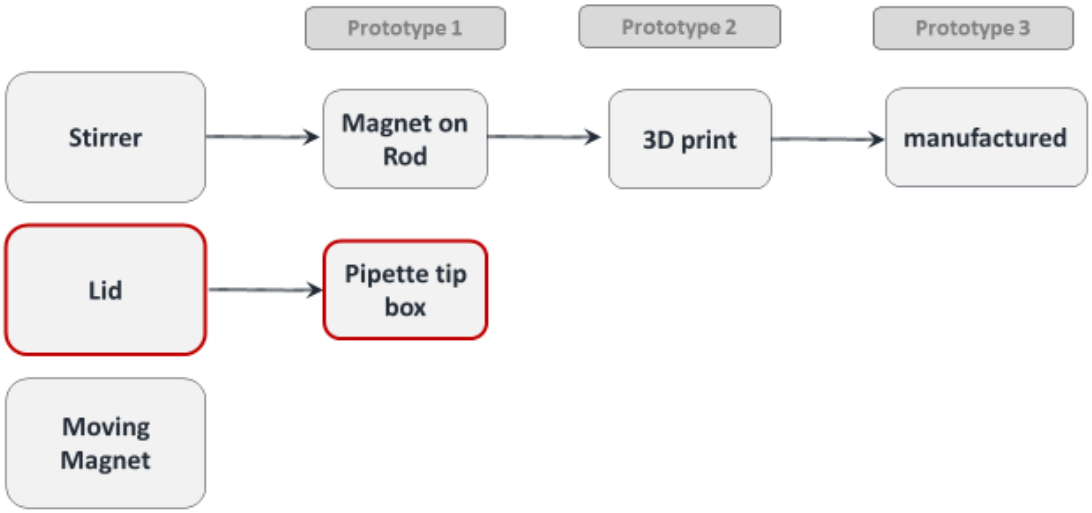

The first lid prototype was built from a pipette tip holder compartment of a pipette tip box, see Figure 5-3 panel C. This lid exactly fits the 96 well plate. However, several issues occurred with this lid during testing. The lid has additional compartments on the outside in order to click into the pipette tip box. These compartments can be removed, however this would leave the lid in an uneven state, causing the lid to be slightly higher on one side than the other. Furthermore, it was difficult to place the lid exactly on the 96 well plate. This bears the risk that the stirrer's mid-point is not placed in a horizontal line with the well's mid-point.

5.2.2 Prototype 2 – PDMS

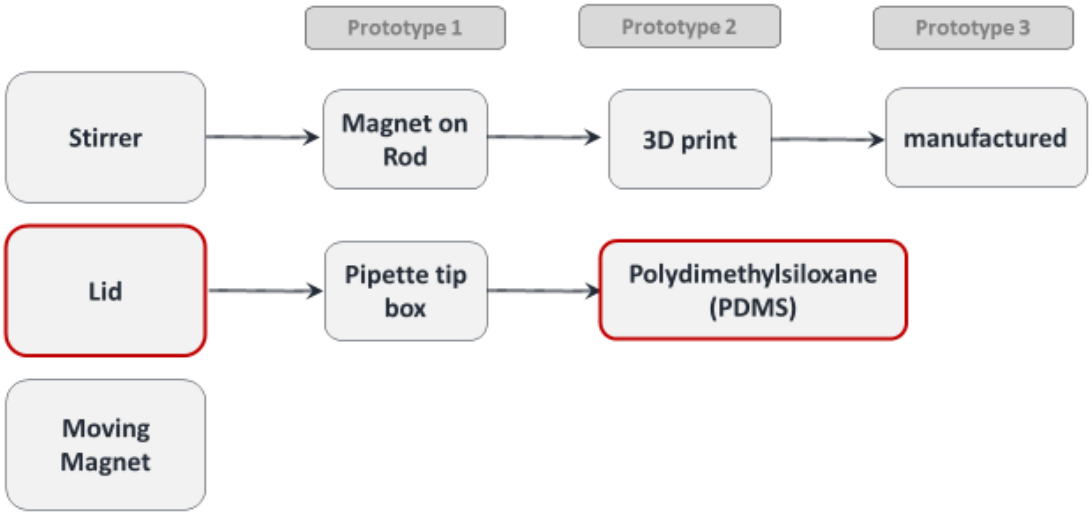

In order to address issues of the 1st prototype, the 2nd prototype was made by moulding PDMS in a 96 well plate lid. Subsequently a 7 mm diameter cutter was used to cut out ball bearing positions of the PDMS mould, see Figure 5-3 panels A and B. Compared to the pipette tip box tip holder, this lid's improvement is an exact fit on the 96 well plate. Furthermore, the PDMS lid adapts perfectly on the 96 well plate, allowing a perfect horizontal alignment on the 96 well plate to be achieved.

The PDMS lid greatly improved the precision of the stirrer's placement in the 96 well plate. However, it was observed that the lid underwent movement when the stirrers were in motion. Furthermore, cutting out the ball bearing positions exactly in the required position was technically challenging. However, this is an unconditional requirement for the correct ball bearing positioning and therefore the stirrer's placement in the 96 well.

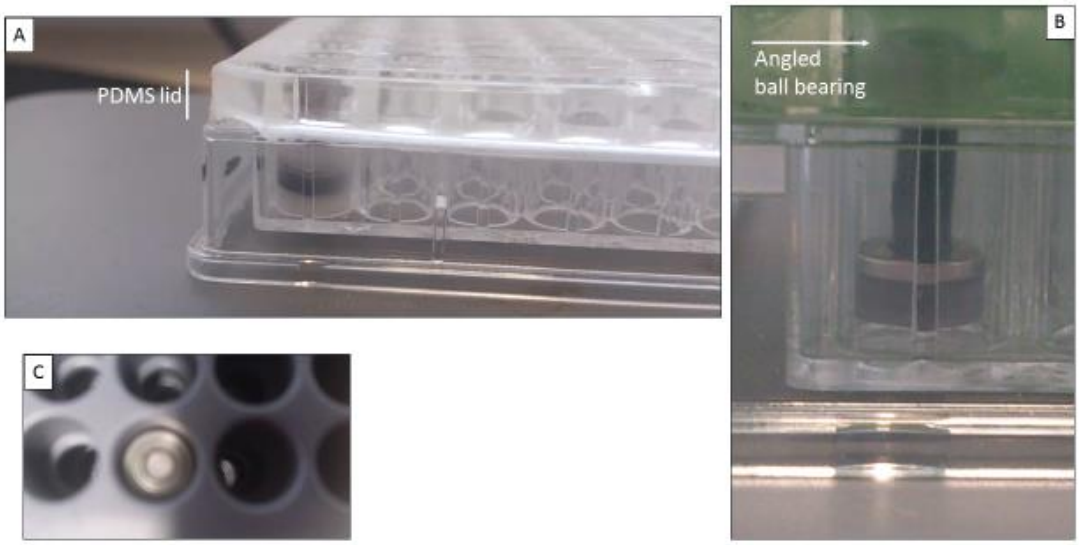

Figure 5-3 Lid prototype 1 and 2

The figure shows the lid prototype 1 and 2. Panel C shows the first prototype, where a pipette tip box holder compartment was used to place the ball bearing and stirrer. The figure shows the top view perspective of the pipette tip box holding compartment including a ball bearing placed in one of the holes. Panels A and B show the second prototype using a self-made PDMS lid. Panel B illustrates the issue of the correct positioning of the ball bearing in the PDMS lid, as described in the text.

5.2.3 Prototype 3 – customised aluminium lid

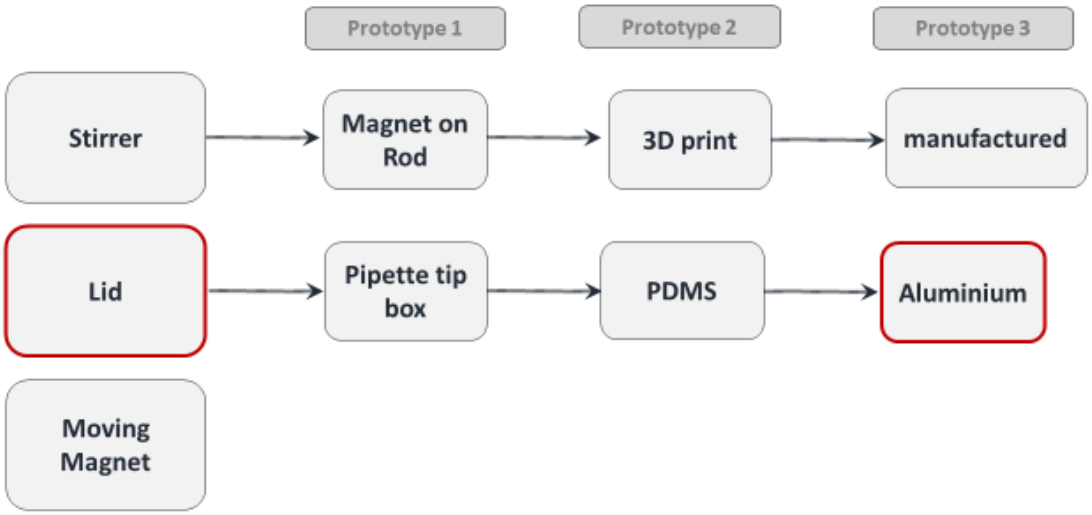

The problems associated with the Prototype 2 PDMS lid included the correct adjustment and positioning of the Mörs stirrer in the lid. Taking together all occurring issues with the PDMS lid, it was decided to design a more robust and reliable lid. This newly designed lid is made of non-magnetic aluminium. The lid contains holes matching exactly a 96 well plate. Furthermore, the holes are designed to fit the ball bearings exactly in the lid holes. Therefore, the vertical alignment of the ball bearing is much improved. Furthermore, the holes are in line with the 96-well plate which ensures that the stirrer's mid-point is in line with the well mid-point. In addition, the lid is designed and built like a 96-well plate lid, including the overhang on the edges, in order to fit and enclose the 96-well plate. Moreover, the lid has a second lid to protect the ball bearing and stirrers from any outside contamination which could be transferred through the ball bearing to the cell culture medium.

Although the third prototype fulfils all requirements for the lid it was noticed that the chosen ball bearings developed signs of rust after repeatedly placing in the humid cell culture incubator (Singh *et al.* 2008). These were replaced with stainless steel ball bearings (Liu *et al.* 2004).

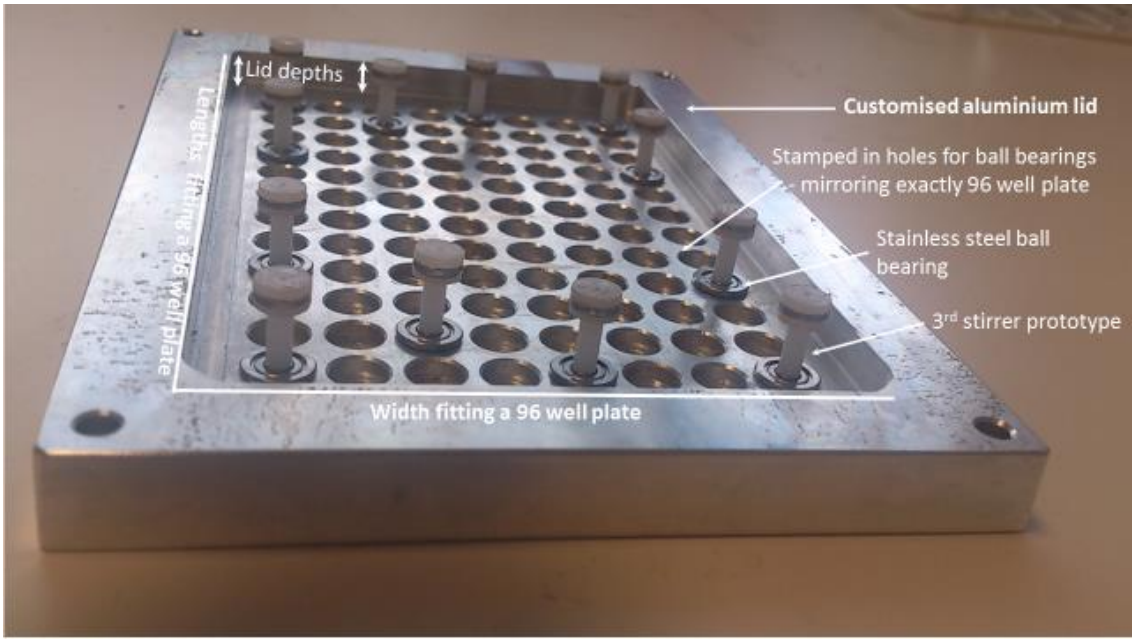

Figure 5-4 customised aluminium lid

The figure displays the 3rd and final lid prototype. The lid's material is non-magnetic aluminium and the inner depths exactly fit a 96 well plate. Moreover, stamped in holes fitting the ball bearings are arranged with the exact same distance in order to place the stirrers within the 96 wells. Therefore the stamped in holes are designed to fit the purchased ball bearings made of stainless steel. The 96 well plate will be enclosed by the lid, thereby the lid secures the correct position of the stirrers in the wells.

5.3 Discussion

Although the lid is not directly involved in the stirring motion nor does it come in contact with the cells, it does hold several very important functions in the overall system. During the prototyping phases a reusable lid was developed. The lid functions to hold the stirrers in the well plate and thereby controlling the distance between stirrer tip and the bottom of the well plate. Furthermore, by holding the ball bearing the lid intermediates between moving and static parts.

The first prototype represented a quick an easy solution by using the insert of a pipette tip box. This prototype was useful to test the principal functionality of the overall system. However, limitations occurred in the precision of placing the lid on the well plate. Furthermore the holes in the lid which hold the ball bearings are not customisable. Consequently, the ball bearing size is restricted to the given outer diameter.

The second prototype attempted to address this issue by having a moulded PDMS lid (Peterson *et al.* 2005). Thereby, holes with the required size were stamped in the PDMS mould (Yesildag *et al.* 2017). However, problems were found in the practical application when stamping the holes in the exact required well distances. Therefore it was challenging to fit the lid holes accurately on top on the well plate. It was also found to be problematic to horizontally align the ball bearing in the holes. This resulted in angled stirrers in the wells. Furthermore, it was suboptimal that the PDMS lid was light-weight, which became an issue when the stirrers were in motion since the lid started to lift up and down.

All issues that arose from prototypes one and two were addressed by building a customised lid. This lid is made of non-magnetic aluminium. The hole diameter was chosen to fit ball bearings with ideal inner and outer diameter for the intended purpose.

In order to fit the lid on the well plate the lid was built with an inner deeper area, whereas the outer lid wall encloses the well plate. Therefore the lid can be placed on the well plate, ensuring a secure fit moreover, it also ensures an accurate stirrer placement in the wells (Anthony & Lee 2016). Thereby each stirrer tip is vertically aligned with each mid-point of the respective well.

Another advantage is the horizontal placement of the stirrers in the holes. Since the positioning of the ball bearing is fixed it is also possible to define the required distance from the stirrer's tip to the bottom of the well. In order to avoid contamination of the cultured cells in the wells a plastic lid was built to put on top, above the ball bearings. The lid final prototype works well in the overall system.

Further optimisation could be done by adapting the ball bearing positioning in order to gain different gap heights (Spruell & Baker 2013). Depending on the application this may be an additional feature with great advantages. Therefore the lid could be built with different stages of hole widths. Consequently, by using different sized ball bearings which fit the holes and by keeping the same stirrer dimensions the gap distance would be changed.

The final lid prototype has precision and functionality for the intended purpose. The only difficulty may be batch dependent tolerances with regard to the 96 well plate sizes from the manufacturer. Therefore, dependent on the batch the 96 well plate may sit very tight, or not as tight in the lid. However, no greater issue should be expected with this matter.

6 Rotating magnet

6.1 Introduction

The fundamental principal of the represented device is the stirrer’s movement by following the magnetic field transmitted of a moving magnet; consequently the stirrer's movement creates the media movement which subsequently initiates the shearing force on the cultured cells (see Figure 2-10). Thereby the moving magnet’s function is the transition of the magnetic field which is intended to be received by the attached magnets on the stirrers. This way the power input in the moving magnet device is transferred wireless; no cables are needed to connect the moving magnet device with the lid or stirrers. Thus, this method reduces cables and therefore represents a user-friendly approach and low maintenance costs.

In order to fulfil this function, the moving magnet device shall have specific properties. Firstly, the moving magnet is made of a magnetic permeable material (Schweizer 1962); thus, the magnetic field created from the moving magnet will be transmitted to the stirrers. In order to direct the stirrer's movement, the created magnetic strengths of the moving magnet must be greater than the stirrer's magnetic strengths.

Secondly, the moving magnet must be suitable for exposure to *in vitro* cell culture conditions of 37°C, 5% CO2 and 100% humidity in order to generate optimal cell culture conditions (Regalia *et al.* 2016). If the moving magnet device needs to be placed in the cell culture incubator the device must meet specific requirements in terms of size and materials, e.g. material resistance in humid conditions (Wolf *et al.* 2013).

Thirdly, the device shall have the possibility to alter the rotational speed of the moving magnets; thus, different effects of shear stress magnitude could be tested. In that respect an optional rotational direction change would be desirable to apply different shear stress magnitudes and directions (Simmons *et al.* 2012).

6.2 Results

6.2.1 Prototype 1 – Laboratory magnetic stirrer

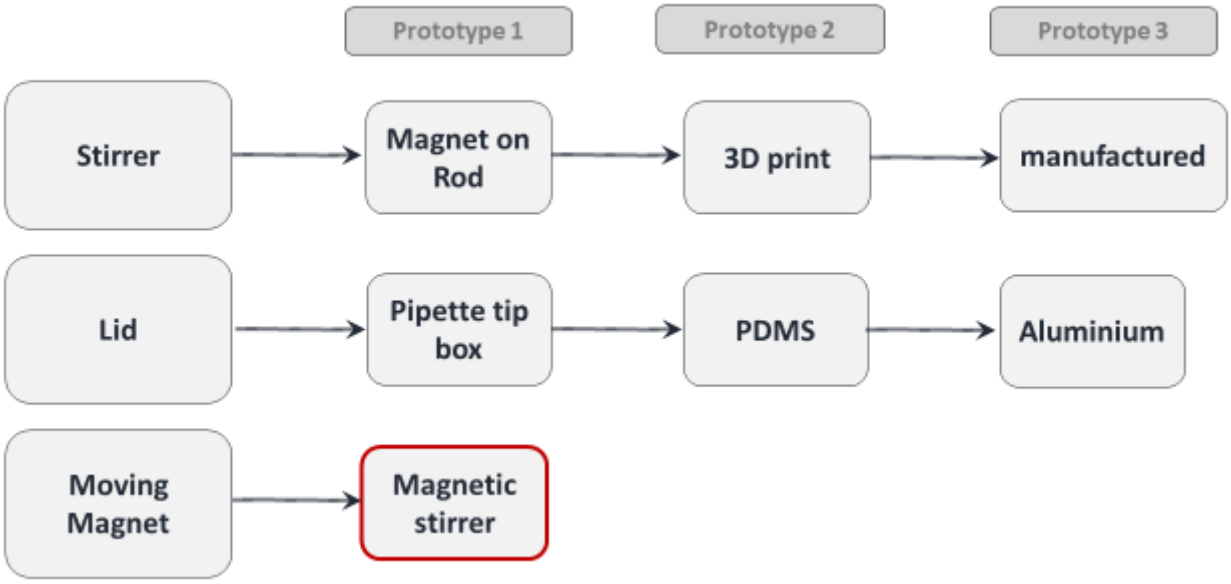

The first moving magnet prototype tested was a laboratory magnetic hotplate stirrer. In order to create cell culture conditions the magnetic stirrer may be placed in the cell culture incubator or the hotplate can be used as controllable heat source in combination with supplementing the cell culture media with HEPES in order to compensate CO_2 absence (Hashem *et al*. 2016).

The use of a laboratory magnetic stirrer as moving magnet device would exhibit the simplest solution for the novel *in vitro* shear stress application system described in this thesis. Therefore specific functions of a commercially available laboratory magnetic stirrer have been tested. In particular, the rotational speed, magnetic properties were investigated. Furthermore, it was tested to see if the ball bearing movement is congruent with the stirrers tip movement, which is crucially important for further validations.

Validation of laboratory magnetic stirrer and Mörs stirrers

Crucial properties of the moving magnet device are to create a magnetic field which is a) strong enough to move all individual stirrers and b) transmitted equally distributed across the 96 well plate. For those reasons the magnetic properties of the laboratory magnetic stirrer itself were examined. In order to easily visualise the magnetic properties bar

magnets were placed individually in wells of a 96 well plate. The tested laboratory magnetic stirrer was set at level 1. In order to record the bar magnet's motion a camera was placed on a dissecting microscope. Subsequently, imageJ was used to create a montage of one bar magnet rotation, and the angular change between frames was measured of three different bar magnets (Andrews *et al*. 2010).

Furthermore, rotational speed of the laboratory magnetic stirrer in combination with the Mörs stirrer was tested. Therefore, a 3D printed stirrer was attached to a ball bearing; the assembled ball bearing- stirrer construct was then placed in the lid (see Prototype 2 - PDMS). The rotational speed was then visualised by marking the ball bearing's inner and outer ring, whereas the inner mobile ring represents the rotational speed of the magnetic stirrer and outer ring functions as control due to its static nature.
Furthermore, this experimental setup was used to answer the key question, do the ball bearing and stirrer tip show a consistent parallel motion when exposed to an external magnetic field? Due to the geometric nature of the ball bearing and the final setup it is a non-trivial challenge to visualise the stirrer's motion within the magnetic field directly. Therefore a piece of white paper, which length is greater than the outer diameter of the ball bearing, was attached on the stirrers tip. This way the stirrer's tip motion is visualised and can be tracked in conjunction with the inner ball bearing motion.

In order to visualise the motion a camera was placed above the assembled device and a video was recorded. Subsequently, imageJ was used to create a montage of selected frames showing the inner ball bearing at a 3 o'clock position thereby completing a full rotational round. The camera used specifies a recording of 30 frames/second; thus allowing calculation of the rounds per minute.

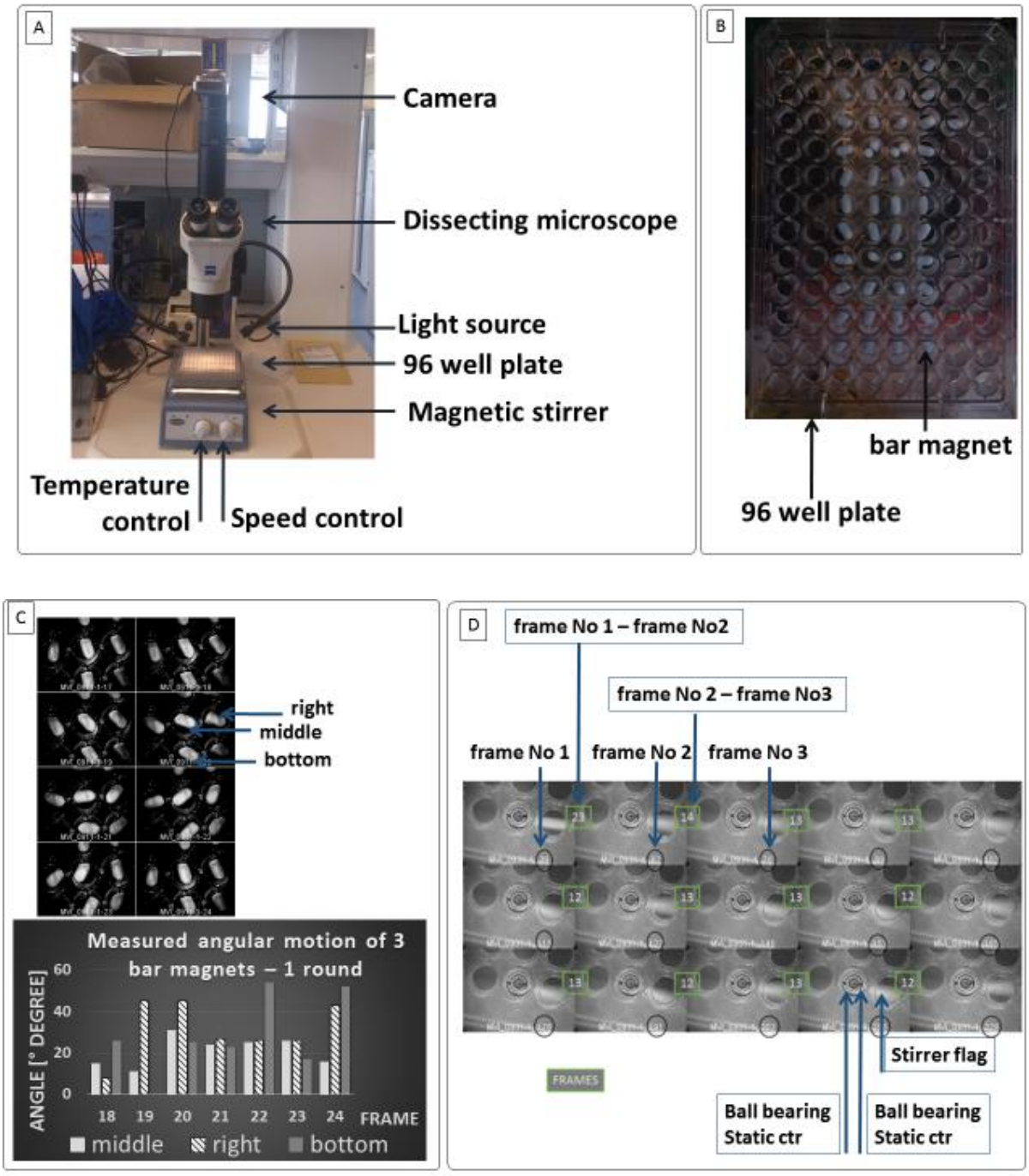

Figure 6-1 Validation prototype 1 moving magnet

The figure illustrates the principal built up of using a laboratory magnetic stirrer for establishing a wireless rotational magnetic field and its setup to validate the laboratory stirrer's angular velocity. Panel A shows the measurement setup, Panel B: 96 well plate including bar magnets placed on the laboratory stirrer. The angular movement of the bar magnets was tracked, as shown in Panel C. In addition it was tested to see if the ball bearings movement run parallel to the stirrers tip.

Magnetic stirrer transmits a non-uniform magnetic field across a 96 well plate

The magnetic field transmitted from the laboratory magnetic stirrer was made identifiable with help of individual bar magnets placed in the 96 well plate. Figure 6-1 provides results obtained from this experiment, Figure 6-1 Panel A presents the experimental setup, Figure 6-1 Panel B shows the static magnetic field transmitted from the laboratory magnetic stirrer, Figure 6-1 Panel C displays a breakdown and the result of angular measurement of the bar magnet's movement when the laboratory magnetic stirrer is switched on.

From Figure 6-1 Panel B it can be seen that the bar magnets manifest themselves differently across the 96 well plate. A linear flat arrangement is formed in the middle of the 96 well plate in 9 wells, whereas the outer regions showing the bar magnets upright and engaged in different directions.

As can be seen from Figure 6-1 Panel C the angular rotation comparing three differently positioned bar magnets differs between frames. One complete round was measured, however, the bar magnet's motion is not uniform.

Speed level 1 of laboratory stirrer moves with 138rpm

Figure 6-1 D illustrates a stack of frames showing the mobile ring of the ball bearing at the 3 o'clock position over time. Numbers in green boxes express the number of frames between two 3 o'clock positions. On average it takes 13 frames for one round, which means that within one second the stirrers will move 2.3 rounds. Given the camera records 30 frames per second this means that the laboratory magnetic stirrer moves 138 rounds in one minute. The very first frame difference of 23 is negotiable. The higher number can be explained by the fact that the stirrer and the ball bearing needed to overcome momentum (Sathyan *et al*. 2008).

Ball bearing and stirrer tip show a consistent parallel motion

Figure 6-1 Panel D also illustrates that the ball bearing movement and the stirrer movement is parallel. When the black marking on the inner ball bearing ring gets to the 3 o'clock position the white flag on the stirrers tip is also found at that position.

Working principal of laboratory magnetic stirrer needs to be investigated

A linear magnetic field has been found at 9 wells positioned in the centre of a 96 well plate. However, wells outside the centre region have been found to show a nonlinear magnetic field. This inconsistency has been confirmed by measuring the angular

movement of the bar magnets when the laboratory stirrer is switched on. In order to optimise the moving magnet device further investigations in the fundamental build-up of the laboratory stirrer may be helpful.

138 rpm, what does this number mean for practical flow application?

It has been found that at level 1 the laboratory magnetic stirrer has a rotational movement of 138 rpm. However, this number does not give any conclusion about the shear stress number applied to the cultured cells. Spruell and Baker (2013) estimated the created shear stress using a cone and plate in a 96 well plate by CFD. Amongst others, this numerical approach considers rpm number, the stirrer's cone tip angle and positioning in the well. Given a 2° stirrer cone tip, a gap height of 100 µm and an angular velocity of 167° rpm the authors predict applied shear stress of 0.5 Pa. Therefore shear stress applied by using the laboratory magnetic stirrer at level 1 shall be below 0.5 Pa. However, this number must be approached very carefully since the Spruell and Baker approach is purely mathematical. Therefore calculated numbers may be subject to change caused by the smoothness of the materials used in this project (Grad & Einav 2000). Furthermore, at this stage of the project prototyping of stirrer and lid was not finished. Therefore, an accurate placement in the 96 well plate cannot be guaranteed, neither can biocompatibility be assured.

Nevertheless, given that this simple solution of a moving magnet device would be ideal, it should be tested if an *in vitro* application of flow on culture cells would be possible in principal.

Ball bearing mobile ring motion is congruent with Mörs stirrer's movement

It has been found that that the circular movement of the mobile ball bearing ring is parallel to the stirrer's movement. This is a crucial important result, especially in regard to further validations. Thereby, the stirrer's movement in the well can be tracked by the ball bearing movement.

6.2.1.1 Identification of the laboratory magnetic stirrer working principal

Further investigation of the laboratory magnetic stirrers principal build up will help draw conclusions about the inconsistency of the observed magnetic field. However, more

importantly in due course, this will provide a further understanding of the device and therefore may help to develop an optimised moving magnet system.
As shown in Figure 6-2 A the laboratory magnetic stirrer consists of a controller board and a platform which holds two magnets opposite each other. By placing the 96 well plate with the bar magnets on top of the platform (Figure 6-2 B) it was observed that the magnets show a similar arrangement as observed in the magnetic field experiment, described in this chapter. However, it is possible to explain these observations by knowing the actual magnet arrangement within the magnetic stirrers. The nine bar magnets in the middle of the well are directly exposed to the linear magnetic field in the middle of the two magnets on the platform (see Figure 6-2 C and Figure 6-2 D). Bar magnets outside the centred wells were found to show a different arrangement.

In summary, the bar magnets show a consistent motion and arrangement when exposed to a linear magnetic field. In contrast, when exposed to a nonlinear magnetic field, the bar magnets show an inconsistent motion and arrange in a chaotic manner. The linear magnetic field is created in-between the two magnets of the laboratory magnetic stirrer only; whereas the nonlinear magnetic field is created outside of the magnets (see Figure 6-2 C and Figure 6-2 D).

Conclusion

In order to increase the number of usable wells and therefore increase the sample throughput of the 96 well plate using the moving magnet device, it shall have opposite magnets assembled extending the lengths of a 96 well plate. Thereby, the magnets must be strong enough to provide a linear magnetic field to the lengths of a 96 well plate (see Figure 6-2 E).

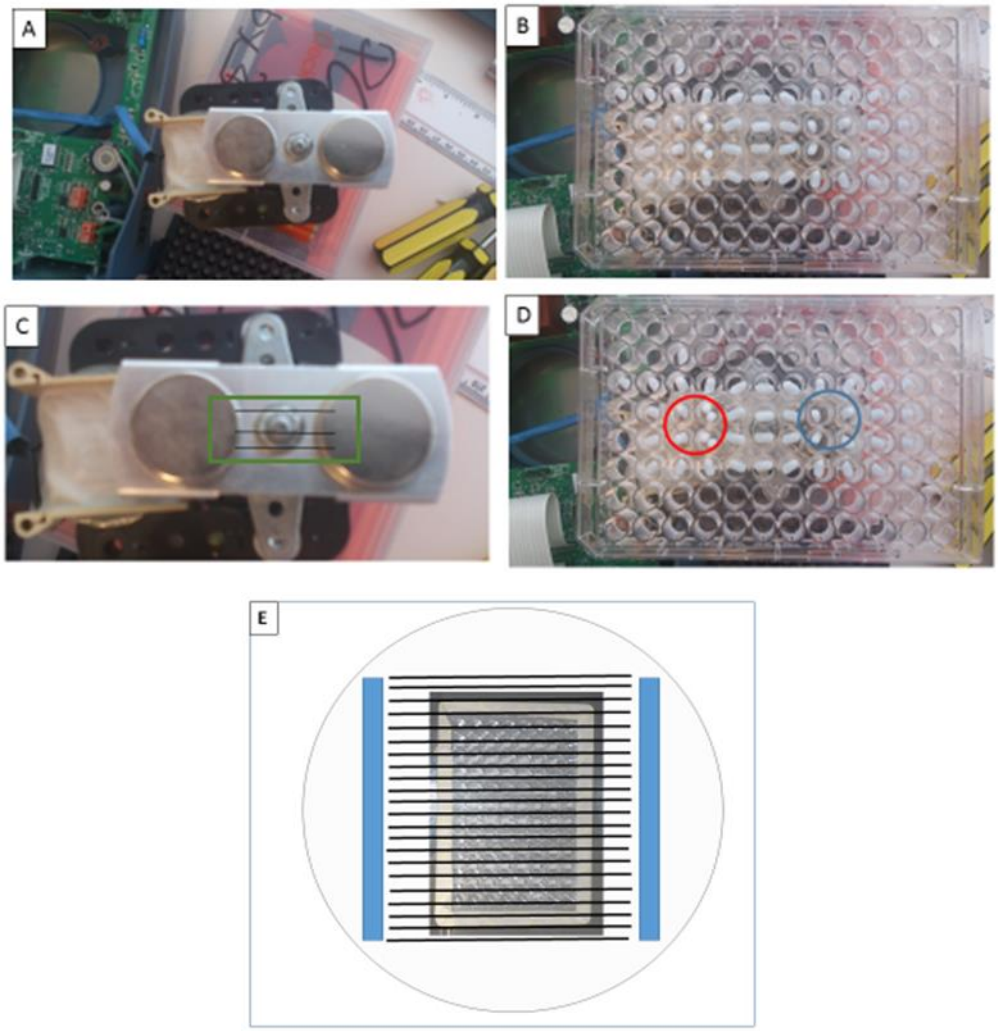

Figure 6-2 Disassembled laboratory magnetic stirrer

The disassembled laboratory magnetic stirrer reveals that the magnetic stirrer works with two magnets which are placed on a platform. The rotational movement of the platform is achieved with a motor, which is electronically controlled (Panel A). When putting a 96-well plate with numerous mini magnets in separate wells, the magnetic field directions created by the stirrer's magnets can be estimated (Panel B). It is shown that linear magnetic field can be found in between the two magnets on the platform (Panel C). The linear magnetic field generates a smooth and linear movement of the bar magnets in the 96-well plate. Whereas bar magnets in the areas outside and above the platform magnets are subject to a non-linear movement (Panel D). Schematic design of an ideal magnetic stirrer for a 96-well plate. Two large magnets (shown in blue) thereby would create a strong magnetic field exerted along a 96-well plate (Panel E).

6.2.1.2 Shear stress application using the laboratory magnetic stirrer

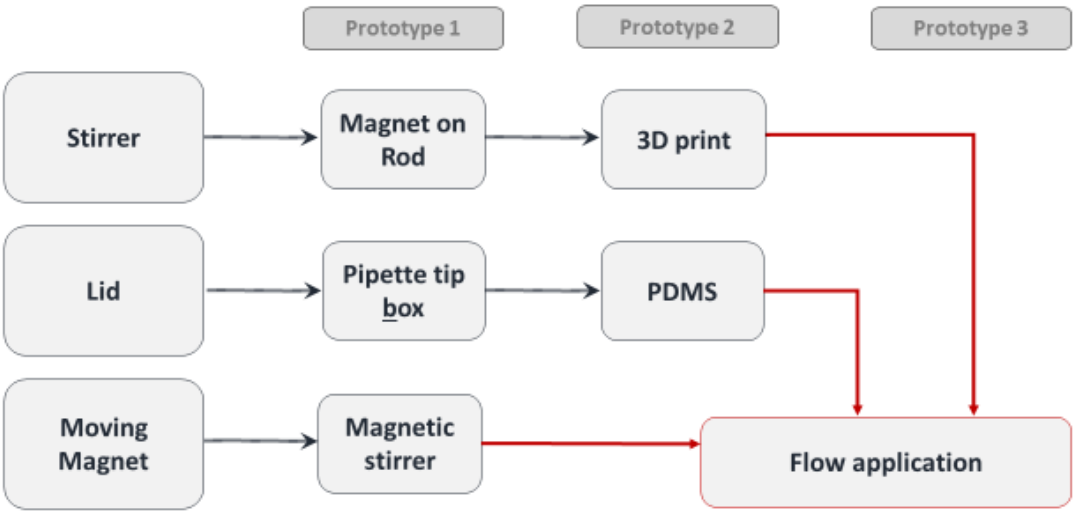

Experimental procedure

In order to test if the proposed device is able to create shear stress on cultured endothelial cells in principal, the very first *in vitro* application was done using the laboratory magnetic stirrer, the 3D printed Mörs stirrer (stirrer Prototype 2, see section 4.2.2) and the PDMS lid (Lid Prototype 2, see section 5.2.2). HUVECs were isolated and cultured to passage 3 and 4000 cells were seeded in one well of a 96 well then allowed to adhere overnight. The cell culture media was removed, the cells were washed with PBS, and media supplemented with HEPES was added to the cells in order to compensate CO_2 absence (Hashem *et al*. 2016; Saalfrank *et al*. 2015).

The PDMS lid and the stirrers were sprayed with 70% Ethanol, wiped thoroughly and assembled in the cell culture hood and placed on the 96 well plate. The 96 well plate was preheated to 37°C and the assembled lid and the wells containing cells were placed in the centre of the laboratory stirrer in order to gain a linear magnetic field. The stirrer was placed in the PDMS lid, so it was as close as possible to the bottom of the 96 well plate but without touching the well. In order to create a 100 µm gap height and a shearing force of approximately 0.5 Pa for 24 h the laboratory stirrer set at level one in the assembly (Spruell & Baker 2013). This procedure obviously has its limitation, as no accurate estimation can be given about the applied shear stress. Nonetheless, at this stage of

prototyping, it was important to test if the fundamental idea of the novel device is purposeful.

After 24 h the cells were fixed and in-well immunofluorescence staining was performed using an antibody directed against VE-Cadherin; a protein playing an important role in the organisation of intercellular junction (Steward *et al*. 2015). Furthermore, the nuclei was stained with DAPI and the cytoskeleton was visualised by using FITC conjugated phalloidine peptide (Knudsen & Frangos 1997). The cells were then examined using a fluorescence microscope.

Results

The functionality of the novel 96 well plate flow device was examined by cell morphology changes comparing cells exposed to shear stress versus static cells, as shown in Figure 6-3 A. It is apparent from this figure that the cells exposed to shear stress show a changed morphology compared to static cells (Davies 2011). The DAPI stain, shown in blue, reveals the stained nuclei (Coleman 1981). Comparing both groups of cells the cell number is reduced in the flow treated well compared to the static control. The red panel, showing the VE-Cadherin staining and therefore the intercellular junctions, illustrates an altered arrangement. The phalloidin panel shows the cytoskeleton and illustrates that the cells exposed to shear stress have a rather elongated and stretched arrangement compared to static cells (Sinha *et al*. 2016).

The results show that the flow application using the novel device caused a cell morphology adaptation. Therefore the fundamental working principal of the device is assured.

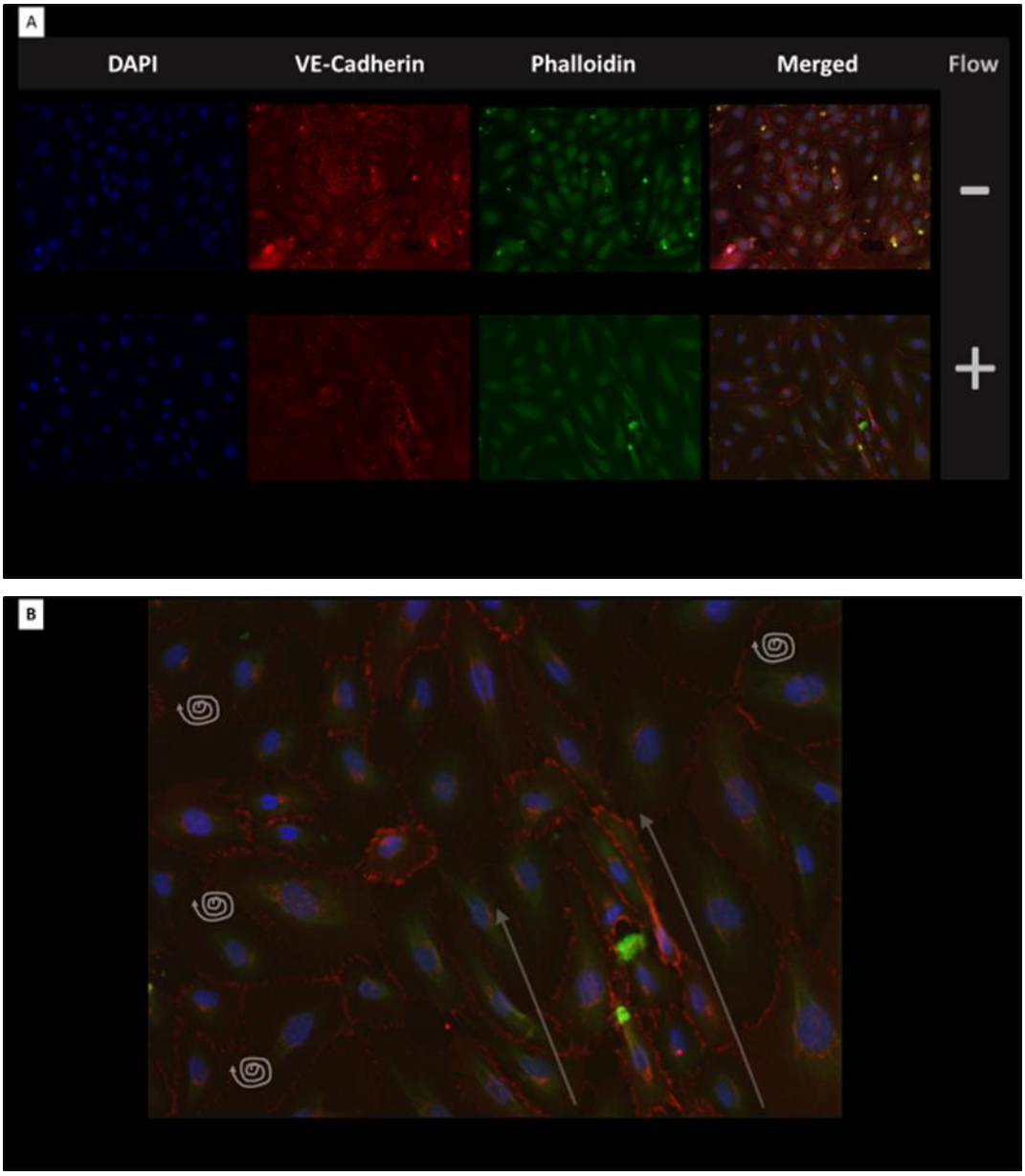

Figure 6-3 Flow application using the laboratory magnetic stirrer

Shear stress was applied to cultured HUVECS using laboratory stirrer, 3D printed stirrers and PDMS lid in order to test the principal functionality of the novel developed device. A shearing force of approximately 0.5 Pa was applied for 24 h. Subsequently, cells were stained with immunofluorescent dyes; visualising the cell's nuclei (DAPI-blue), the cytoskeleton using phalloidin (F-actin – green) and VE-cadherin (red). Cells were imaged using a fluorescent microscope. Panel A shows results obtained from well without or with flow application. Panel B illustrates the predicted fluid dynamic from the obtained result.

Discussion

It has been shown that cells treated to flow undergo a phenotypical change compared to the static cultured cells. In particular the cytoskeleton shows an altered morphology (Sulistyowati *et al*. 2017). By comparing this morphological change with experiments from Franzoni *et al*. 2016, the grade of cell alignment looks similar. This paper also shows that a full cell alignment triggered by flow is reached after three days.

Cell death in of flow treated cells

Overall the cell number of the flow treated cells seems to be reduced compared to the static control, this can be easily seen in the DAPI and the phalloidin channels. Thereby, several explanations may be possible.

Firstly, the cells were exposed to flow on a laboratory stirrer on a laboratory bench, outside the cell culture incubator; although the CO_2 absence was compensated by supplementing HEPES in the cell culture media and in addition the temperature was set on the laboratory stirrer to 37°C . However, the laboratory stirrer's temperature was not tested to be functional over a long period. Consequently, the laboratory stirrer does not keep a constant temperature and therefore the temperature may fluctuate over time, which are suboptimal cell culture conditions (Saalfrank *et al*. 2015). Furthermore, the temperature flux may not be as optimal as in the cell culture incubator (Rebelo *et al*. 2015). The heat of the laboratory stirrer is provided via a plate, whereas the cell culture incubator heating is distributed equally with a fan in the chamber. Therefore, cells cultured in the cell culture incubator are surrounded by the same temperature. However, cells on the hotplate are exposed to the heat source only via the bottom of the 96 well plate.

Furthermore, the PDMS lid most likely did not enclose the 96 well completely. Therefore it could be possible that the cultured cells may have been exposed to an external contamination transmitted by air (Wolf *et al*. 2013).

Secondly, 3D printed Mörs stirrer's (stirrer prototype 2) were used for this experiment, which have been shown to upregulate apoptotic and inflammatory genes and therefore are not biocompatible (see section 4.2.2; Lusis 2000).

Overall, the exact shear stress rate as well as the fluid dynamics in the well itself are unclear (Grad & Einav 2000). In particular, as limitations of the PDMS lid in regard to lid up-and-down movement when in motion and the correct placement of the ball bearing in the lid have been identified. Therefore it may be possible that applied fluid dynamics are not linear across the well. Figure 6-3 B shows aprediction of the fluid dynamics on the basis of the cell morphology changes of the cytoskeleton (Davies 2011). Thereby, at the edges of the presented field of view oscillatory flow may be predominant. Whereas a linear fluid flow may be found in the middle of the picture, since the cytoskeleton and cell nuclei are extended towards a mutual direction (Davies *et al*. 2014).
It will be crucially important to further investigate prevailing fluid dynamics as soon as the final prototype is developed. This can be done by CFD and PIV (Pekkan *et al*. 2005).

6.2.2 Prototype 2 - customised magnetic stirrer

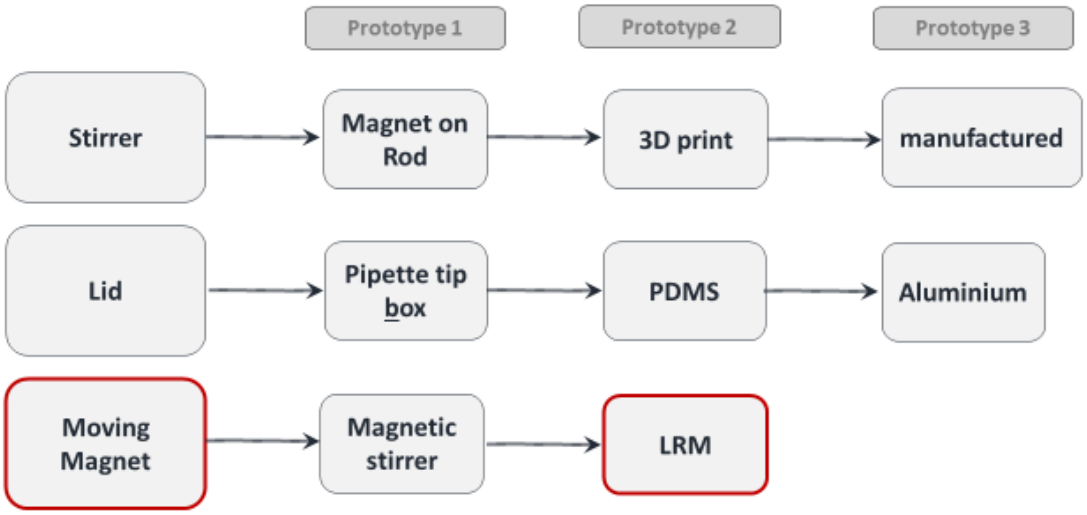

The magnetic stirrer prototype 1 has shown suboptimal results for the intended application. Especially the lack of a linear magnetic field across the entire lengths of a 96 well plate is not ideal. However, with help of the principal prototype 1 build-up it is possible to optimise the system for the anticipated purpose.
The moving magnet device's most important features are the rotating magnets which will be placed with opposing polarities on a platform. Thereby the distance of those magnets shall extend the lengths of a 96 well plate (see Figure 6-2 E). The platform holding those magnets must be able to rotate to create the angular movement. In order to generate the rotation the platform will be mounted to a motor, which will be connected to a

microcontroller. By programming the microcontroller the motors rotation can be regulated (Petru & Mazen 2015). In order to place the 96 well plate on the moving magnet device a cell culture incubator suitable box will be built around the described assemble. The 96 well plate and the lid containing the 96 stirrers will then be placed on top of the box. Consequently, stirrers in the wells will be exposed to the magnetic field transmitted from the rotating magnets.
Drawings for the moving magnet device have been done using the open-source software SketchUp (Lee & Yan 2016). The drawings were discussed with the medical workshop in the Royal Hallamshire Hospital. The workshop then implemented the practical building of the moving magnet device.

In summary, this device will hold two large magnets which are supposed to rotate; therefore in laboratory jargon we called this device large rotating magnet, or short LRM.

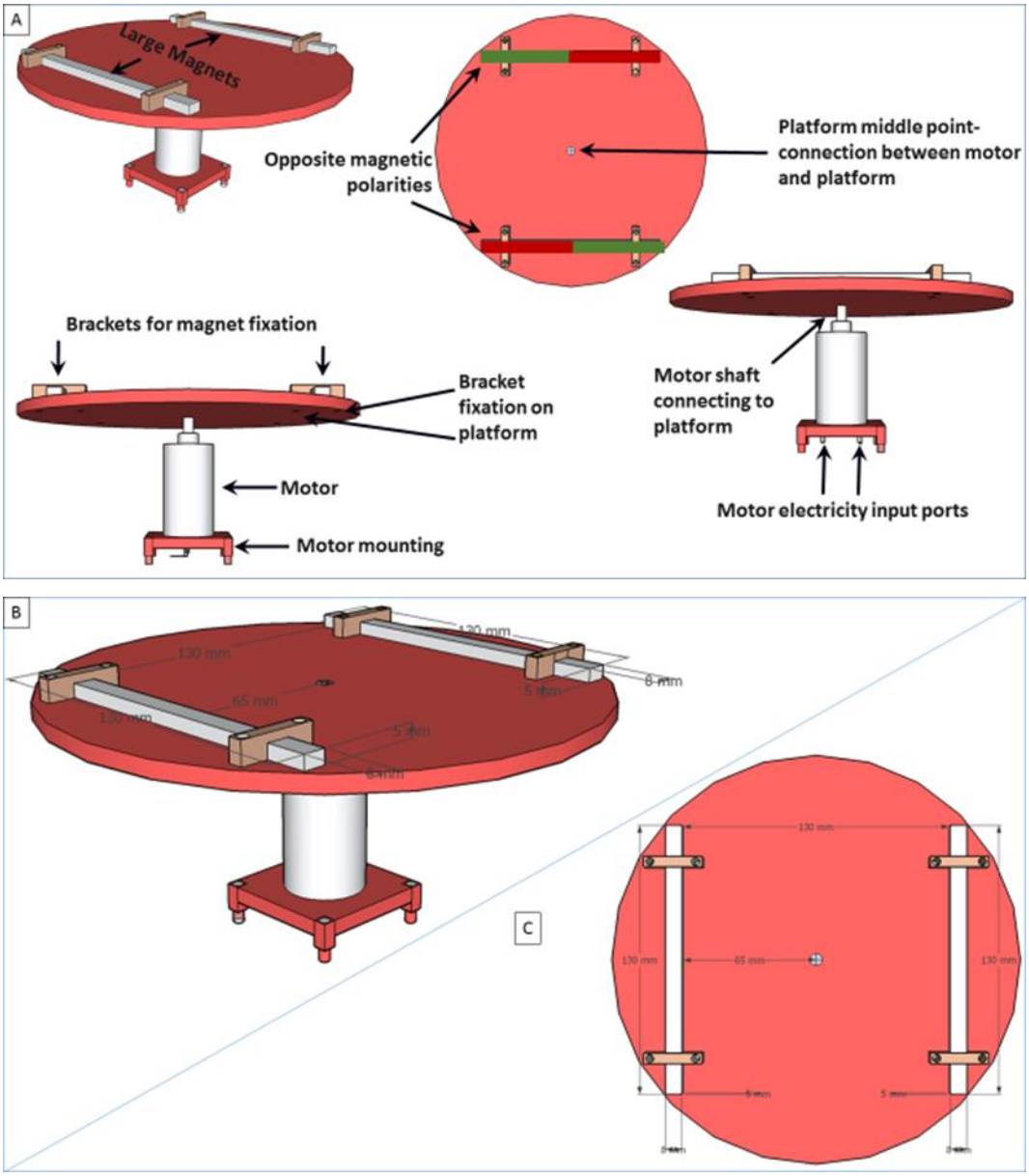

Figure 6-4 Drawing moving magnet Prototype 2

The figure shows CAD drawing to build the second prototype of the moving magnet, namely large rotating magnet (LRM). The build-up derives from a laboratory stirrer/hotplate, however the design has been optimised for the intended purpose of the newly developed device. Panel A: Two large magnets are placed with opposite magnetic polarities on a platform and being held in place with brackets. The platform is assembled on a motor shaft, which allows rotational movement of the platform. Panel B represents a side view and Panel C the top view. Thereby illustrating that the distance between the magnets is chosen so a 96 well plate will fit in-between.

LRM- magnets

This device consists of two magnets which are placed on opposite sides and with opposing polarities on a platform. In order to develop an optimised prototype a few requirements shall be considered. Firstly, the magnetic field should be strong enough to reach above the entire length of the 96 well plate. Secondly, the magnetic field should be strong enough to move the stirrers in the 96 well plate. Finally, those magnets should span the 96 well plate in order to expose the magnetic field across the whole of the 96 well plate.

The distance between these magnets on the platform were chosen to be 133 mm (see Figure 6-4), thereby extending the lengths of a 96 well plate of 128 mm by 5 mm, in order to achieve the intended linear magnetic enclosing the entire lengths of the 96 well plate.

In order to create a magnetic field which meets the requirements for its purpose neodymium magnets are chosen which are 130 mm long, 8 mm wide and 5 mm thick. According to the manufactures specification, one of those neodymium magnets has a pull of 23.8 kg and weighing 250 g. Neodymium magnets were chosen since it has been found that the energy production of neodymium magnets is greater compared to any other permanent magnet materials (Herbst 1991).

LRM- platform and box

The moving magnet's platform occupies two main functions. Firstly, the platform holds the magnets and secondly, the platform connects the magnets to the motor.

Polymethyl methacrylate (PMMA) was chosen as material since it is easy to handle and process (Salimgareeva & Kolesov 2005). Importantly, spacers to hold the magnets were stamped in as well as fixtures for brackets to secure the magnets in their position. This way important health and safety aspects are being addressed and the magnets are secured to enclose the entire 96 well plate. Furthermore, the centre was specifically processed to connect the platform with the stirrer's shaft. The platform is built from non-magnetic materials, including non-magnetic screws; thus, decreasing the chance of interrupting magnetic interactions. PMMA also occupies the advantage that it is a lightweight material (Ali *et al*. 2015), thus reducing loading weight to the motor. The box material is PMMA, a transparent plastic which allows the movement of the motors/platform to be tracked (Salimgareeva & Kolesov 2005). Furthermore, the material characteristics were found to be stable in the cell culture incubator environment. In general the device was designed as small as possible in order to fit it in an incubator (Wolf *et al*. 2013).

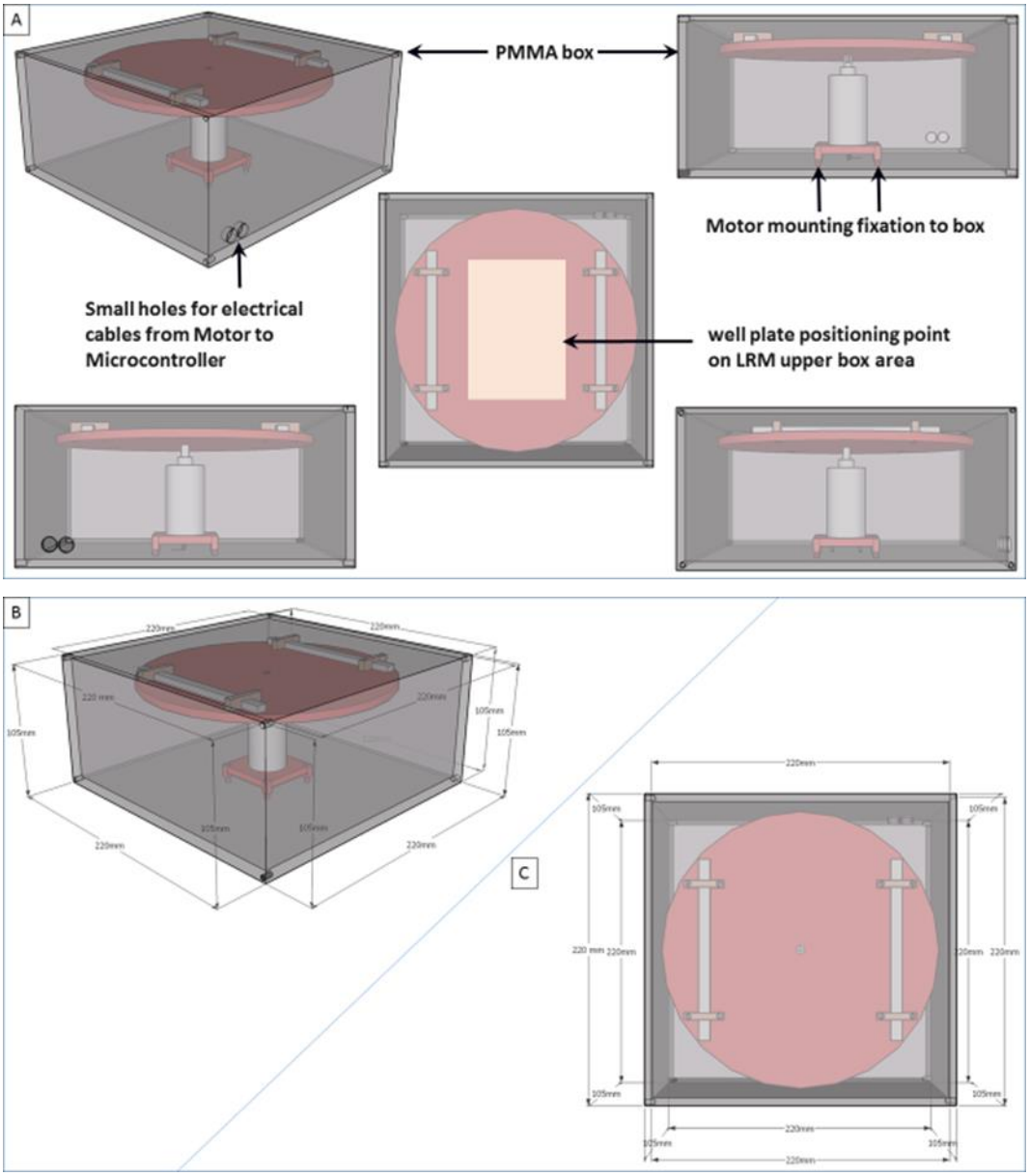

Figure 6-5 Drawing moving magnet Prototype 2 - box

This figure shows the CAD drawing of the LRM placed in the box.
Panel A: The box enables the placement of the 96 well plate on top of the box as well as the mounting and humidity exposure control of the motor. The box also contains two small holes in order to connect a microcontroller externally to the motor.
Panel B shows a side view and Panel C shows the top view of the box including the dimensions for the build.

LRM - Motor

The motor function is the angular circulation of the platform holding the large magnets. In order to create a shearing force in a physiologically relevant range, a motor with an angular velocity up to 350 rpm was chosen. Thereby, the maximum number was estimated from the orbital shaker device which creates 1.5 Pa in the periphery of the 6 well, when the orbital shaker rotates at 210 rpm (Warboys *et al*. 2010b).

In order to meet those requirements, a geared DC motor was chosen. The gearing reduces the rpm number of a motor compared to non-geared motors from which the rpm number reaches typically several thousands (Khabou *et al*. 2011). Furthermore the motor's specific stall torque was considered, which describes the maximal load until the motor's shaft rotation becomes zero. Stall torque is described in [g cm], thereby it was calculated that a stall torque above 5000 g cm is required, given the weights o the magnets (250 g per magnet) and the platform's radius of 10 cm. The weight of the PMMA platform itself was neglected, since the platform was not built and it was considered that the PMMA is a light material (Ali et al. 2015). For the same reason, weights of brackets and screws on the platform were neglected as well. Moreover, the Arduinos maximum operating voltage of 12V needed to be considered as well as the actual motor size in order to fit in the device (Petru & Mazen 2015).

A 30:1 geared motor, with lengths of 52 mm and a diameter of 37 mm was chosen. The 12V DC motor's output is 350 rpm, and has a stall torque of 7823.2 g cm

LRM – Motor control

In order to induce the motor's rotation the motor needs an electrical input. Therefore, the simplistic way would be to connect the motor's output cables to a battery and subsequently, the motor starts to rotate.

The motor's rpm number depends on the voltage input

The effective motor's shaft output speed depends on the voltage input, which itself is influenced by three factors. Firstly, as already mentioned in the previous section, the motor's specific stall torque; secondly, the motor's own voltage input maximum, and thirdly, the voltage capacity of the connected electrical source influences the motor's effective output speed. The higher the effective voltage input to the motor, the higher the motor's output, measureable in the rpm number. Thereby, the motor's own voltage input depends on the manufactured motor design. In addition, the external electrical source depends on the live voltage coverage to the motor. For example, if a 6V motor is

connected to a fully charged 9V battery, the motor will be on full capacity until the battery charging level drops below 6V. Consequently, the motor's maximal speed capacity will no longer be reached and the motor's speed will be reduced in accordance with the battery power level. Therefore the principal of motor controlling is simply possible by controlling the motor's voltage input (Petru & Mazen 2015).

The Arduino Microcontroller can be used for motor control

The Arduino Uno microcontroller board was tested in order to control the motor rotation (D'Ausilio 2012). The motor is connected to the Arduino microcontroller. The Arduino needs to be programmed in order to signal voltage inputs to the motor. Consequently, the motor will transduce the electronic input in mechanical energy in form of angular rotation.

First attempts of motor control with the Arduino were fulfilled with a classic breadboard for building electronic circuits (Williams 2013). Thereby the microcontroller was connected to the breadboard, which itself was equipped with a 9V battery as power supply and the motor. There were several options to control the motor which are going to be explained in more detail. Firstly, a potentiometer was used to manually control the voltage input to the motor. Potentiometers can be found in several everyday applications and a simple way of visualising the fundamental functionality is a light dimming switch; thereby the user increases or decreases the voltage input to the bulb by turning the dimmer which results in an increase or decrease of the light intensity. In the same way a potentiometer works for the motor's voltage input; increasing the voltage increases the angular velocity and decreasing the input voltage decreases the angular velocity.

Regulating the motor's speed by using a breadboard and potentiometer

The potentiometer basically consists of consecutive resistors, thereby controlling the final voltage output to the motor. The more elegant solution to a potentiometer is the use of PWM. Thereby the voltage input to the motor can be controlled with the software written and applied to the Arduino microcontroller (Petru & Mazen 2015).

In order to identify the best way of controlling the motor for the intended purpose, the breadboard method was combined with either potentiometer or PWM. For this purpose a mini DC motor was used as shown in Figure 6-6 C.

Conclusions of motor control with breadboard and potentiometer

The breadboard was equipped with a potentiometer therefore it was possible to control the motor's speed. However, this method is limited by inaccuracy and is dependent on a physical attendance when the angular velocity needs to be changed. Therefore, the motor control with the breadboard in combination with a potentiometer is possible, however too many limitations have been found with that system.

Regulating the motor's speed and direction with the Arduino motor shield

The Arduino motor shield brings the advantage that the motor control elements are built in a circuit board, which is easily stackable to the Arduino Uno (Figure 6-6 B and Figure 6-6 C). The Arduino motor shield is equipped to run two motors independently of each other. The PWM mode is available from two channels; channel A pin D3 and channel B pin D11. For power supply the Arduino motor shield has a 2.1 mm plug which can be combined with an AC/DC adapter to a wall socket. The motor is directly connected to the motor shield and no other electronic components are required (Ventura *et al.* 2014).

Testing the LRM

In order to test the functionality of the built LRM the motor was connected to a simple 9V battery to achieve rotational movement of the platform. As soon the motor was provided with energy support, the platform started to move. Indicating that a 9V power supply is sufficient for the motor to achieve a rotational movement including the platform load.

Furthermore it was verified that the LRM fulfils its purpose with a 3D printed stirrer (see page 49) placed in the aluminium lid (see page 67). Thereby it was observed that the stirrers follow the rotational movement of the LRM. However, it was also observed that multiple stirrers placed in the lid would not always move within the magnetic field of the LRM (see Figure 6-8). In more detail, the stirrers would not move when they are placed side by side in the lid. It appears that the magnetic strengths of the stirrer magnet are too strong or *vice versa* that the linear magnetic field created by the two large rotating magnets is too weak.

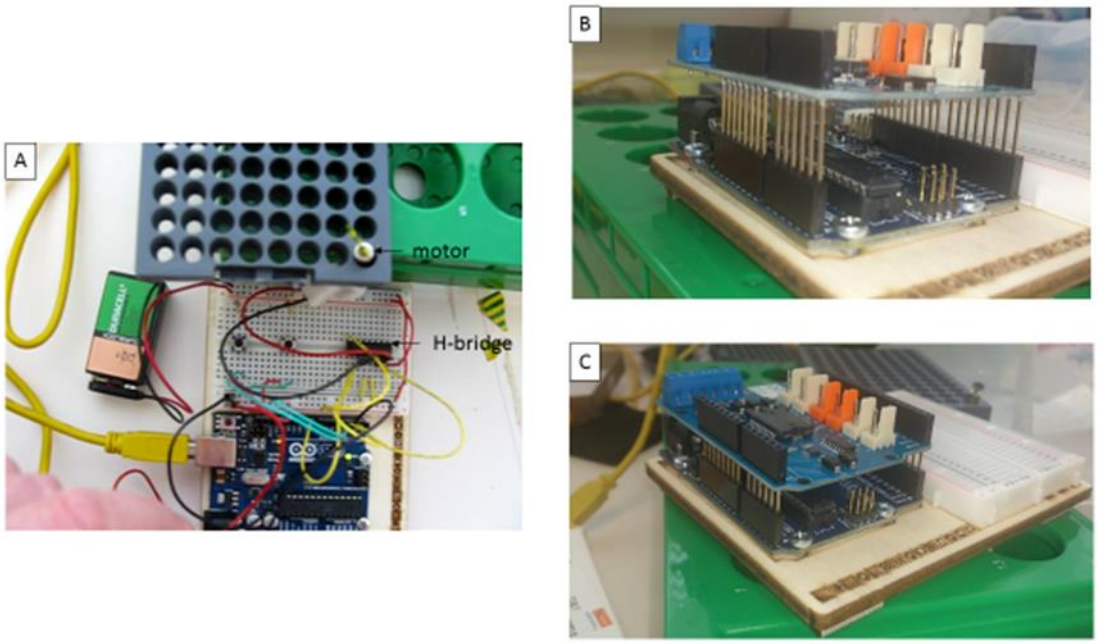

Figure 6-6 LRM motor control

Electronic circuits were built using a prototyping bread board. The speed was controlled with PWM on the Arduino Uno and an H-bridge built in the electronic circuit (Panel A). In order to simplify the motors control and to create a more stable base the Arduino motor shield was used (Panel B, motor shield on top of Arduino Uno). The shield has the same pin configurations as the Arduino Uno and is therefore easily stackable on the Arduino Uno (Panel C).

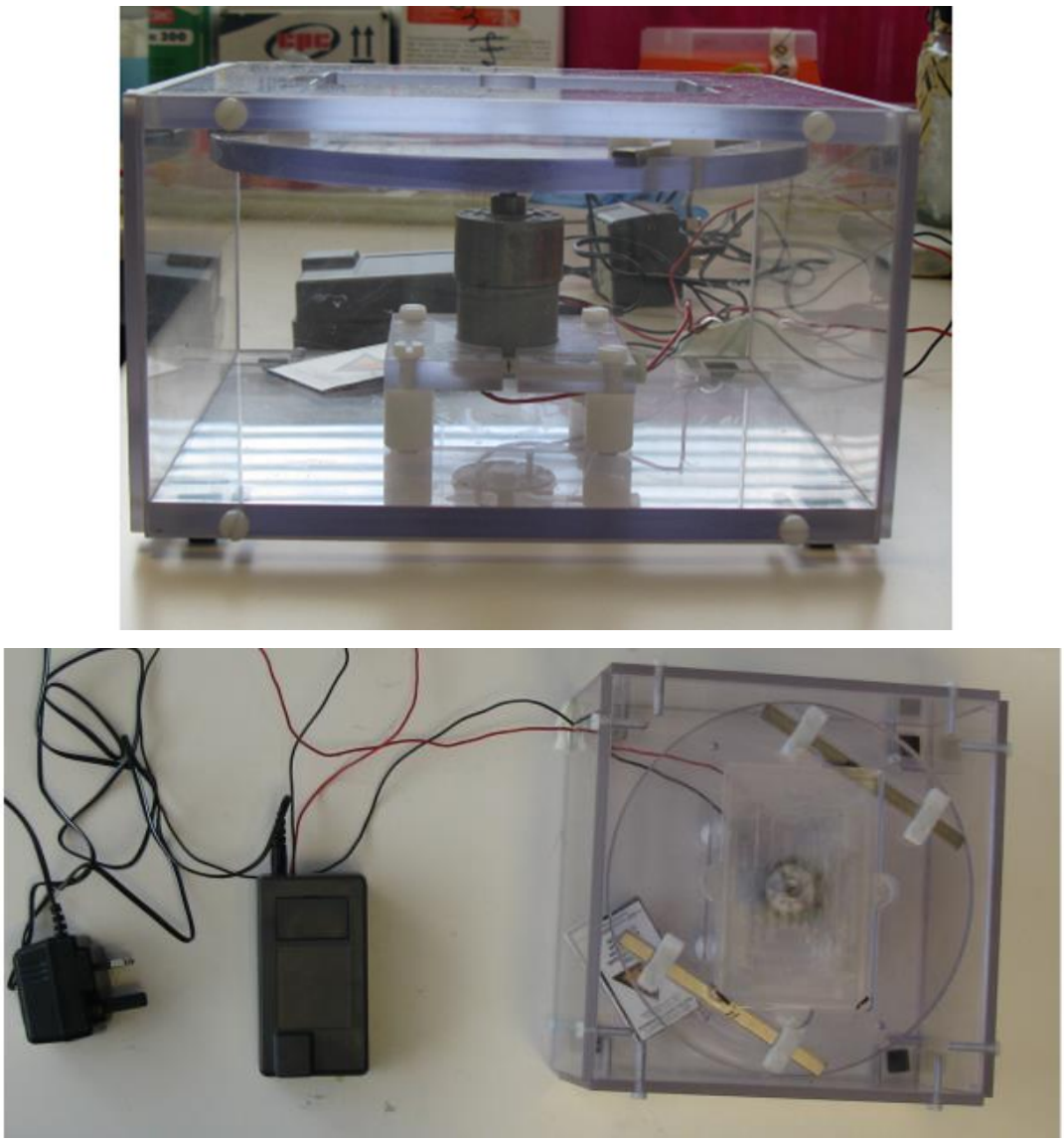

Figure 6-7 Built LRM device

The figure shows pictures of the LRM device. The LRM's function is the creation of a linear magnetic field across a 96 well plate. Therefore a controllable motor is connected to a platform holding two magnets distancing the lengths of the 96 well plate. In order to fulfil the function of creating shear stress, the multi well plates are placed on top of the LRM. Shear stress will then be created by placing the Mörs stirrers in the wells. Consequently the Mörs stirrers will follow the magnetic field created by the LRM. Subsequently the cell culture media will be moved, which will finally create the shearing force on the cultured cells in the well plate.

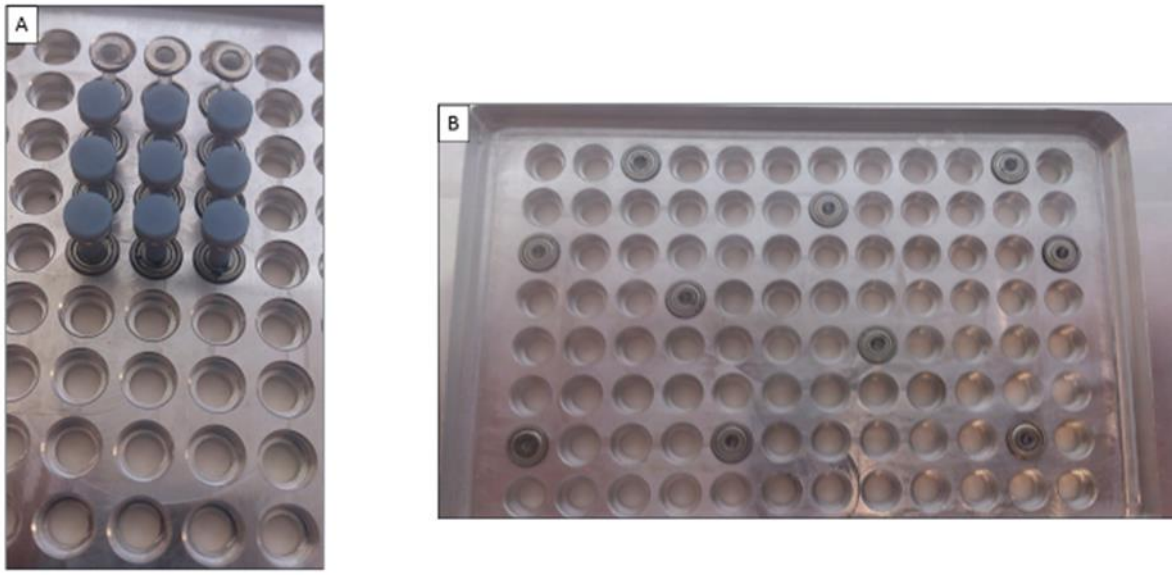

Figure 6-8 LRM functionality test, Mörs stirrer arrangement

The LRM functionality was tested by applying a rotational platform movement to Mörs stirrers. Application with one Mörs stirrer show a consistent stirrer movement achieved by following the moving platform. Mörs stirrer arrangement as shown in Panel A resulted in a chaotic and interrupted stirrer movement. However, configuration B, generated a smooth stirring motion when the stirrers are placed on the LRM.
Only 10 3D printed stirrers were available at the time of testing.

6.2.3 Prototype 3 - LRM.2

The main function of the LRM is the rotation of the large magnets in order to transmit a linear magnetic field. Subsequently, the Mörs stirrers, each containing a magnet and being assembled in the lid, will receive the transmitted magnetic field and consequently start moving following the movement of the large magnets.

The LRM's functionality was tested by putting a single stirrer in the lid and testing it on the LRM device. This stirrer showed a regular consistent movement by following the LRM's platform. Furthermore, arranging stirrers in the lid as shown in Figure 6-8 B generated a regular movement. However, when placing the stirrers next to each other the stirrers did not move (see Figure 6-8 A). At that time of prototyping only ten 3D printed stirrers were available, therefore limiting the number of possible configurations which could be checked.

From the results obtained it was hypothesised that the magnetic strength of the magnetic discs attached to the each of the Mörs stirrers is bigger than the magnetic strength of the two large magnets of the LRM. Thus, the magnet interaction of the Mörs stirrer's is greater than the LRM magnetic strengths, as a result the Mörs stirrers are not lead by the LRM. In order to explain and optimise this observation the magnetic field strengths in the system was measured with a Gauss meter (Chou & Yeh 2008). Theoretically, two approaches may be possible to improve the magnetic flux in the system. Firstly, it may be possible to rearrange the configuration of the large magnets on the LRM to strengthen and increase the magnetic flux. Secondly, the magnetic strength of the Mörs stirrer magnets may be weakened by a different magnet arrangement. Alternatively, the Mörs stirrer magnets may be changed.

Measuring magnetic strengths

Firstly, the magnetic strengths between the two large magnets on the actual placement of the 96 well plate can be assessed. Secondly, the magnetic strength of a single magnet can be measured, and it may be possible to predict the magnetic strength by calculating the interaction with a second magnet (Holstein & Primakoff 1940). This way it may be possible to examine if a turn of the large magnets would increase the magnetic field. In addition, the magnetic strengths of the Mörs stirrer may be measured starting at the magnetic disc itself followed by measuring the magnetic strength at different distances. Thereby addressing the central question of how much actual magnetic strength is transmitted to the neighbouring wells on the 96 well plate.

Initially three measurements using a Gauss Meter were performed. Firstly, the magnetic strengths on actual stirrers position across the 96-well plate in-between the large magnets with the moving magnet were measured. Secondly, the probe was kept in the same position as measurement 1, but the lid of the large moving magnet was removed. With this measurement it can be determined if the material weakens or interrupts the magnetic flux. Thirdly, the magnetic strength of the magnetic disc of the Mörs stirrer was measured by starting at the disc outer touching point and finishing at the next well.

Results magnetic strengths

1. Actual magnetic strengths in-between the large magnets

The measurement shows that the strongest magnetic field can be found at the magnet with a value of 20 mT. The magnetic strength then continuously drops and reaches a minimum value at the middle of the 96-well plate length of 1.2 mT.

2. Actual magnetic strengths in-between the large magnet but without LRM box lid

The probe was kept at the same height as in measurement 1, but the lid of the large moving magnet was removed. It was found that there was no difference compared to measurement 1. This confirms that the magnetic flux is not interrupted by the plastic lid of the box.

3. The magnetic strength on the outer edge of the magnetic disc

The magnetic disc strength was measures to be 108 mT. At a distance of 4 mm, which approximately corresponds to the next well distance, the magnetic strength was measured to be 6 mT. At a further distance of 8 mm, which is approximately corresponds to the distance to the next well thereafter, the magnetic strength was measured to be 1.82 mT.

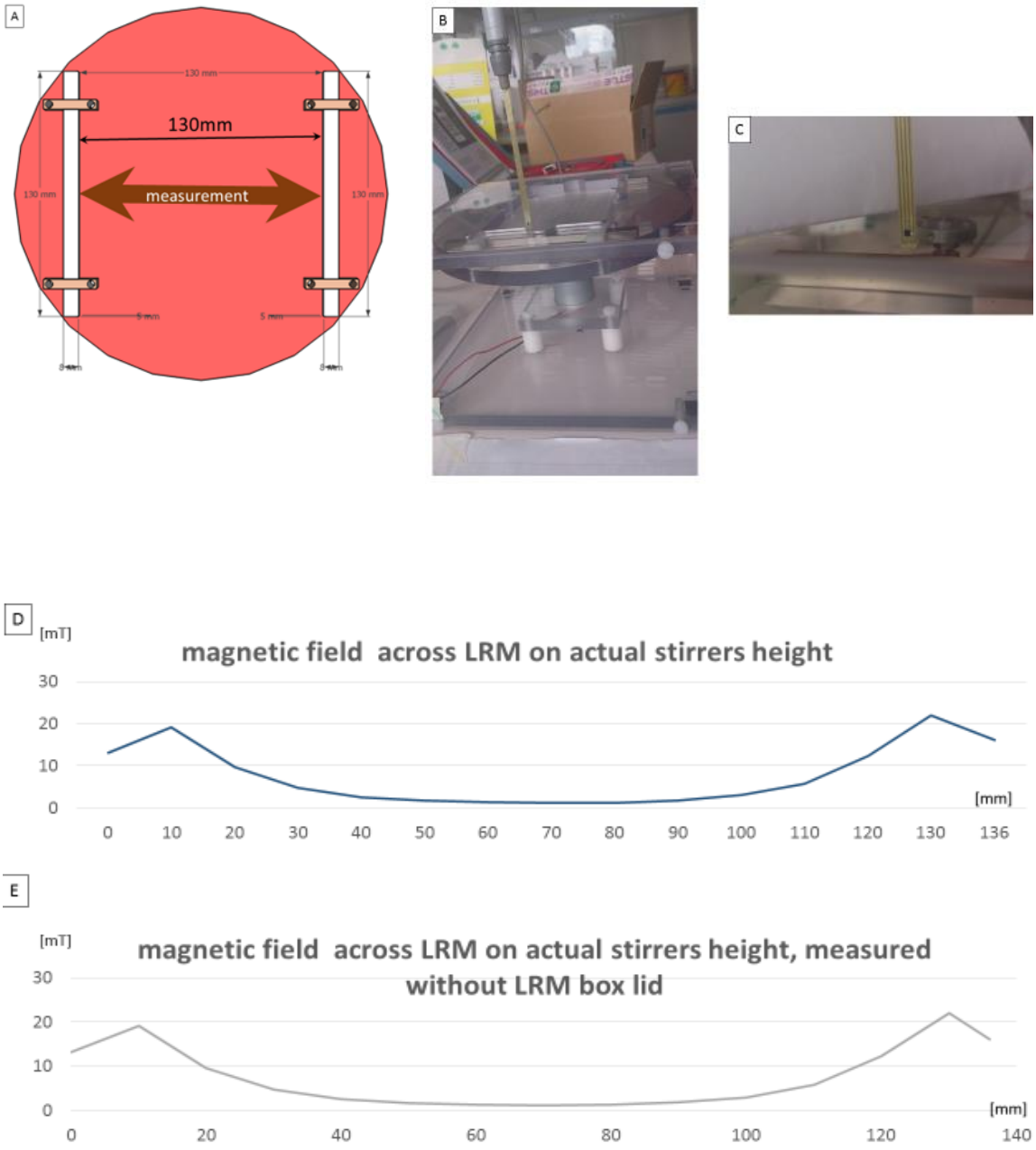

Figure 6-9 Magnetic strength LRM magnets

The figure shows the magnetic strength across the LRM created by the two large magnets (Panel A) measured with and without box lid (Panel B and Panel C). The result in panels D and E shows, that the magnetic strength is the same in both cases; thus, demonstrating that the transmitted magnetic field is not altered by the box lid.

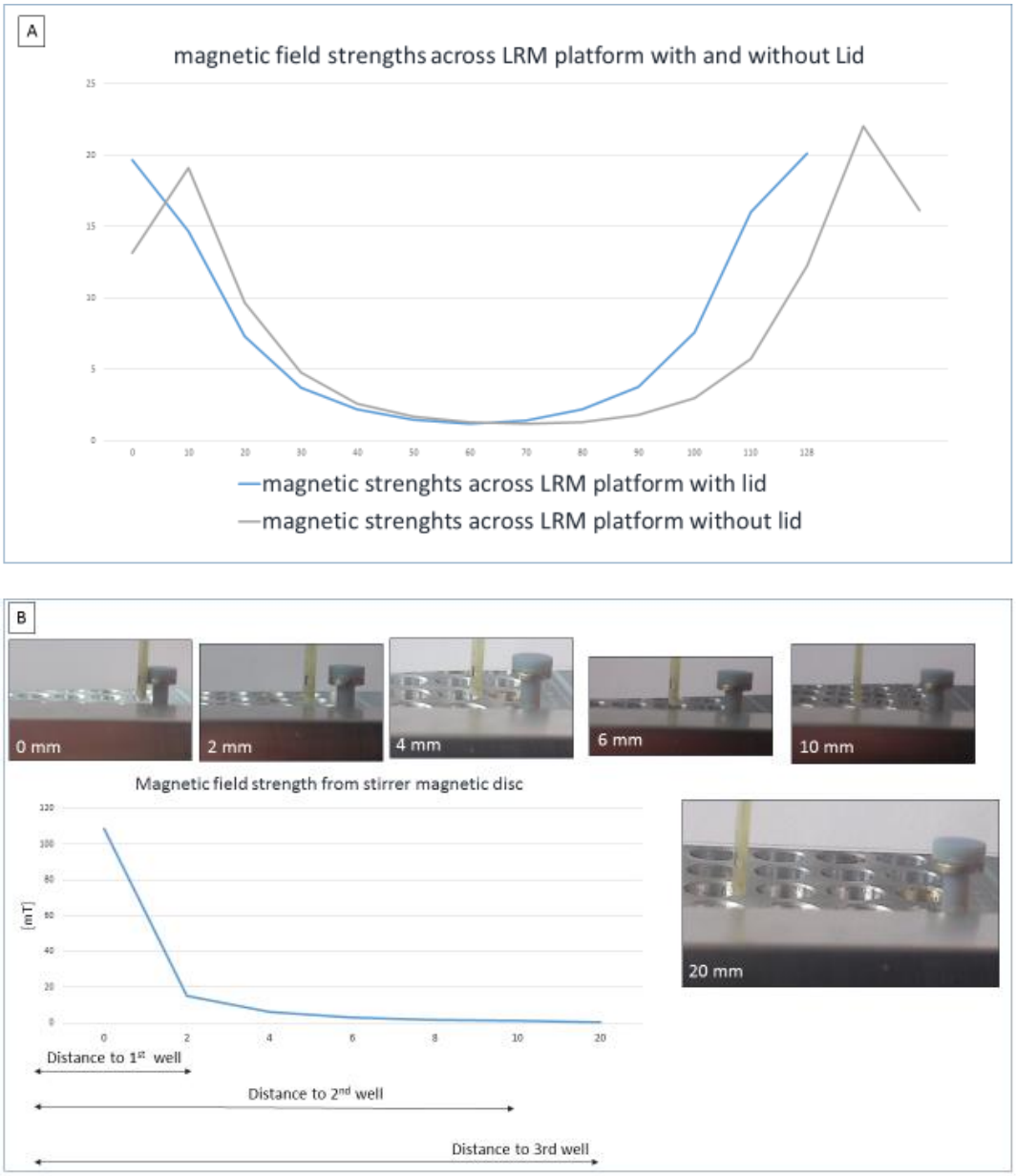

Figure 6-10 Magnetic strength measurements

The figure shows in Panel A the magnetic strength across the LRM created by the two large magnets, measured with and without box lid. The result shows, that the magnetic strength is the same in both cases. The curve shift can be explained by placing the probe at slightly different measuring points.

Panel B illustrates the magnetic strength of the magnetic disc at the stirrer. The magnetic strength was measured at different distances in order to predict the drop off to the neighbouring wells.

Discussion and troubleshoot magnetic strengths measurement

The measurements explain the different movements of the stirrers depending on the arrangement in the lid. The magnetic discs of the Mörs stirrers are much stronger than the magnetic field created by the large moving magnet device. Therefore it can be concluded that the magnets of the Mörs stirrers interact strongly with each other. However, in order to control the Mörs stirrers the magnetic strengths of the moving magnet device should be greater than the interaction strength of the Mörs stirrers. Therefore investigations were conducted if the magnetic strength can be improved, by turning the LRM magnets.

For the first optimisation measurement the probe was moved, closer to magnet to test if magnetic field strength increases. It was also hypothesised that a decrease in the thickness of the lid box, in addition to altering the positioning of the 96 well plate and the Mörs stirrers so that they are closer to the moving magnet, may create a stronger magnetic field transmitted by moving magnet device. For the measurement the probe was positioned at the outer edge of the large magnet and was measured at the opposite side of the other magnet. The measured values show that the actual magnetic field is weaker than in the current position. The weakest magnetic field was found in the middle of the 96 well plate length of 0.68 mT. This result may be explained by the magnetic curve formation.

For the second optimisation measurement the magnetic strength of a single large magnet was measured towards the outer side. It was hypothesized that it is possible to predict the magnetic strength of two opposing magnets by measuring the strengths of a single one. Since the magnet interacts with the opposing magnet, it was hypothesised that the measured values can be multiplied by a factor of two in order to estimate the magnetic strength of two interacting magnets. Since the actual measurements of the magnetic strength in-between the two large magnets were already performed, this method has the potential to verify whether the magnetic strength prediction is a valuable method. The result shows (see Figure 6-11) that the measured and the predicted magnetic strengths are in the same range. Therefore, it was concluded that it is a valid method to predict the magnetic strength.

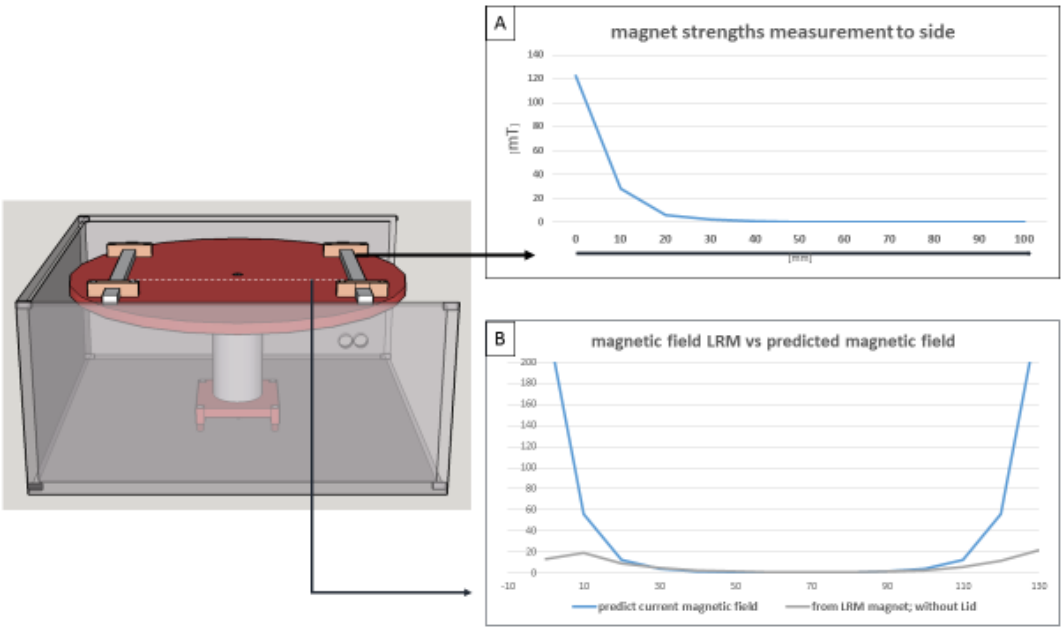

Figure 6-11 Verification of magnetic strength prediction

The figure illustrates the validation of the magnetic strength prediction method. Magnet strengths measurements starting at the magnet and measured towards the outside of the LRM device were taken (Panel A). Values obtained were multiplied by two in order to predict the actual magnetic strengths from a second interacting magnet.

Panel B compares the predicted magnetic field strengths to the actual measured magnetic strengths of the LRM. The comparison shows that the predicted magnetic field is similar to the actual magnetic strength. Therefore this method was considered to be valid for the prediction of the magnetic strength in the case of a magnet turn, which may result in a magnetic strength increase. The increased magnetic strength may be helpful in order to address the stirrer moving issue, as described in the text.

6.2.3.1 Optimisation

It has been found that stirrers do not move in a smooth consistent way when placed next to each other and exposed to the LRMs magnetic field. Therefore, magnetic strength measurements have been performed and it has been found that the magnetic strength of the LRMs magnet is not strong enough. In order to increase the magnetic strength it was tested if a magnet turn on the LRM platform may address the found issue.

For this purpose the vertical magnetic field at several distances above one large magnet were measured. In the case of a magnet turn this side would be directed towards the middle and opposite the other large magnet. The measurement shows that the single magnetic strength at a distance of 64 mm, which is approximately the middle of the 96-well plate, is found to be 2.31 mT. Since the magnet would experience an interaction with the opposite large magnet this strength can be doubled. This method was validated as described in the previous section (see Figure 6-11).

The result of the predicted magnetic turn shows that the system would benefit from an increase of the magnetic strength (see Figure 6-12). Consequently, the magnet's turn was fulfilled by stamping the magnets width as an area in the LRM's platform whilst being held with brackets. Subsequently, the stirrer's configuration was re-tested, showing an improvement of the stirrer's movement. However, it was also found that the stirrers were only functional when only every other well was equipped with a stirrer. This observation is congruent with the result obtained from the predicted magnetic strengths measurement. Figure 6-12 B illustrates that the magnetic strength of the stirrers is still greater even with the magnet turn. In addition, the interaction of the stirrer's magnet have not been taken into consideration (Holstein & Primakoff 1940). Consequently, it is likely that the actual interaction of the stirrer magnets drastically increases the shown magnetic strengths (see Figure 6-12). In order to address this issue either stronger LRM magnets or weaker stirrer magnets need to be used. Alternative commercially available magnets could not be found in the required dimensions. Therefore an alteration of the magnetic disc positioning on the Mörs stirrers was tested (see Figure 6-13). However, when the altered Mörs stirrers were tested in the system the stirring motion was not improved.

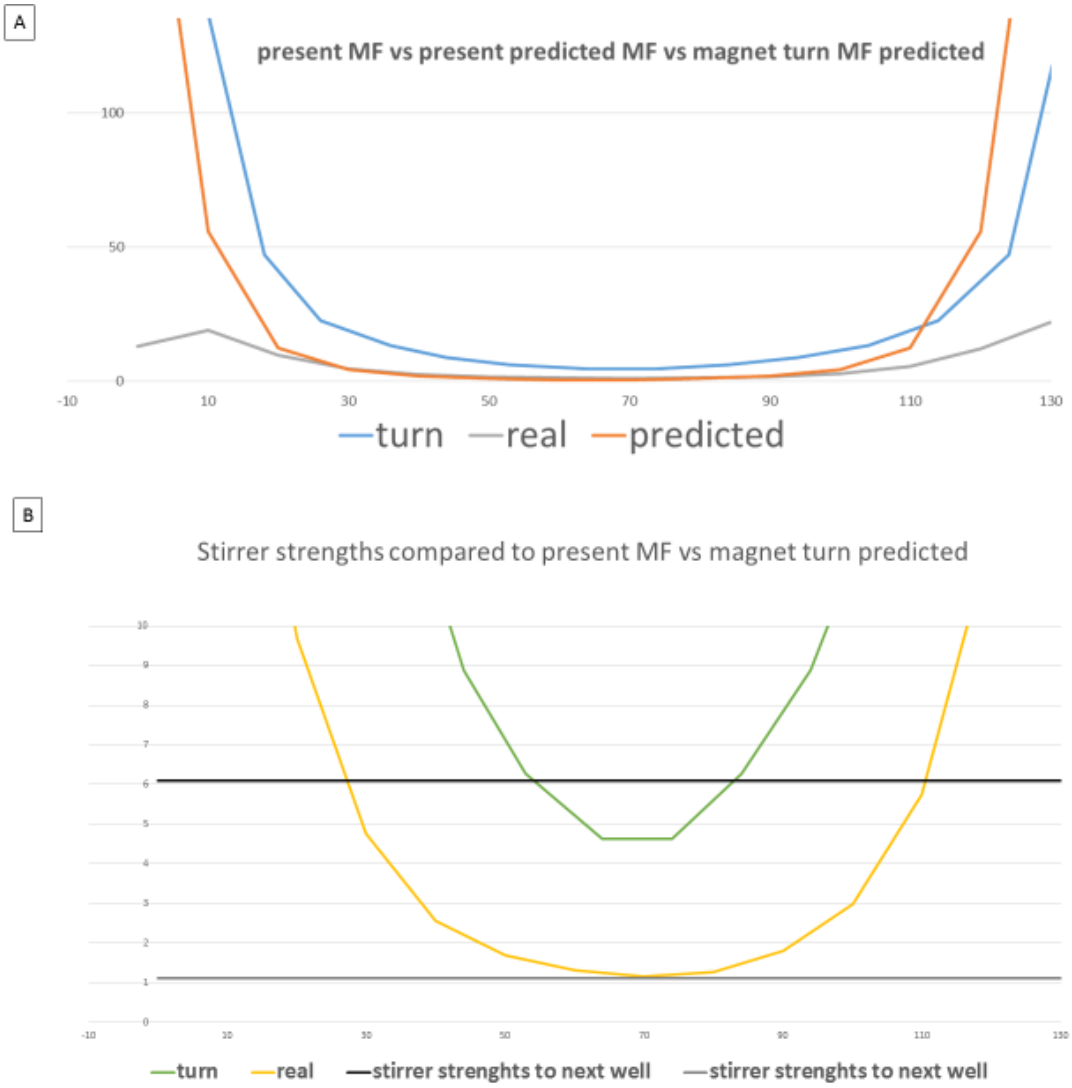

Figure 6-12 LRM's magnet turn - predicted magnetic field strengths

Shown in this figure are results obtained from predicting the magnetic field (MF) if the LRM magnets were turned by 90°.

Panel A compares the MF strengths without turn including predicted results obtained from this configuration as well as the predicted MF strengths of the magnet configuration when being turned.

Panel B illustrates the effects of the magnet turn by plotting the curves of no turn and turn in comparison with the stirrers MF strengths.

Results obtained show that the MF strengths can be improved by turning the magnets by 90° on the LRM platform.

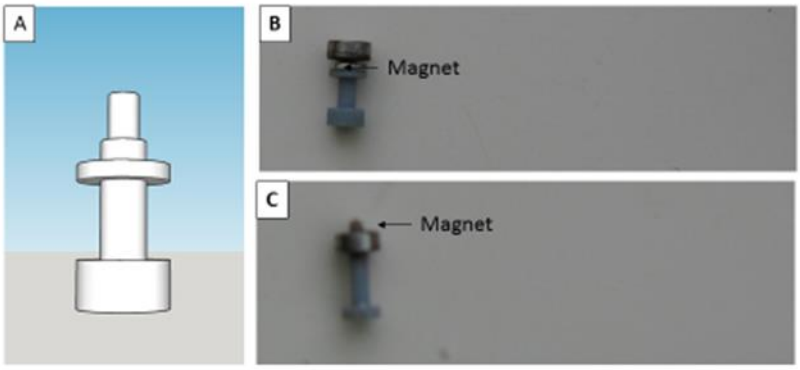

Figure 6-13 Altered stirrer design

The figure illustrates attempts to alter the stirrer design to improve magnetic flux and the number of stirrers which can be used in the system. The principal idea is an offset arrangement of upper and lower placed magnets on the stirrers thereby reducing the magnetic interaction of the stirrers' magnets. Panel A shows a CAD drawing with a second platform to hold the magnetic disc, thereby the stirrer's tip has been elongated by the width of the magnetic disc. Panel B displays the 3D printed stirrer assembled with magnetic disc and ball bearing. Panel C shows a classic stirrer design, but without magnetic disc on the stirrer's tip. Instead a bar magnet was glued on the mobile ring of the ball bearing.

6.2.3.2 Validation

Speed validation

The LRMs rotational speed depends on the voltage input to the motor (Ventura *et al.* 2014). For example, an increase in voltage input results in an increase of the platforms rotation, and consequently, in an increase in the stirrers rotational speed which subsequently leads to an increase in shear stress applied to the cultured cells (Buschmann *et al.* 2005). Therefore it is crucially important to relate voltage input numbers to the resulting rotational speed. Given a known stirrer placement in the wells it is then possible to estimate the applied shear stress (Spruell & Baker 2013).

In order to validate the rotation speed the voltage input was changed in steps of 10 bits and three different videos have been taken. Videos were validated by counting frames in-between one fulfilled round of one of the magnets on the LRM's platform. Given the camera records 30 frames per second, this data in combination with the counted number of frames for one successful round allows the calculation of the respective rpm number. The result shown in **Error! Reference source not found.** illustrates bit inputs in resulting rpm number of the LRM. Numbers were interpolated in-between the counted 10 bits marks. The result shows that a maximal rpm number of 200 can be achieved with the maximal bits input of 255.

Gas exchange

Gas exchange probabilities have been tested using the final prototypes of this project, namely the customised aluminium lid (see Figure 5-4) and the LRM. A sufficient gas exchange is crucially important for the cells cultured in the multi well plate (Saalfrank *et al.* 2015).

In order to validate the gas exchange possibilities two plates with HUVECs were seeded. The cells were allowed to attach to the multi well plates overnight. Subsequently, one plate was placed on the LRM with attached lid whereas the second plate was placed in the incubator next to the LRM device. After 24h cell morphology and media colour was examined (see Figure 6-15). The cell phenotype and the media colour was similar in the two plates. These observation lead to the conclusion that the system provides a sufficient gas exchange to culture mammalian cells *in vitro*.

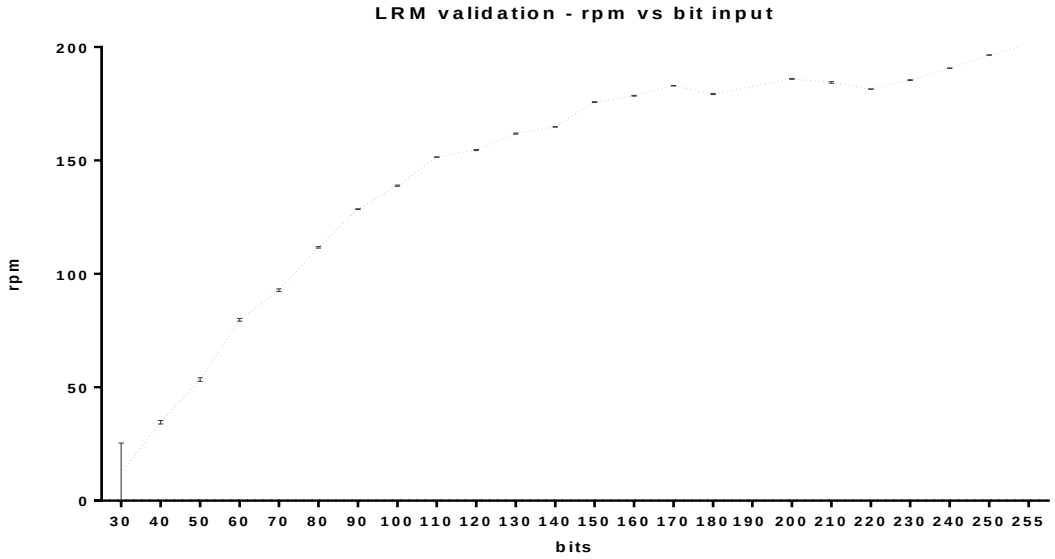

Figure 6-14 LRM speed validation

The figure relates the voltage input to the achieved rpm number. The bit number was changed in steps of 10 bits and videos of the rotating platform were taken. Frames in-between one full platform round were counted. With help of the frames per second camera specification the respective rpm number was calculated. Three different videos of one bit input were taken and each video was analysed by counting five successive rounds per video. The maximal bit input of 255 can create 200 rpm.

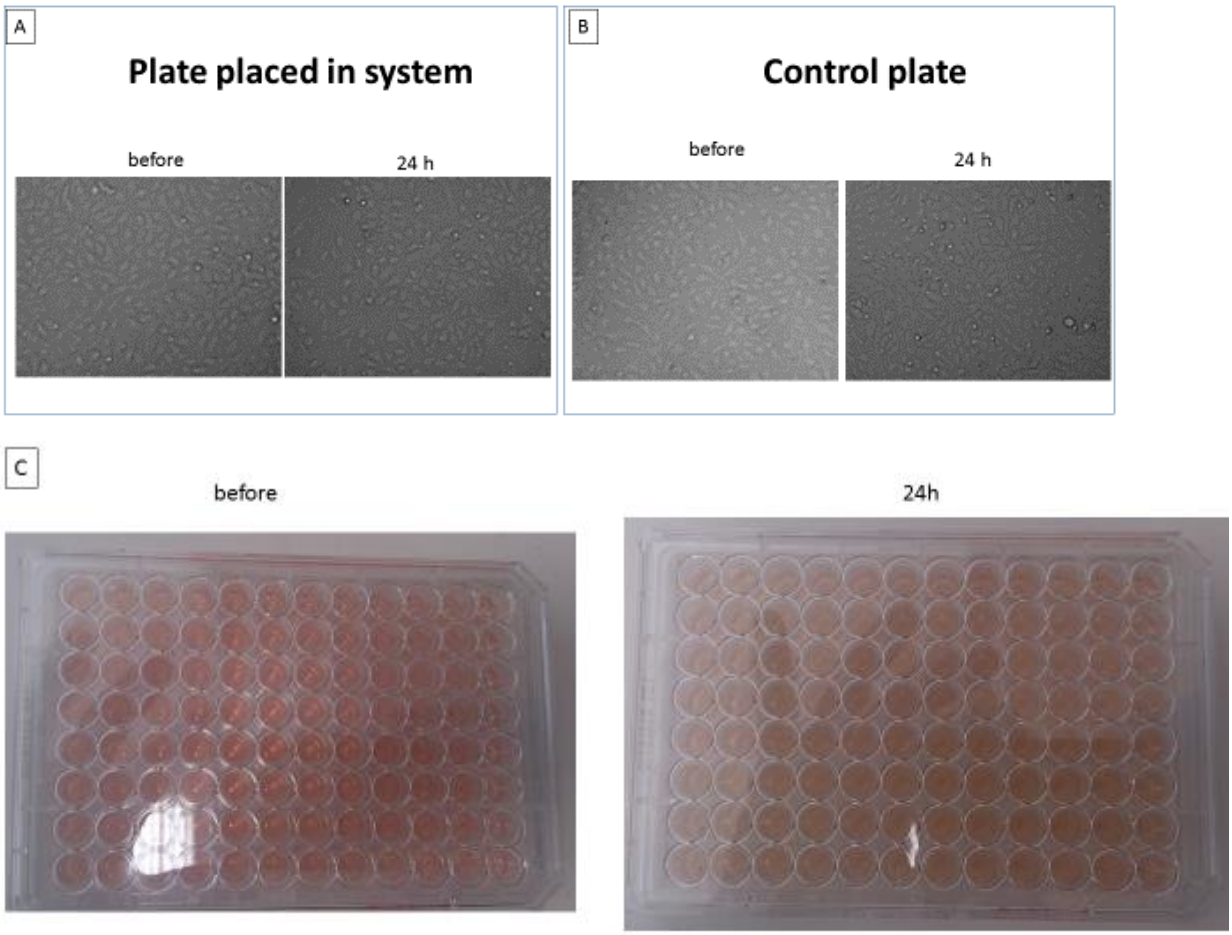

Figure 6-15 LRM and lid gas exchange validation

The system was tested for gas exchange possibilities in order to verify that the system is suitable for in vitro cell culture conditions. Two plates of cultured HUVECs were placed in the cell culture incubator either on the novel developed system or placed beside as a control plate. Panel A shows pictures of the cells in the novel system before placing in the LRM and 24 h after. Panel B shows pictures of the control plate. Panel C shows pictures of the plates in the novel system to compare the media colour, which an indication of gas exchange.

Overall the result indicates that the LRM and the lid provide the cells with a sufficient gas exchange.

6.3 Discussion

The moving magnet device occupies the function of rotating magnets in order to move the stirrers in the wells. The first prototype used to fulfil this function was a commercially available laboratory magnetic stirrer hotplate, commonly used in the laboratory to mix substances. This prototype was found to be functional for a limited number of wells. Further investigation has shown that this is caused by the magnetic configuration of the stirrer. Using this prototype flow was applied to HUVECs and subsequent immunofluorescent staining of the cytoskeleton, the nuclei and the cell junction protein VE-Cadherin was performed (Ross *et al*. 2013). Application of flow caused an altered cell morphology compared to static conditions (Davies 2011). In particular a rearrangement of the cytoskeleton was observed, strongly indicating a successful application of shear stress (Tzima *et al*. 2005). Thereby verifying the principal functionality of the device presented in this dissertation.

However, in order to increase throughput numbers and therefore the effectiveness of the novel system, a device addressing the limitations was built. This device name: large rotating magnet, indicates that the device works with large magnets. Therefore the distance between the magnets was set to enclose a 96 well plate. With an increased distance it was aimed to achieve a linear magnetic field across the full lengths of a 96 well plate, which was intended to guarantee a smooth movement of the stirrers in the wells. The LRM's speed and direction is fully controllable by the motor attached to the Arduino microcontroller (Williams 2013).
During practical tests of the LRM it was found that the device works well itself, however, during the validation process and practical application limitations were found.

Mörs stirrer moving issue

It was found that Mörs stirrers placed close to each other in the lid were not moved by the LRM. In order to address this issue magnetic strength measurements were performed, investigating the magnetic strengths of the LRM magnets as well as the stirrer magnets. Results obtained indicate that the magnetic strength of the LRM magnets were too weak to be fully functional for the stirrers movement. From the results obtained it was possible to improve LRM's magnetic strengths by a magnet turn of 90^{o}. In addition an altered magnetic configuration and a different type of magnet attached to the stirrer did not show an improvement.

However, further optimisation work needs to be done to address this issue. Ideally either stronger LRM magnets or weaker stirrer magnets can be found, or could be manufactured for the intended purpose. In addition, a magnetic shield may be used on top of the lid (Schweizer 1962). The magnetic shield thereby would reflect the magnetic field towards the stirrers and LRM. Therefore it could be possible to increase the magnetic strength from the LRM. However, this could also result in an increase of the stirrer magnet strength. Another possibility might be to use magnetic shielding material in-between the 96 well plates. This way, the stirrer's magnets cannot interact with each other anymore. However, this also bears the risk of shielding the LRMs transmitted magnetic field.

Another idea may be to work with a stirrer containing an enclosed magnet, as suggested in 4.2.3. However, instead of the magnetic disc a small permanent magnet may be used in order to reduce magnetic strengths (Herbst 1991). To a certain extent this was tested, see Figure 6-13 C. However, this attempt was limited since a sufficient attachment site can only be found on top of the stirrers tip, or as shown in the figure, on top of the ball bearing. However, ideally the bar magnet's mid-point would be placed at the horizontal stirrer axis mid-point.

Speed validation

The speed validation shows that at a maximal bit input of 255 the resulting rpm number is 200. Since the device shall be optimised to have a gap distance of 100 µm and a cone angle of 2°, the mathematical approach from Spruell & Baker 2013 may be applicable. Therefore a shearing force of 0.5 Pa would be applied when using the maximal possible voltage input. Consequently, the motor could be changed in order to increase the rotational output.

A motor should be chosen with a higher voltage and/or an increased stall torque. Alternatively the weight of the platform and magnets could be reduced. However, regarding the light weight of the PMMA material this would be challenging (Ali *et al.* 2015). In order to gain a 1.5 Pa shearing force the angular rotation should be 350 rpm.

Gas exchange

Results obtained from the gas exchange validation showing that the device, in combination with the aluminium lid, is fully compatible with culture of mammalian cells within the device *in vitro* (Saalfrank *et al.* 2015).

7 Flow application of latest prototypes

7.1 Introduction

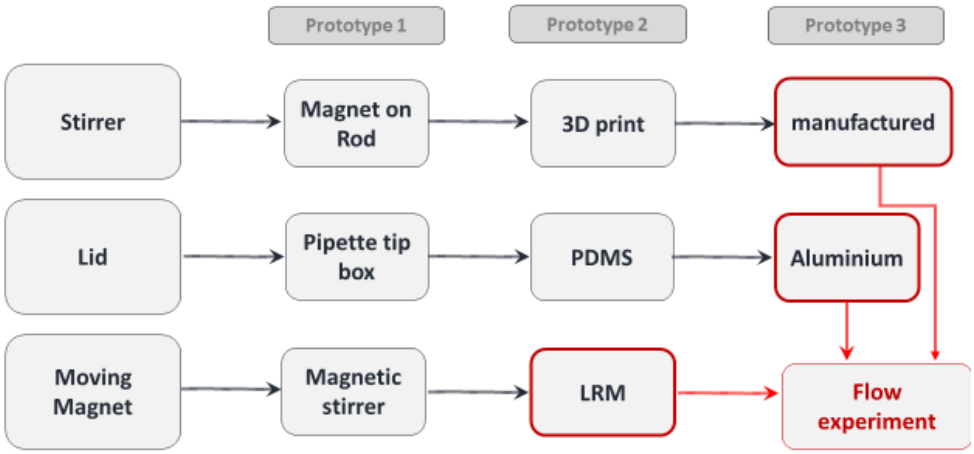

A flow experiment was performed using the manufactured stirrers (see 4.2.3), the aluminium lid (see 5.2.3) and the LRM (see 6.2.2). Shear stress was applied to HUVECs cultured in a 96 well plate for 6 h. This time point was specifically chosen, since previous results indicate no significant change of selected genes caused by the magnet's coating (see 4.2.2). The experiment was performed in the cell culture incubator and using static conditions as a control plate (O'Keeffe *et al.* 2009b). In order to inhibit corrosion of the LRM device, which could be caused by humidity, a bag with silica beads was placed in the LRM box (see Figure 7-1 Panel A).

The LRM was programmed to gradually increase rpm number. The gradual increase of the rpm number was found to be laboratory standard; cell loss was observed when cells were exposed to higher shear stress numbers without adaption time.

Total RNA using cells from 10 wells were pooled and the mRNA was then used to identify transcriptional levels of eNOS, e-selectin, MCP1 and c-jun, which were proven to be flow responsive using the orbital shaker system (see Figure 4-3; Dardik *et al.* 2005b). The experiment was repeated three times using independent donor cells. The stirrers were distributed across the 96 well plate and a functional stirrer movement was carefully tested before running the experiment. In addition, immunofluorescence staining of the nuclei as well as VE-Cadherin was performed by applying 200 rpm for 12 h (Gulino-Debrac 2013).

It was hypothesised, that a transcriptional as well as phenotypical change would be apparent compared to control cells, thereby verifying the prototypes presented in this thesis.

7.2 Results

qPCR

The qPCR result indicates that transcriptional levels of selected flow responsive genes are altered. MCP1 and e-selectin show a decrease,and eNOS and c-Jun an increase, of relative mRNA expression normalised to static cells (see Figure 7-1). Differences between mRNA levels were calculated by an un-paired, two tailed t-test showing a significance of $p<0.05$ for e-selectin.

Immunofluorescence staining

The immunofluorescence staining of nuclei and VE-Cadherin shows an altered phenotype following exposure to shear stress compared to static cells. The flow treated cell nuclei size appears to be reduced and the VE-Cadherin levels appear to be increased. Furthermore it can be detected that cell number is reduced compared to static cultured cells (see Figure 7-2).

Programming

The programme was written to gradually increase the rotational speed of the LRM by increasing the bit number by 10 between configurations (see Table 7-1). The setup pin configurations were chosen as follows: pin 12 was defined as the output break for motor channel A; written: pinMode (12, OUTPUT);. pin 9 was the functional break for pin 1; written: pinMode (0, OUTPUT);. The pin configuration execution of pin 12 was chosen to be high in order to achieve a forward rotation of the motor; written: digitalWrite (12,HIGH);. Since a constant motor rotation was desirable the respective break of pin 9 was disabled; written: digitalWrite (9, LOW);. In order to control rotational speed the analog written PWM needed to be written in addition in the programme. Thereby pin3 function is the PWM, by writing the bit input number the rotational speed can then be defined; written: analogWrite (3,40);, in this case 40 bits input. The previous obtained result of validating the LRM's rotational speed relates the bit input to respective rpm output of the LRMs platform (see **Error! Reference source not found.**. Bit inputs were chosen to gradually increase in steps of ten and each bit input was applied for 300000 ms before the following input was applied; written: delay (300000);. The final 255 bit input was written as loop and the flow application was stopped manually.

B

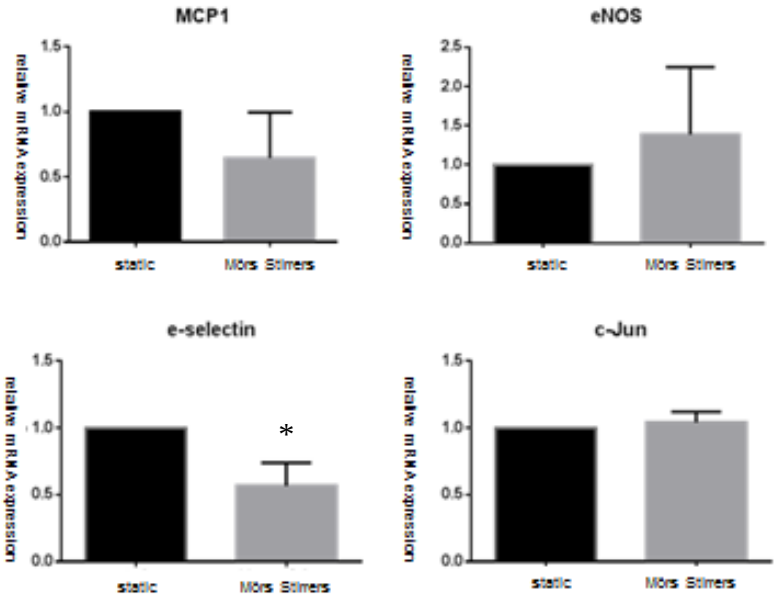

Figure 7-1 qPCR results using final prototypes

The figure shows results obtained from a flow experiment using the final prototypes of the novel device. Panel A is picture taken from the Mörs stirrers placed in the cell culture incubator. Panel B shows the result obtained from the transcriptional analysis. Shear stress at a rotational speed of 200 rpm was applied to 10 wells of a 96 well plate for 6 h. Wells were pooled and total RNA was isolated and relative mRNA levels of e-selectin, c-Jun, MCP1 and eNOS were quantified by qPCR. Data shows three independent experiments and the mean level of mRNA is shown including the standard errors. Differences between mRNA levels from flow applied cells and control cells and were calculated by an un-paired, two-tailed t-test. It was found that E-selectin expression shows a difference of $p<0.05$.

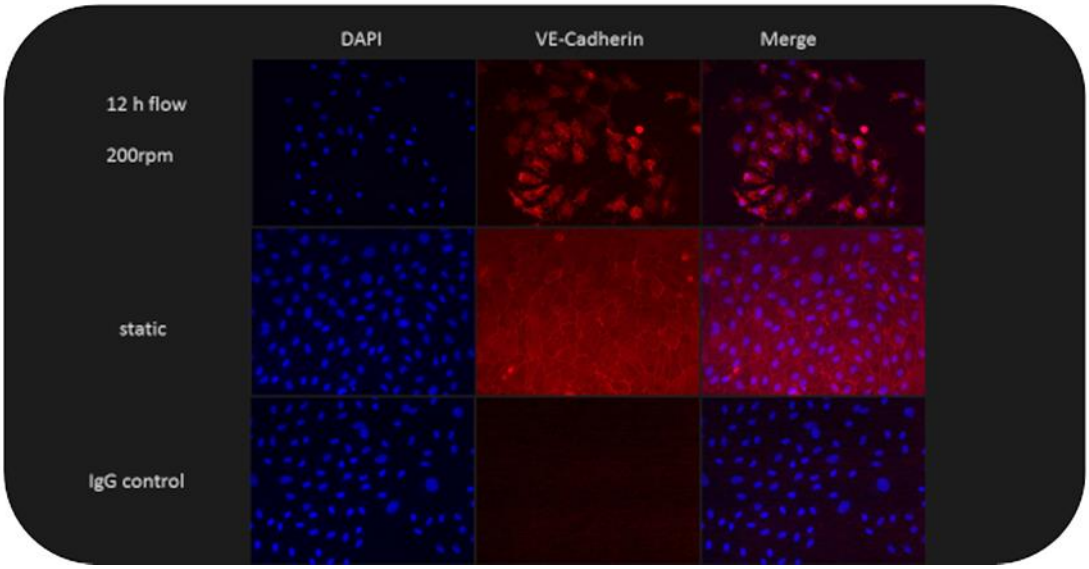

Figure 7-2 Immunofluorescence staining result using final prototypes

The figure shows results obtained from immunofluorescence staining of flow treated cells using the final prototypes of the Mörs stirrers. A rotational speed of 200 rpm was applied for 12 h on cultured HUVECs. Subsequently cells were stained with DAPI, shown in blue, and VE-Cadherin, shown in red. The figure also presents a merged picture, in order to identify the VE-Cadherin location. Species-specific IgG control was used as negative control.

VE-Cadherin levels appear to be increased whereas the nuclei size seems to be reduced in the flow treated group. The IgG control does not show any staining. In addition, less cells are noticeable in the flow treated group.

Table 7-1 Programme: 200 rpm, unidirectional, with gradient

Cell 1 - start	Continue from cell 1

void setup() {
 	
pinMode (12, OUTPUT);
 	
pinMode (0, OUTPUT);
 	
digitalWrite (12,HIGH);
digitalWrite (9, LOW);
analogWrite (3,40);
delay (300000);
 	
digitalWrite (12,HIGH);
digitalWrite (9, LOW);
analogWrite (3,50);
delay (300000);
 	
digitalWrite (12,HIGH);
digitalWrite (9, LOW);
analogWrite (3,60);
delay (300000);
 	
digitalWrite (12,HIGH);
digitalWrite (9, LOW);
analogWrite (3,70);
delay (300000);
 	
digitalWrite (12,HIGH);
digitalWrite (9, LOW);
analogWrite (3,80);
delay (300000);
 	
digitalWrite (12,HIGH);
digitalWrite (9, LOW);
analogWrite (3,90);
delay (300000);
 	
digitalWrite (12,HIGH);
digitalWrite (9, LOW);
analogWrite (3,100);
delay (300000);
 	
digitalWrite (12,HIGH);
digitalWrite (9, LOW);
analogWrite (3,110);
delay (300000);
 	
digitalWrite (12,HIGH);
digitalWrite (9, LOW);
analogWrite (3,120);
delay (300000);
 	
digitalWrite (12,HIGH);
digitalWrite (9, LOW);
analogWrite (3,130);
delay (300000);
 	
digitalWrite (12,HIGH);
digitalWrite (9, LOW);
analogWrite (3,140);
delay (300000);
 	
digitalWrite (12,HIGH);
digitalWrite (9, LOW);
analogWrite (3,150);
delay (300000);
	digitalWrite (12,HIGH);
	digitalWrite (9, LOW);
	analogWrite (3,160);
	delay (300000);
	
	digitalWrite (12,HIGH);
	digitalWrite (9, LOW);
	analogWrite (3,170);
	delay (300000);
	
	digitalWrite (12,HIGH);
	digitalWrite (9, LOW);
	analogWrite (3,180);
	delay (300000);
	
	digitalWrite (12,HIGH);
	digitalWrite (9, LOW);
	analogWrite (3,190);
	delay (300000);
	
	digitalWrite (12,HIGH);
	digitalWrite (9, LOW);
	analogWrite (3,200);
	delay (300000);
	
	digitalWrite (12,HIGH);
	digitalWrite (9, LOW);
	analogWrite (3,210);
	delay (300000);
	
	digitalWrite (12,HIGH);
	digitalWrite (9, LOW);
	analogWrite (3,220);
	delay (300000);
	
	digitalWrite (12,HIGH);
	digitalWrite (9, LOW);
	analogWrite (3,230);
	delay (300000);
	
	digitalWrite (12,HIGH);
	digitalWrite (9, LOW);
	analogWrite (3,240);
	delay (300000);
	
	digitalWrite (12,HIGH);
	digitalWrite (9, LOW);
	analogWrite (3,255);
	
	delay (300000);
	}
	
	void loop(){
	
	digitalWrite (12,HIGH);
	digitalWrite (9, LOW);
	analogWrite (3,255);

7.3 Discussion

The qPCR result may give an indication that transcriptional changes take place; however, the result is inconclusive. Therefore more repeats are necessary to perform as well as clarification about the applied fluid flow in the well. The shearing force could be estimated with the approach from Spruell and Baker 2013 which have performed a CFD of a rotating cone in a 96 well plate. Thereby the group investigated in different cone angles as well as different gap distances between cone tip and bottom of the well. By using this published publication'smathematical considerations shear stress applied would be approximately 0.5 Pa, given a gap distance of 100 µm and a cone angle of 2°. However, previous attempts to measure the gap distance (Figure 4-6) indicate that the gap distance present is greater than 100 µm, which would decrease the shear stress applied to the cells (see Equation 2-9). Furthermore the gap distance experiment indicates that a cone angle is present, however, this was not successfully quantified. Moreover, smoothness of used materials differs from the mathematical approach, which will have an effect on the fluid dynamics. Therefore it is crucially important to perform a CFD analysis of the novel device and furthermore, more repeats are needed to gain more evidence of transcriptional changes of gene expression due to shear stress manipulation.

For phenotypical changes were treated to flow for 12 h. Overall it was observed that phenotypical changes occurred by applying flow with the Mörs stirrers. After 12 h the cell's morphology changed compared to the static control cells.. Moreover, due to the 12 h application, knowing the cytotoxic effects of the stirrer's magnet, the cell loss was presumably due to apoptosis and is apparent compared to the static cells. In general it was noticed that the auto-fluorescence of the 96 well's plastic is not ideal for fluorescence microscopy (Piruska *et al.* 2005).

qPCR

Mörs stirrer flow application changes transcriptional level of selected genes

Overall there is not enough evidence of transcriptional changes of HUVECs treated with fluid flow using the final Mörs stirrer prototypes. Furthermore are the results obtained inconclusive considering previous results obtained from the orbital shaker experiment,

Unfortunately, the number of manufactured stirrers was limited therefore the static control was performed without stirrers in the well. All available stirrers were used in the flow experiment in order to gain a sufficient amount of RNA. Although the previous biocompatibility experiment (see Figure 4-5) indicates no transcriptional change of the selected genes in cells exposed to flow after 6 h, an experiment using static cells with stirrer exposure would further assure that the transcriptional changes are indeed induced by flow. However, the comparison of mRNA levels from both experiments (flow treated cells and static biocompatibility test with stirrers) shows an opposite trend of e-selectin expression. Flow treated HUVECS show a decrease, whereas cells with exposure to the stirrers but without flow application show a slight increase, both normalised to static cells without stirrers. However, further evidence is needed to support this observations.

Comparing flow systems? Mörs *stirrer vs orbital shaker*

ResBoth platforms use the movement of the cell culture media as a source to create the shearing force on the cultured cells. The orbital shaker is a well-established system in the scientific community.However, could results obtained from the orbital shaker be compared to the novel device?

In order to answer this question both systems and experimental setups must be critically reviewed in depth.

Firstly, there are different time scales; the orbital shaker experiment was set up for three days whereas the Mörs stirrer experiment was set up for 6 h. Taking that into consideration, it may be possible that shear stress responses are time depended and short-term signalling may differ from the long term response. In addition, the orbital shaker gene expression was normalised to the high shear region. Results of an orbital shaker experiment for 6 h normalising low shear regions to static cells would give further insights.

Secondly, differences may be found considering the specificity of low shear stress applied. By definition low shear stress describes flow with a low magnitude. However, CFD analysis of the orbital shaker describes the centre region as low and oscillatory shear stress, implying low amplitudes but also different velocity directions (Warboys *et al*. 2014). No CFD analysis has been performed for the Mörs stirrers at present, consequently a fluid dynamic comparison is not possible. However, these two systems present different types of low shear stress, caused by the nature of mechanical

movement, namely: shaking vs stirring. Thereby the amplitude may be the same, however, oscillation could influence the cell signalling response.

Thirdly, the cellular responses are different as the shear stress distribution differs across the wells. The 6 well on the orbital shaker experiences high and low shear regions in the same well (Warboys *et al*. 2014). This may effect signalling of the centre regions which may be changed by biochemical signals from the high shear region. Looking at the Mörs stirrer well, theoretically, we should find predominantly a low shear stress region, except in the mid-point of the well and the outer region between stirrer and well wall (Spruell & Baker 2013). In theory these two regions shall be subjected to no flow. However, the no flow region of the 96 well may be neglected at the current theoretical configuration, due to the small surface area. Taken together, the 6 well plate orbital shaker system reproduces signalling responses of merging low and high shear regions as can be found *in vivo*. In contrast, the current Mörs stirrer configuration may reproduce one specific shear stress pattern. Nevertheless, more capacities can be achieved by further understanding and optimisation the Mörs stirrers. Crucially important is the prediction of fluid dynamics in the well at the current configuration (Sucosky *et al*. 2008). Furthermore, different configurations shall be investigated such as greater gap distances, altered cone angles and stirrer diameter. These results could identify Mörs stirrer configurations which can be used depending on the scientific question asked. For example, if a greater gap distance is desirable this may induce a shear stress pattern similar to the orbital shaker. Consequently, the same device can be used in order to address different scientific questions. The Mörs stirrers have the potential to permanently change the way flow experiments can be conducted in the laboratory by simplifying the process and providing flexible configurations.

In summary, the Mörs stirrer is a self-contained system. Results obtained cannot be directly compared to results from the orbital shaker system.

8 General discussion

A strong relationship between haemodynamic forces and cardiovascular diseases has been found. Therefore *in vitro* flow application systems have been developed in order to investigate cell signalling in response to shear stress (Kroutvar & Guttenberg 2013; Dardik *et al.* 2005b). Those systems are based on the cell culture media motion in order to create the shearing force by pumping, shaking or stirring.

The device presented in this thesis functions on the basis of stirring a conical shaped stirrer in individual wells of a 96 well plate. Key advantages are user-friendliness, high throughput number as well as plate reader compatibility. Through several rounds of prototyping individual parts, it was possible to coordinate and match those parts to combine a working prototype. The functionality was tested by applying shear stress to cultured HUVECs; results obtained show that phenotypical and transcriptional cellular characteristics are altered in response to the shear stress created. However, due to a limited data set (n=3) results obtained must be critically reviewed. In particular more repeats must be performed as well as a better understanding of the actual applied shear stress distribution in the 96 well must be obtained in order to gain further insights. In due course the present inconclusive data set, compared to the orbital shaker result, can be explained accordingly.

Biocompatibility

Biocompatibility is a crucial factor for the proposed device in order to culture living cells and to achieve reliable results of the flow application. Non-biocompatible materials influence the cellular response and consequently it would be impossible to distinguish between cell-toxic and shear stress induced effects. Unfortunately, the 3D printed stirrers as well as the disc magnet were identified to be non-biocompatible. The 3D printed stirrers were subsequently optimised by manufacturing the stirrers with the biocompatible delrin material (Urban 1985). Nonetheless, 3D printing technology occupies greater advantages, in particular, regarding precision and reproducibility. Therefore, 3D print using biocompatible and strong materials, such as Ti-6Al-4V shall be considered (Tan *et al.* 2016). In combination with newest technologies, such as selective laser melting or selective electron beam melting, high precision and accuracy should be guaranteed. In addition, the titanium's high melting point will avoid stirrer deformation when placed in the cell culture incubator, as it was noticed with the 3D

printing material used in this project. Liu *et al*. 2004 investigated in biocompatible coating materials for titanium based biomedical applications, which could be applied for stirrers. Nonetheless, experiments regarding cell biocompatibility must be performed when coating procedures were applied. Furthermore, effect on the fluids dynamic must be considered due to different surface properties and an increase of the stirrer dimensions. The biocompatibility issue which arose from the magnetic disc is most likely due to the magnet's nickel and copper coating. Strategies to address this problem are either to change the magnet or prevent the magnet contacting the cell culture media. Unfortunately, it was impossible to find a diametrical magnetised magnet with the required dimensions, which was desired in order to keep the developed stirrer design. Consequently, it shall be considered to either manufacture magnets with biocompatible properties or apply a biocompatible coating such as silica, ceramic or parylene. Coating procedures use chemical vapour deposition in order to create a thin equal coverage on the magnet's surface as described by Sik Song *et al*. 2013 or Liu *et al*. 2004.
Alternatively, the manufacturing process could be changed in order to embed the magnet within the stirrers tip. This was attempted when the 3rd stirrer prototype was designed however, it was found technically not feasible with the available machinery. Therefore an improved manufacturing process may be possible. However, another way would be via 3D printing two stirrer parts. Thereby, the stirrers tip, including a platform fitting the magnet, and an exact fitting top could be printed individually. After the printing process the magnet can be placed in the tip's platform and the stirrer's top can be assembled mechanically or via gluing. Another possibility would be to use cutting edge 4D printing process using smart materials, a novel technology recently described by Momeni *et al*. 2017. Embedding the magnet may also improve fluid dynamics created by the stirrer. The stirrer presented in this project was built by attaching the magnet to the stirrers cone tip. However, by embedding the magnet this attachment side would become no longer necessary and the stirrer's cone tip would be smoothened.

The gas exchange biocompatibility test confirms a sufficient gas exchange when the cell culture plate is placed on the LRM enclosed by the lid. Thereby making sure that mammalian cells can be cultured under standard *in vitro* conditions.

Magnetic field

It was also found that the stirrer's movement is interrupted when placed closed to each other. Magnetic strength measurements were performed, which lead to the conclusion that the stirrer magnets were too strong for the intended purpose. Herbst 1991 published interesting insights of permanent magnets. Therefore, the stirrer's magnet could be exchanged with a permanent magnet with a lesser amount of magnetic strength. However, other possibilities could be considered. Firstly, the magnet could be partly demagnetised by heating it up close to their specific curie temperature. Secondly, a magnetic shield may be attached to the magnet. However, since magnetic shielding works on redirection of the magnetic field, the shielding material should only be used on the magnets outer side in order to block interaction with next well neighbouring magnets. This way the stirrer magnet would be able to receive the exposed magnetic field from the LRM. However, the stirrer's redirected magnetic field may interrupt the magnetic field created from the LRM magnets. Consequently, stronger LRM magnets may be needed to overcome the stirrer's magnetic field, which would represent another solution to address the described issue itself.

Furthermore it was tested whether a different magnet configuration may solve the issue of the stirrer's magnet interaction. Firstly, a stirrer was designed and 3D printed by adding an additional platform above the stirrer's tip. However, a strong interaction of the magnet with the metallic ball bearing was found, resulting in an interrupted rotational movement. Secondly, a bar magnet was attached to mobile ball bearing ring. This configuration was found too weak to move the stirrer. In order to address this issue, a novel design may be used by using customised ball bearings. These ball bearings could either be used as magnetic source itself by using magnetised ball bearing balls or by including a diametrically magnetised magnet within the ball bearing. The ball bearing material shall be plastic or a non-magnetic metal, in order to reduce further magnetic interactions within the system. Furthermore, magnetic shielding should be applied on the ball bearings outer ring. This novel approach would address issues which arose from the stirrers moving capability as well as the biocompatibility issue of the stirrer magnet used.

Fluid dynamics

Crucially important is the investigation of fluid dynamics applied with-in the well (Sucosky *et al*. 2008). Therefore CFD modelling as well as PIV should be performed. Issues may arise performing PIV caused by the lid on top which restricts visual access with the microscope (Sucosky *et al*. 2004). A possible solution may be to use non-fluorescent beads which can be examined with a camera placed underneath the 96 well.
Fluid dynamics analysis shall consider different gap heights in combination with different cone angles as well as various angular rotational speed. Results obtained will give a crucially important understanding for potential configurations of the system in order to address a various numbers of possible scientific demands which could be addressed by using the Moers stirrers.

Gap height and cone angle

Gap height and cone angle play an important role regarding shear stress pattern and applied force (Spruell & Baker 2013; Buschmann *et al.* 2005). Therefore it is important that a reliable method to measure and validate these factors should be developed. The presented method used a PDMS mould which was hand-cut in cross section and then examined using a light microscope. Although this method did not show ideal results, the working principal could be further optimised. An idea may be, to use modelling material which is placed in the well. The stirrers are put on top and thereby the modelling material represents the room between well bottom and stirrer. Subsequently, the stirrers and modelling material could be removed. The modelling material may be frozen and then cross-sectioned using a cryostat. This way sectioning can be performed more precisely by cross-sectioning in the µm range which can be used to model the entire space between well plate and stirrer. Subsequently measurements of gap heights and cone angle can be performed. In addition, the gap distance shall be accurately measured by using a commercially available nanometre which would require to remove part of the well wall in order to place the measuring probe. Once the correct gap distance is determined, a laser beam equipped on the side of the 96 well plate may be calibrated with this measuring tool. Thereby, providing the correct distance between cone tip and plate. Once the required calibrations are performed, the light source could be placed next to well plate, and the stirrers can be placed in wells. If the gap distance is smaller then required

light beam will be refracted from the stirrers and no light will pass through. The correct gap distance can be determined by moving the lid. The configuration which just allows light to pass through to the opposite side of the 96 well plate therefore would be the desired gap distance. Depending on the light beam configuration, this method could be used as a calibration tool or be performed on a day-to-day basis prior setting up experiments.

Well surface

The designed stirrer allows the application of flow on 86% of the well's surface. A 100% efficiency is technically impossible, since the stirrer's diameter must be smaller than the well diameter. In addition, a no flow region can be found below the stirrer's mid-point. However, it shall be considered that cells will also be present at those no flow regions which may influence signalling of flow treated cells in the well. Therefore no flow regions could be coated with a hydrophobic reagent in order to prevent cell attachment and subsequent cell migration (Okano *et al.* 1993). In order to simplify the coating process, a stamp-like lid could be build, with an individual stamp for each well. The hydrophobic coating material could be applied to the stamp, and subsequently, all wells of the 96 well plate could be coated at the same time.

However, the coating procedure may influence the cells behaviour, in particular due to contact sensing. In case of an artificial gap, HUVECs may sense a loss of barrier function, which may result in an inflammatory response.

LRM's speed and direction

The LRM exposes the magnetic field which is received by the stirrer's magnet. In order to create a rotating magnetic field the LRM magnets were attached to a platform, which itself is attached to a motor creating the angular movement. The LRMs rotational speed depends on the voltage input, which can be defined with the attached microcontroller. Thereby higher voltage inputs create an increased rotation movement and *vice versa*, a lower voltage input creates a decrease of rotational movement (Ventura *et al.* 2014). Therefore different voltage inputs were related to the resulting rpm number of the LRM's platform. The result obtained shows that the maximum voltage input results in a rotational movement of 200 rpm, which is estimated to create a shearing force of 0.5 Pa,

given a gap distance of 100 µm and a cone angle of 2°. Therefore it shall be considered to exchange the motor in order to gain an increased rpm number.

In order to improve the flexibility of possible flow applications, a rotational direction change shall be considered to apply oscillatory flow (Johnson *et al.* 2011). The motors directional change can be programmed in combination with the rotational speed (Williams 2013). Consequently different flow directions and amplitudes can be achieved. Therefore further validations are desirable in order to identify rotational delay times when the motor changes its direction.

The Arduino motorshield also occupies two possible motor connections (Ventura *et al.* 2014). Consequently, two Mörs stirrers' experiments could be performed in parallel, thereby further increasing the throughput number.

Potential applications of the novel device

The device functionality is the creation of a rotational stirring motion in a multi well plate by using individual stirrers in the wells. The device proposed in this thesis was built to apply flow to cultured cells in a 96 well plate, since a higher throughput number and the plate reader compatibility was anticipated. However, the device's working principal could be further extended to be used in other multi well formats (Lob *et al.* 2007). The multi wells dimensions differ in height and well size, however lengths and widths are congruent. Therefore, the current LRM device can be used as an external magnetic source. Nonetheless, different sized stirrers in addition to an adaptation of the lid must be performed. Cutting edge technology may allow in the future for production of stirrers and ball bearings which could fit 396 well plate. Using this format, robotic high throughput techniques can be used for large scale experiments, such as RNAi screening (Belougne *et al.* 2012).

The device also may be used as a generic laboratory device for mixing substances in a well plate or in order to optimise experimental procedures such as immunofluorescence staining.

Furthermore the Mörs stirrers could be used for biotechnology scale down experiments. Therefore, using the fluid flow in order to verify ideal fermentation conditions of mammalian or bacterial cells in suspension for large scale productions.

9 Conclusion

The fundamental principles of the Mörs stirrer offers a self-consistent system including flexible adaption possibilities for various applications. The principal functionality was proven as described in this thesis. Hence, further validation and optimisation is necessary in order to fully utilise the system's potential.

- CFD and PIV for different gap height, cone angles, rotational speeds, stirrer dimensions, fluid flows as well as different multi well formats

- Improved stirrer movement through new magnet or redesign

- Biocompatible coating of stirrer magnet

- Validation time delay of motor directional change in order create oscillatory flow conditions

- Well plate stamp to apply hydrophobic coating to no flow regions

10 References

Abudayyak, M., Guzel, E. & Özhan, G., 2017. Nickel Oxide Nanoparticles Induce Oxidative DNA Damage and Apoptosis in Kidney Cell Line (NRK-52E). *Biological Trace Element Research*, 178(1), pp.98–104. Available at: http://link.springer.com/10.1007/s12011-016-0892-z.

Alan Dardik PhD, Leiling Chen, MD, Jared Frattini, MD, Hidenori Asada, MD, Faisal Aziz, MD, M.D. & Fabio A. Kudo PhD, and Bauer E. Sumpio, MD, PhD, M.D., 2005a. Differential effects of orbital and laminar shear stress on endothelial cells. *The Society for Vascular Surgery*, 41(5), pp.869–880.

Alan Dardik PhD, Leiling Chen, MD, Jared Frattini, MD, Hidenori Asada, MD, Faisal Aziz, MD, M.D. & Fabio A. Kudo PhD, and Bauer E. Sumpio, MD, PhD, M.D., 2005b. Differential effects of orbital and laminar shear stress on endothelial cells. *The Society for Vascular Surgery*, 41(5), pp.869–880.

Ali, U., Karim, K.J.B.A. & Buang, N.A., 2015. A Review of the Properties and Applications of Poly (Methyl Methacrylate) (PMMA). *Polymer Reviews*, 55(4), pp.678–705. Available at: http://www.tandfonline.com/doi/full/10.1080/15583724.2015.1031377.

Amini, N. et al., 2014. Requirement of JNK1 for endothelial cell injury in atherogenesis. *Atherosclerosis*, 235(2), pp.613–618.

Andrews, S., Gilley, J. & Coleman, M.P., 2010. Difference Tracker: ImageJ plugins for fully automated analysis of multiple axonal transport parameters. *Journal of Neuroscience Methods*, 193(2), pp.281–287. Available at: http://dx.doi.org/10.1016/j.jneumeth.2010.09.007.

Anthony, G. & Lee, J.A., 2016. An optimized small tissue handling system for immunohistochemistry and in situ hybridization. *PLoS ONE*, 11(8), pp.1–11.

Barbee, K. a., Davies, P.F. & Lal, R., 1994. Shear stress-induced reorganization of the surface topography of living endothelial cells imaged by atomic force microscopy. *Circulation Research*, 74(1), pp.163–171. Available at: http://circres.ahajournals.org/cgi/doi/10.1161/01.RES.74.1.163 [Accessed October 27, 2014].

Barnes, K.W., Hutton, J. & Walters, K., 1989. *An Introduction to Rheology H.A. Barnes, K. Walters*, Amsterdam: Elsevier Science Publishers.

Baskurt, O.K. et al., 2003. Blood Rheology and Hemodynamics. *Seminars in Thrombosis*

and Hemostasis, 29(5), pp.435–450.

Bataineh, K.M., 2014. Computers & Fluids Numerical investigation of secondary flow effect in cone – plate viscometer. *COMPUTERS AND FLUIDS*, 101, pp.105–113. Available at: http://dx.doi.org/10.1016/j.compfluid.2014.06.009.

Batra, N. et al., 2012. Mechanical stress-activated integrin α5β1 induces opening of connexin 43 hemichannels. *Proceedings of the National Academy of Sciences of the United States of America*, 109(9), pp.3359–64. Available at: http://www.pubmedcentral.nih.gov/articlerender.fcgi?artid=3295295&tool=pmcentrez&rendertype=abstract [Accessed November 7, 2014].

Bellin, R.M. et al., 2009. Defining the role of syndecan-4 in mechanotransduction using surface-modification approaches. *Proceedings of the National Academy of Sciences of the United States of America*, 106(52), pp.22102–7. Available at: http://www.pubmedcentral.nih.gov/articlerender.fcgi?artid=2796905&tool=pmcentrez&rendertype=abstract [Accessed November 7, 2014].

Belougne, J. et al., 2012. Quantitative and Automated High-throughput Genome-wide RNAi Screens in &lt. *Journal of visualized experiments JoVE.*, (60).

Bingham, C.E., 1846. RHEOLOGY. I. THE NATURE OF FLUID FLOW EUGENE. *Journal of chemical education*, 6(6), pp.1113–1119.

Boyle, J.J., 2005. Macrophage Activation in Atherosclerosis : Pharmacology of Plaque Rupture Pathogenesis and. *Current Vascular Pharmacology*, pp.63–68.

Bryan, M.T. et al., 2014. Mechanoresponsive networks controlling vascular inflammation. *Arteriosclerosis, thrombosis, and vascular biology*, 34(10), pp.2199–205. Available at: http://www.ncbi.nlm.nih.gov/pubmed/24947523 [Accessed October 31, 2014].

Buchhave, P., 1992. Particle Image Velocimetry. *Experimental Thermal and Fluid Science*, 5(92), pp.586–604.

Buschmann, M.H. et al., 2005. Analysis of flow in a cone-and-plate apparatus with respect to spatial and temporal effects on endothelial cells. *Biotechnology and bioengineering*, 89(5), pp.493–502. Available at: http://www.ncbi.nlm.nih.gov/pubmed/15648084 [Accessed December 7, 2014].

Caro, C.G., 2009. Discovery of the role of wall shear in atherosclerosis. *Arteriosclerosis, thrombosis, and vascular biology*, 29(2), pp.158–61. Available at: http://www.ncbi.nlm.nih.gov/pubmed/19038849 [Accessed November 7, 2014].

CARO, C.G., FITZ-GERALD, J.M. & SCHROTER, R.C., 1969. Arterial Wall Shear and Distribution of Early Atheroma in Man. *Nature*, 223(5211), pp.1159–1161.

Available at: http://dx.doi.org/10.1038/2231159a0.

Caro, C.G. & Nerem, R.M., 1973. Transport of 14C-4-Cholesterol between Serum and Wall in the Perfused Dog Common Carotid Artery. *Circulation Research*, 32(2), pp.187–205. Available at: http://circres.ahajournals.org/cgi/doi/10.1161/01.RES.32.2.187 [Accessed November 13, 2014].

Chang, T.Y. et al., 2007. Cell and protein compatibility of parylene-C surfaces. *Langmuir*, 23(23), pp.11718–11725.

Chen, J.S. & Chen, K.W., 2005. Bearing load analysis and control of a motorized high speed spindle. *International Journal of Machine Tools and Manufacture*, 45(12–13), pp.1487–1493.

Chien, S., 2003. Molecular and mechanical bases of focal lipid accumulation in arterial wall. *Progress in Biophysics & Molecular Biology*, 83(2), pp.131–151.

Chou, C.-S. & Yeh, C.-H., 2008. Effect of a rotating magnetic field on the moving pattern and collision attrition of magnetic particles. *Advanced Powder Technology*, 19(3), pp.253–275. Available at: http://dx.doi.org/10.1163/156855208X294627.

Cicha, I. et al., 2008. Endothelial dysfunction and monocyte recruitment in cells exposed to non-uniform shear stress. *Clinical Hemorheology and Microcirculation*, 39(1–4), pp.113–119.

Civelek, M. et al., 2009. Chronic endoplasmic reticulum stress activates unfolded protein response in arterial endothelium in regions of susceptibility to atherosclerosis. *Circulation research*, 105(5), pp.453–461. Available at: http://www.pubmedcentral.nih.gov/articlerender.fcgi?artid=2746924&tool=pmcentrez&rendertype=abstract.

Coleman, J.R., 1981. Mithramycin- Staining for Fluorescence Microspectrophotometric Measurement Nuclei , of D NA in. *Measurement*.

Cuhlmann, S. et al., 2011. Disturbed blood flow induces RelA expression via c-Jun N-terminal kinase 1: a novel mode of NF-$κ$B regulation that promotes arterial inflammation. *Circulation research*, 108(8), pp.950–959. Available at: http://www.ncbi.nlm.nih.gov/pubmed/21350211.

D'Ausilio, A., 2012. Arduino: A low-cost multipurpose lab equipment. *Behavior Research Methods*, 44(2), pp.305–313. Available at: https://doi.org/10.3758/s13428-011-0163-z.

Dai, G. et al., 2004. Distinct endothelial phenotypes evoked by arterial waveforms derived from atherosclerosis-susceptible and -resistant regions of human

vasculature. *Proceedings of the National Academy of Sciences*, 101(41), pp.14871–14876.

Davies, P.F., 2008. Endothelial transcriptome profiles in vivo in complex arterial flow fields. *Annals of biomedical engineering*, 36(4), pp.563–70. Available at: http://www.ncbi.nlm.nih.gov/pubmed/17978875 [Accessed October 27, 2014].

Davies, P.F., 2011. Flow-Mediated Endothelial Mechanotransduction Peter. , 75(3), pp.519–560.

Davies, P.F., 1995. Flow-Mediated Mechanotransduction. *Physiol Rev.*, 75(3), pp.519–560.

Davies, P.F., 2009. Hemodynamic shear stress and the endothelium in cardiovascular pathophysiology. *Nature clinical practice. Cardiovascular medicine*, 6(1), pp.16–26. Available at: http://www.pubmedcentral.nih.gov/articlerender.fcgi?artid=2851404&tool=pmcentrez&rendertype=abstract [Accessed October 13, 2014].

Davies, P.F. et al., 2013. The atherosusceptible endothelium: endothelial phenotypes in complex haemodynamic shear stress regions in vivo. *Cardiovascular research*, 99(2), pp.315–27. Available at: http://www.pubmedcentral.nih.gov/articlerender.fcgi?artid=3695748&tool=pmcentrez&rendertype=abstract [Accessed October 13, 2014].

Davies, P.F. et al., 2014. Turbulent fluid shear stress induces vascular endothelial cell turnover in vitro. , 83(7), pp.2114–2117.

Dutta, A. & Tarbell, J.M., 1996. Influence of Non-Newtonian Behavior of Blood on Flow in an Elastic Artery Model. *Journal of Biochemical Engineering*, 1(February 1996), pp.111–119.

El-Ali, J., Sorger, P.K. & Jensen, K.F., 2006. Cells on chips. *Nature*, 442(7101), pp.403–11. Available at: http://www.ncbi.nlm.nih.gov/pubmed/16871208 [Accessed July 10, 2014].

Enesa, K. et al., 2008. NF-kappaB suppression by the deubiquitinating enzyme Cezanne: a novel negative feedback loop in pro-inflammatory signaling. *The Journal of biological chemistry*, 283(11), pp.7036–45. Available at: http://www.ncbi.nlm.nih.gov/pubmed/18178551 [Accessed October 27, 2014].

Ernst, E. et al., 1986. Blood rheology in vegetarians. , 29, pp.555–560.

Evans, P.C. & Kilshaw, P.J., 2000. Interleukin-13 protects endothelial cells from apoptosis and activation - Association with the protective genes A20 and A1. *Transplantation*, 70(6), pp.928–934.

Finn, A. V et al., 2010. Concept of vulnerable/unstable plaque. *Arteriosclerosis, thrombosis, and vascular biology*, 30(7), pp.1282–1292. Available at: http://www.ncbi.nlm.nih.gov/pubmed/20554950.

Franzoni, M. et al., 2016. Design of a cone-and-plate device for controlled realistic shear stress stimulation on endothelial cell monolayers. *Cytotechnology*, 68(5), pp.1885–1896.

Fung, Y.C., 1996. *Biomechanics: Circulation* 2nd ed., New York Berlin Heidelberg: Springer Verlag. Available at: http://www.amazon.co.uk/gp/product/0387943846 [Accessed December 3, 2014].

Garin, G. et al., 2007. Flow antagonizes TNF-alpha signaling in endothelial cells by inhibiting caspase-dependent PKC zeta processing. *Circulation research*, 101(1), pp.97–105. Available at: http://www.ncbi.nlm.nih.gov/pubmed/17525369.

Geudens, I. & Gerhardt, H., 2011. Coordinating cell behaviour during blood vessel formation. *Development (Cambridge, England)*, 138(21), pp.4569–4583. Available at: http://www.ncbi.nlm.nih.gov/pubmed/21965610.

Glagov, S. et al., 1987. Compensatory enlargement of human atherosclerotic coronary arteries. *New England Journal of Medicine*, 316, pp.1371–1375.

Glagov, S., 1994. Intimal Hyperplasia , Vascular Modeling , and the Restenosis Problem. *CIRCULATION*, 89(6), pp.2888–2891.

Goel, R. et al., 2008. Site-specific effects of PECAM-1 on atherosclerosis in LDL receptor-deficient mice. *Arteriosclerosis, thrombosis, and vascular biology*, 28(11), pp.1996–2002. Available at: http://www.pubmedcentral.nih.gov/articlerender.fcgi?artid=3013511&tool=pmcentrez&rendertype=abstract [Accessed November 7, 2014].

Grad, Y. & Einav, S., 2000. Spectral and instantaneous flow field characteristics of the laminar to turbulent transition in a cone and plate apparatus. *Experiments in Fluids*, 28, pp.336–343.

Gulino-Debrac, D., 2013. Mechanotransduction at the basis of endothelial barrier function. *Tissue barriers*, 1(2), pp.e24180–e24180.

Hajra, L., 2000. The NF-kappa B signal transduction pathway in aortic endothelial cells is primed for activation in regions predisposed to atherosclerotic lesion formation. *Proc. Natl Acad. Sci. USA*, 97, pp.9052–9057. Available at: http://dx.doi.org/10.1073/pnas.97.16.9052.

Harry, B.L. et al., 2008. Endothelial cell PECAM-1 promotes atherosclerotic lesions in areas of disturbed flow in ApoE-deficient mice. *Arteriosclerosis, thrombosis, and*

vascular biology, 28(11), pp.2003–8. Available at: http://www.pubmedcentral.nih.gov/articlerender.fcgi?artid=2651147&tool=pmcentrez&rendertype=abstract [Accessed October 25, 2014].

Hashem, N. et al., 2016. 141 BOVINE EMBRYO DEVELOPMENT RATES ARE AFFECTED WHEN OOCYTES ARE MATURED IN DIFFERENT VIALS CONTAINING HEPES/BICARBONATE BUFFERED MEDIUM. *Reproduction, Fertility and Development*, 29(1), p.179. Available at: https://doi.org/10.1071/RDv29n1Ab141.

Hayden, M.S. & Ghosh, S., 2004. Signaling to NF- kB. *GENES & DEVELOPMENT*, 18, pp.2195–2224.

Van der Heiden, K. et al., 2011. Role for primary cilia as flow detectors in the cardiovascular system. *International review of cell and molecular biology*, 290, pp.87–119. Available at: http://www.ncbi.nlm.nih.gov/pubmed/21875563 [Accessed November 7, 2014].

Van der Heiden, K. et al., 2010. Role of nuclear factor kappa B in cardiovascular health and disease. *Clinical Science*, 118(9–10), pp.593–605.

Henninger, H.B. et al., 2010. Validation of computational models in biomechanics. *Proceedings of the Institution of Mechanical Engineers, Part H: Journal of Engineering in Medicine*, 224(7), pp.801–812. Available at: http://pih.sagepub.com/lookup/doi/10.1243/09544119JEIM649.

Heo, K.-S. et al., 2011. PKC$ζ$ mediates disturbed flow-induced endothelial apoptosis via p53 SUMOylation. *The Journal of cell biology*, 193(5), pp.867–884. Available at: http://www.pubmedcentral.nih.gov/articlerender.fcgi?artid=3105539&tool=pmcentrez&rendertype=abstract.

Herbst, J.F., 1991. R2Fe14B materials: Intrinsic properties and technological aspects. *Reviews of Modern Physics*, 63(4), pp.819–898.

Hierck, B.P. et al., 2008. Primary cilia sensitize endothelial cells for fluid shear stress. *Developmental dynamics : an official publication of the American Association of Anatomists*, 237(3), pp.725–35. Available at: http://www.ncbi.nlm.nih.gov/pubmed/18297727 [Accessed November 7, 2014].

Holstein, T. & Primakoff, H., 1940. Field Dependence of the Intrinsic Domain Magnetization of a Ferromagnet. *Phys. Rev.*, 58(12), pp.1098–1113. Available at: https://link.aps.org/doi/10.1103/PhysRev.58.1098.

HUBBE, M.A., 1981. ADHESION AND DETACHMENT OF BIOLOGICAL CELLS

IN VITRO. *Progress in Surface Science*, 11(2), pp.65–137.

Huebsch, N. et al., 2010. Harnessing traction-mediated manipulation of the cell/matrix interface to control stem-cell fate. *Nature materials*, 9(6), pp.518–526. Available at: http://www.pubmedcentral.nih.gov/articlerender.fcgi?artid=2919753&tool=pmcentrez&rendertype=abstract.

Jacobs, C., 2013. *Introduction to cell mechanics and mechanobiology* 1st ed., New York: Garland Science.

Jang, S.M. et al., 2012. Characteristic analysis on permanent magnet synchronous machines with three types of diametrically magnetized rotors under magnetic circuit construction conditions. *2012 IEEE Vehicle Power and Propulsion Conference, VPPC 2012*, (3), pp.227–230.

Jin, X. et al., 2002. Induction of human inhibitor of apoptosis protein-2 by shear stress in endothelial cells. *FEBS Letters*, 529(2–3), pp.286–292. Available at: http://linkinghub.elsevier.com/retrieve/pii/S0014579302033616.

Johnson, B.D., Mather, K.J. & Wallace, J.P., 2011. Mechanotransduction of shear in the endothelium: basic studies and clinical implications. *Vascular medicine (London, England)*, 16(5), pp.365–77. Available at: http://www.ncbi.nlm.nih.gov/pubmed/22003002 [Accessed November 7, 2014].

Khabou, M.T. et al., 2011. Study of a spur gear dynamic behavior in transient regime. *Mechanical Systems and Signal Processing*, 25(8), pp.3089–3101. Available at: http://dx.doi.org/10.1016/j.ymssp.2011.04.018.

Kishi, H. et al., 2017. Carbon fiber reinforced thermoplastic composites from acrylic polymer matrices: Interfacial adhesion and physical properties. *Express Polymer Letters*, 11(4), pp.334–342.

Knudsen, H.L. & Frangos, J.A., 1997. Role of cytoskeleton in shear stress-induced endothelial nitric oxide production. *American Journal of Physiology - Heart and Circulatory Physiology*, 273(1), p.H347 LP-H355. Available at: http://ajpheart.physiology.org/content/273/1/H347.abstract.

Kostenko, V. et al., 2010. Staphylococcus aureus biofilm formation and tolerance to antibiotics in response to oscillatory shear stresses of physiological levels. *FEMS immunology and medical microbiology*, 59(3), pp.421–431. Available at: http://www.ncbi.nlm.nih.gov/pubmed/20528928.

Kroutvar, M. & Guttenberg, Z., 2013. *ibidi Pump System Instructions*.

Ku, D. & DN Ku, DP Giddens, C.Z. and S.G., 1985. Pulsatile Flow and Atherosclerosis in the Human Carotid Bifurcation Positive Correlation between Plaque Location

and Low and Oscillating Shear Stress. *Arteriosclerosis, Thrombosis, and Vascular Biology*.

Kurth, F. et al., 2012. A new mechanobiological era: microfluidic pathways to apply and sense forces at the cellular level. *Current opinion in chemical biology*, 16(3–4), pp.400–408. Available at: http://www.ncbi.nlm.nih.gov/pubmed/22525494.

Lee, S. & Yan, J., 2016. The impact of 3D CAD interfaces on user ideation: A comparative analysis using SketchUp and Silhouette Modeler. *Design Studies*, 44, pp.52–73. Available at: http://dx.doi.org/10.1016/j.destud.2016.02.001.

Leonhardt, H., Arntz, H.-R. & Klemens, U.H., 1977. Studies of plasma viscosity in primary hyperlipoproteinaemia. *Atherosclerosis*, 28(1), pp.29–40. Available at: http://www.sciencedirect.com/science/article/pii/0021915077901964 [Accessed November 4, 2014].

Libby, P., 2012. Inflammation in atherosclerosis. *Arteriosclerosis, thrombosis, and vascular biology*, 32(9), pp.2045–2051. Available at: http://www.pubmedcentral.nih.gov/articlerender.fcgi?artid=3422754&tool=pmcentrez&rendertype=abstract.

Libby, P., 2002. Inflammation in atherosclerosis. *Nature*, 420(6917), pp.868–74. Available at: http://apps.webofknowledge.com/full_record.do?product=UA&search_mode=GeneralSearch&qid=31&SID=P2d6OT9iznQE1PLVn9o&page=3&doc=24&cacheurlFromRightClick=no [Accessed July 14, 2014].

Liu, X., Chu, P.K. & Ding, C., 2004. Surface modification of titanium, titanium alloys, and related materials for biomedical applications. *Materials Science and Engineering R: Reports*, 47(3–4), pp.49–121.

Lob, V. et al., 2007. Automated live cell screening system based on a 24-well-microplate with integrated micro fluidics. *Medical and Biological Engineering and Computing*, 45(11), pp.1023–1028.

Lumpkin, E. a, Marshall, K.L. & Nelson, A.M., 2010. The cell biology of touch. *The Journal of cell biology*, 191(2), pp.237–48. Available at: http://www.pubmedcentral.nih.gov/articlerender.fcgi?artid=2958478&tool=pmcentrez&rendertype=abstract [Accessed August 14, 2014].

Lusis, A.J., 2000. Atherosclerosis. *Nature*, 407(September), pp.233–241.

M. MEHDI SALEK 2 POORIA SATTARI, 2 and ROBERT J. MARTINUZZI1, 2, 1, 2011. Analysis of Fluid Flow and Wall Shear Stress Patterns Inside Partially Filled Agitated Culture Well Plates. *Annals of Biomedical Engineering*, 40(3), pp.707–

728.

Matthews, B.D. et al., 2010. Ultra-rapid activation of TRPV4 ion channels by mechanical forces applied to cell surface beta1 integrins. *Integrative biology : quantitative biosciences from nano to macro*, 2(9), pp.435–42. Available at: http://www.pubmedcentral.nih.gov/articlerender.fcgi?artid=3147167&tool=pmcentrez&rendertype=abstract [Accessed October 28, 2014].

McKENNELL, R., 1954. Cone-Plate Viscometer Comparison with Coaxial Cylinder Viscometer. *Analytical Chemistry*, 28(11), pp.1710–1714.

Melling, a, 1997. Tracer particles and seeding for particle image velocimetry. *Measurement Science and Technology*, 8(12), pp.1406–1416. Available at: http://stacks.iop.org/0957-0233/8/i=12/a=005?key=crossref.828d3477f9cf4538526e17cfeed03203.

Momeni, F. et al., 2017. A review of 4D printing. *Materials and Design*, 122, pp.42–79. Available at: http://dx.doi.org/10.1016/j.matdes.2017.02.068.

Nagel, T. et al., 1994. Shear stress selectively upregulates intercellular adhesion molecule-1 expression in cultured human vascular endothelial cells. *J. Clin. Invest.*, 94(August), pp.885–891.

Nichols, M. et al., 2013. Cardiovascular disease in Europe: epidemiological update. *European heart journal*, 34(39), pp.3028–34. Available at: http://www.ncbi.nlm.nih.gov/pubmed/24014390 [Accessed November 12, 2014].

O'Keeffe, L.M. et al., 2009a. Vascular cell adhesion molecule-1 expression in endothelial cells exposed to physiological coronary wall shear stresses. *Journal of biomechanical engineering*, 131(8), p.81003. Available at: http://www.ncbi.nlm.nih.gov/pubmed/19604015.

O'Keeffe, L.M. et al., 2009b. Vascular cell adhesion molecule-1 expression in endothelial cells exposed to physiological coronary wall shear stresses. *Journal of biomechanical engineering*, 131(8), p.81003. Available at: http://www.ncbi.nlm.nih.gov/pubmed/19604015 [Accessed January 7, 2015].

Ohm, G.S., 1891. *The galvanic circuit investigated mathematically.*, New York, D. Van Nostrand company. Available at: http://hdl.handle.net/2027/uc1.b4534705 [Accessed December 3, 2014].

Okano, T. et al., 1993. A novel recovery system for cultured cells using plasma-treated polystyrene dishes grafted with poly(N-isopropylacrylamide). *Journal of biomedical materials research.*, 27(10), pp.1243–1251.

Pasceri, V., Willerson, J.T. & Yeh, E.T.H., 2000. Direct Proinflammatory Effect of C-

Reactive Protein on Human Endothelial Cells. *Circulation*, 102(18), pp.2165–2168. Available at: http://circ.ahajournals.org/content/102/18/2165.short.

Passerini, a. G. et al., 2004. Coexisting proinflammatory and antioxidative endothelial transcription profiles in a disturbed flow region of the adult porcine aorta. *Proceedings of the National Academy of Sciences*, 101(8), pp.2482–2487. Available at: http://www.pnas.org/cgi/doi/10.1073/pnas.0305938101.

dela Paz, N.G. et al., 2012. Role of shear-stress-induced VEGF expression in endothelial cell survival. *Journal of cell science*, 125(Pt 4), pp.831–843. Available at: http://www.pubmedcentral.nih.gov/articlerender.fcgi?artid=3311927&tool=pmcentrez&rendertype=abstract.

Pekkan, K. et al., 2005. Physics-Driven CFD Modeling of Complex Anatomical Cardiovascular Flows?A TCPC Case Study. *Annals of Biomedical Engineering*, 33(3), pp.284–300. Available at: http://link.springer.com/10.1007/s10439-005-1731-0.

Peterson, S.L. et al., 2005. Poly(dimethylsiloxane) thin films as biocompatible coatings for microfluidic devices: cell culture and flow studies with glial cells. *Journal of biomedical materials research. Part A*, 72(1), pp.10–8. Available at: http://www.ncbi.nlm.nih.gov/pubmed/15534867 [Accessed January 5, 2015].

Petru, L. & Mazen, G., 2015. PWM control of a DC motor used to drive a conveyor belt. *Procedia Engineering*, 100(January), pp.299–304. Available at: http://dx.doi.org/10.1016/j.proeng.2015.01.371.

Piruska, A. et al., 2005. The autofluorescence of plastic materials and chips measured under laser irradiation. *Lab on a chip*, 5(12), pp.1348–1354.

Raffel, M. et al., 2007. *Particle image velocimetry* 2nd ed., Heidelberg: Springer Verlag. Available at: https://www.dawsonera.com/abstract/9783540723080 [Accessed January 7, 2015].

Rebelo, S.P. et al., 2015. Establishing Liver Bioreactors for In Vitro Research BT - Protocols in In Vitro Hepatocyte Research. In M. Vinken & V. Rogiers, eds. New York, NY: Springer New York, pp. 189–202. Available at: https://doi.org/10.1007/978-1-4939-2074-7_13.

Regalia, G. et al., 2016. Development of a bench-top device for parallel climate-controlled recordings of neuronal cultures activity with microelectrode arrays. *Biotechnology and Bioengineering*, 113(2), pp.403–413.

Ross, T.D. et al., 2013. Integrins in mechanotransduction. *Current opinion in cell biology*, 25(5), pp.613–8. Available at:

http://www.ncbi.nlm.nih.gov/pubmed/23797029 [Accessed July 22, 2014].

Rua, Y., Muren, R. & Reckinger, S., 2015. Limitations of Additive Manufacturing on Microfluidic Heat Exchanger Components. *Journal of Manufacturing Science and Engineering*, 137(3), p.34504. Available at: http://manufacturingscience.asmedigitalcollection.asme.org/article.aspx?doi=10.1115/1.4030157.

Rusina, T.P. et al., 2007. Polymer selection for passive sampling: A comparison of critical properties. *Chemosphere*, 68(7), pp.1344–1351.

Saalfrank, D. et al., 2015. Incubator-independent cell-culture perfusion platform for continuous long-term microelectrode array electrophysiology and time-lapse imaging. *Royal Society Open Science*, 2(6), p.150031. Available at: http://rsos.royalsocietypublishing.org/content/2/6/150031.abstract.

Salimgareeva, V.N. & Kolesov, S. V., 2005. Plastic scintillators based on polymethyl methacrylate: A review. *Instruments and Experimental Techniques*, 48(3), pp.273–282.

Sathyan, K. et al., 2008. Development of a lubrication system for momentum wheels used in spacecrafts. *Tribology Letters*, 32(2), pp.99–107.

Saxer, T., Zumbuehl, A. & Müller, B., 2013. The use of shear stress for targeted drug delivery. *Cardiovascular research*, 99(2), pp.328–333. Available at: http://www.ncbi.nlm.nih.gov/pubmed/23645574.

Schweizer, F., 1962. Magnetic shielding factors of a system of concentric spherical shells. *Journal of Applied Physics*, 33(3), pp.1001–1003.

Schwenke, D.C. & Carew, T.E., 1989. Initiation of atherosclerotic lesions in cholesterol-fed rabbits. I. Focal increases in arterial LDL concentration precede development of fatty streak lesions. *Arteriosclerosis, Thrombosis, and Vascular Biology*, 9(6), pp.895–907. Available at: http://atvb.ahajournals.org/cgi/doi/10.1161/01.ATV.9.6.895 [Accessed November 13, 2014].

Sengupta, R. et al., 2007. A Short Review on Rubber / Clay Nanocomposites With Emphasis on Mechanical Properties. *Engineering*, 47, pp.21–25. Available at: http://doi.wiley.com/10.1002/pen.20921.

Serbanovic-Canic, J. et al., 2016. Zebrafish Model for Functional Screening of Flow-Responsive Genes. *Arteriosclerosis, Thrombosis, and Vascular Biology*, pp.130–143.

Sik Song, J. et al., 2013. Improved Biocompatibility of Parylene-C Films Prepared by

Chemical vapor Deposition and the Subsequent Plasma Treatment. *Polymers and Polymer Composites*, 21(7), pp.449–456.

Simmons, C.S., Petzold, B.C. & Pruitt, B.L., 2012. Microsystems for biomimetic stimulation of cardiac cells. *Lab on a Chip*, 12(18), p.3235.

Singh, D.D.N., Yadav, S. & Saha, J.K., 2008. Role of climatic conditions on corrosion characteristics of structural steels. *Corrosion Science*, 50(1), pp.93–110.

Sinha, R. et al., 2016. Endothelial cell alignment as a result of anisotropic strain and flow induced shear stress combinations. *Nature Publishing Group*, (April), pp.1–12. Available at: http://dx.doi.org/10.1038/srep29510.

Sloop, G.D. & Mercante, D.E., 1998. Opposite effects of low-density and high-density lipoprotein on blood viscosity in fasting subjects. *Clinical hemorheology and microcirculation*, 19(3), pp.197–203. Available at: http://www.ncbi.nlm.nih.gov/pubmed/9874355 [Accessed November 4, 2014].

Sochi, T., 2013. *Non-Newtonian Rheology in Blood Circulation*, Available at: http://arxiv.org/abs/1306.2067v1.

Spruell, C. & Baker, A.B., 2013. Analysis of a high-throughput cone-and-plate apparatus for the application of defined spatiotemporal flow to cultured cells. *Biotechnology and bioengineering*, 110(6), pp.1782–93. Available at: http://www.ncbi.nlm.nih.gov/pubmed/23280552 [Accessed December 7, 2014].

Steward, R. et al., 2015. Fluid shear, intercellular stress, and endothelial cell alignment. *American Journal of Physiology - Cell Physiology*, p.ajpcell.00363.2014. Available at: http://ajpcell.physiology.org/lookup/doi/10.1152/ajpcell.00363.2014.

Sucosky, P. et al., 2008. Design of an ex vivo culture system to investigate the effects of shear stress on cardiovascular tissue. *Journal of biomechanical engineering*, 130, p.35001.

Sucosky, P. et al., 2004. Fluid mechanics of a spinner-flask bioreactor. *Biotechnology and bioengineering*, 85(1), pp.34–46. Available at: http://www.ncbi.nlm.nih.gov/pubmed/14705010 [Accessed September 28, 2014].

Sulistyowati, E., Permatasari, N. & Aris Widodo, M., 2017. Combined effects of shear stress and glucose on the morphology, actin filaments, and VE-cadherin of endothelial cells in vitro. *IJC Heart & Vasculature*, 15, pp.31–35. Available at: http://linkinghub.elsevier.com/retrieve/pii/S2352906716300975.

Sumpio, B.E., Timothy Riley, J. & Dardik, A., 2002. Cells in focus: endothelial cell. *The International Journal of Biochemistry & Cell Biology*, 34(12), pp.1508–1512. Available at:

http://www.sciencedirect.com/science/article/pii/S1357272502000754 [Accessed October 26, 2014].

Sutera, P.S. & Skalak, R., 1993. THE HISTORY OF POISEUILLE â€™ S. *Annual Review of Fluid Mechanics*.

Taba, Y. et al., 2003. 15-Deoxy-12,14-prostaglandin J2 and laminar fluid shear stress stabilize c-IAP1 in vascular endothelial cells. *Am J Physiol Heart Circ Physiol*, 285(1), pp.38–46.

Tabas, I., García-Cardeña, G. & Owens, G.K., 2015. Recent insights into the cellular biology of atherosclerosis. *Journal of Cell Biology*, 209(1), pp.13–22.

Tan, X.P. et al., 2016. Metallic powder-bed based 3D printing of cellular scaffolds for orthopaedic implants: A state-of-the-art review on manufacturing, topological design, mechanical properties and biocompatibility. *Materials Science and Engineering C*, 76, pp.1328–1343. Available at: http://dx.doi.org/10.1016/j.msec.2017.02.094.

Tarbell, J.M. et al., 2014. Fluid Mechanics, Arterial Disease, and Gene Expression John. , pp.591–614.

Tarbell, J.M. & Pahakis, M.Y., 2006. Mechanotransduction and the glycocalyx. *Journal of internal medicine*, 259(4), pp.339–50. Available at: http://www.ncbi.nlm.nih.gov/pubmed/16594902 [Accessed November 4, 2014].

Thurston, G.B., 1972. Viscoelasticity of human blood. *Biophysical journal*, 12(9), pp.1205–17. Available at: http://www.pubmedcentral.nih.gov/articlerender.fcgi?artid=1484135&tool=pmcentrez&rendertype=abstract [Accessed November 19, 2014].

Tzima, E. et al., 2005. A mechanosensory complex that mediates the endothelial cell response to fluid shear stress. *Nature*, 437(7057), pp.426–31. Available at: http://www.ncbi.nlm.nih.gov/pubmed/16163360 [Accessed July 22, 2014].

Urban, J.F.J.S.F.V.A.M.J.O.G.W.R.R.M., 1985. Biocompatibility of Delrin 150: a creep-resistant polymer for total joint prostheses. *Journal of biomedical materials research*, Vol.19(5)(5), p.p.519-533.

Ventura, H. et al., 2014. ARDOLORES: an Arduino based motors control system for DOLORES. *GROUND-BASED AND AIRBORNE INSTRUMENTATION FOR ASTRONOMY V*, 9147, p.91474X.

Verhaar, J., Sanders, R. & Krijnen, G., 2015. 3D printed features in the 100 μm range for application in sensing. *2015 IEEE SENSORS - Proceedings*, pp.5–8.

Versteg, H. & Malalasekera, W., 2007. *An introduction to computational fluid dynamics*

2nd ed., Essex CM20 2JE: Pearson Education Limited. Available at: http://scholar.google.com/scholar?hl=en&btnG=Search&q=intitle:An+Introduction+to+Computational+Fluid+Dynamics#0 [Accessed January 7, 2015].

Voyvodic, P.L., Min, D. & Baker, A.B., 2012. A multichannel dampened flow system for studies on shear stress-mediated mechanotransduction. *Lab on a Chip*, 12, p.3322.

Warboys, C.M. et al., 2010a. Acute and chronic exposure to shear stress have opposite effects on endothelial permeability to macromolecules. *American Journal of Physiology-Heart and Circulatory Physiology*, 298(6), pp.H1850--H1856. Available at: %3CGo.

Warboys, C.M. et al., 2010b. Acute and chronic exposure to shear stress have opposite effects on endothelial permeability to macromolecules. *American Journal of Physiology-Heart and Circulatory Physiology*, 298(6), pp.H1850–H1856.

Warboys, C.M. et al., 2014. Disturbed Flow Promotes Endothelial Senescence via a p53-Dependent Pathway. *Arteriosclerosis Thrombosis and Vascular Biology*, 34(5), pp.985–995.

Weinbaum, S. et al., 2011. An Integrative Review of Mechanotransduction in Endothelial, Epithelial (Renal) and Dendritic Cells (Osteocytes). *Cellular and molecular bioengineering*, 4(4), pp.510–537. Available at: http://www.pubmedcentral.nih.gov/articlerender.fcgi?artid=3748935&tool=pmcentrez&rendertype=abstract [Accessed November 7, 2014].

Weinbaum, S. et al., 2003. Mechanotransduction and flow across the endothelial glycocalyx. *Proceedings of the National Academy of Sciences of the United States of America*, 100(13), pp.7988–95. Available at: http://www.pubmedcentral.nih.gov/articlerender.fcgi?artid=164700&tool=pmcentrez&rendertype=abstract.

Williams, W.B., 2013. LabVIEW and Arduino as a gateway to PLC programming. *2013 ASEE ANNUAL CONFERENCE*.

Wolf, P. et al., 2013. Automated platform for sensor-based monitoring and controlled assays of living cells and tissues. *Biosensors and Bioelectronics*, 50, pp.111–117.

Xiang, J. et al., 2014. CFD : Computational Fluid Dynamics or Confounding Factor Dissemination ? The Role of Hemodynamics in Intracranial Aneurysm Rupture Risk Assessment. *American Journal of Neuroradiology*, 35, pp.1849–1857.

Yesildag, C., Tyushina, A. & Lensen, M., 2017. Nano-contact transfer with gold nanoparticles on PEG hydrogels and using wrinkled PDMS-stamps. *Polymers*, 9(6).

Zakkar, M. et al., 2011. Dexamethasone Arterializes Venous Endothelial Cells by Inducing Mitogen-Activated Protein Kinase Phosphatase-1 A Novel Antiinflammatory Treatment for Vein Grafts? *Circulation*, 123(5), pp.524-U141.

Zeng, L. et al., 2009. Sustained activation of XBP1 splicing leads to endothelial apoptosis and atherosclerosis development in response to disturbed flow OB OB. *PNAS*, 106(20), pp.8326–8331.

Zhanhai, Y., Ying, G. & Jinghua, Y., 2002. Thermal properties and morphology of noncrosslinking linear low-density polyethylene-grafted acrylic acid. *Journal of Applied Polymer Science*, 86(10), pp.2626–2630. Available at: http://doi.wiley.com/10.1002/app.11218.

Zhou, J., Li, Y.-S. & Chien, S., 2014. Shear stress-initiated signaling and its regulation of endothelial function. *Arteriosclerosis, thrombosis, and vascular biology*, 34(10), pp.2191–2198.